



Faculté des Sciences Appliquées  
Département d'Aérospatiale et de Mécanique  
Laboratoire de Thermodynamique  
Professeur Jean Lebrun



**IEA SHC Task 34 / ECBCS Annex 43  
Subtask D: Mechanical Equipment and Control Strategies**

# **Simulation of HVAC Components with the Help of an Equation Solver**

*Authors:*

**Vincent Lemort, Andres Rodríguez and Jean Lebrun**

**March 2008**



*International Energy Agency*  
**Energy Conservation in  
Buildings and Community  
Systems Programme**

---

Campus du Sart Tilman – Bâtiment B 49 – Parking P 33 – B-4000 LIEGE (Belgium)  
tel : +32 (0)4 366 48 00 – fax : +32 (0)4 366 48 12  
thermoap@ulg.ac.be - <http://www.labohtap.ulg.ac.be>

<b>NOMENCLATURE</b> .....	<b>4</b>
<b>INTRODUCTION</b> .....	<b>7</b>
<b>1 CHILLER</b> .....	<b>7</b>
<b>1.1 Description of the model</b> .....	<b>7</b>
1.1.1 Scroll compressor model.....	7
1.1.2 Chiller global model.....	13
<b>1.2 Parameters identification</b> .....	<b>15</b>
1.2.1 Available information.....	15
1.2.2 Procedure for identifying the parameters (at full load).....	19
1.2.3 Description of part load operation and condenser fans control.....	25
1.2.4 Influence of glycol concentration on the performances.....	28
<b>1.3 Simulation results analysis</b> .....	<b>29</b>
1.3.1 Analysis of empirical test I.....	29
1.3.2 Analysis of the measurements.....	35
<b>2 COOLING COIL</b> .....	<b>48</b>
<b>2.1 Description of the model</b> .....	<b>48</b>
<b>2.2 Parameters identification</b> .....	<b>51</b>
2.2.1 “Nominal” point given by the manufacturer ( <i>Comparative Test</i> ).....	51
2.2.2 Quasi steady-state points extracted from experimental data (empirical tests).....	57
<b>2.3 Simulation results analysis</b> .....	<b>66</b>
2.3.1 Analysis of the comparative tests.....	66
2.3.2 Analysis of the empirical tests.....	72
<b>3 CONDENSING BOILER</b> .....	<b>75</b>
<b>3.1 Description of the model</b> .....	<b>75</b>
<b>3.2 Parameters identification</b> .....	<b>78</b>
3.2.1 Available information.....	78
3.2.2 Procedure for identifying the parameters.....	81
<b>3.3 Simulation results analysis</b> .....	<b>82</b>
3.3.1 Analysis of the comparative tests.....	82
3.3.2 Analysis of the empirical test.....	86
<b>4 HEATING COIL</b> .....	<b>105</b>
<b>4.1 Description of the model</b> .....	<b>105</b>
<b>4.2 Parameters identification</b> .....	<b>105</b>
4.2.1 “Nominal” point given by the manufacturer (comparative test).....	105

4.2.2	Quasi steady-state points extracted from experimental data (empirical tests).....	108
<b>4.3</b>	<b>Simulation results analysis .....</b>	<b>112</b>
4.3.1	Analysis of the comparative tests.....	112
4.3.2	Analysis of the empirical test.....	115
<b>5</b>	<b>CONCLUSIONS .....</b>	<b>120</b>
5.1	Chiller .....	120
5.2	Cooling coil.....	120
5.3	Condensing boiler.....	120
5.4	Heating coil.....	121
5.5	Summary of the models parameters.....	121
	<b>LIST OF REFERENCES .....</b>	<b>121</b>

## Nomenclature

A	area, m <sup>2</sup>
AU	heat transfer coefficient, W/K
c	specific heat, J/kg-k
$\dot{C}$	capacity flow rate, W/K
COP	coefficient of performance
d	diameter, m
gain	temperature gain, 1/K
h	enthalpy, J-kg or convective heat exchange coefficient, W/m <sup>2</sup> -K
HHV	high heating value, J/kg
k	thermal conductivity, W/m-K
LHV	low heating value, J/kg
$\dot{M}$	mass flow rate, kg/s
N	rotational speed, rpm
n	number, -
NTU	Number of thermal units, -
Nu	Nusselt number, -
P	pressure, Pa
Pr	Prandtl number, -
R	heat transfer resistance, K/W
Re	Reynolds number, -
RH	relative humidity, -
s	entropy, J/kg-K
SHR	sensible heat ratio, -
$\dot{Q}$	thermal power, W
t	temperature, C
v	volume, m <sup>3</sup> /kg
V	volume, m <sup>3</sup>
$\dot{V}$	volume flow rate, m <sup>3</sup> /s
W	specific humidity, -
$\dot{W}$	mechanical power, W
x	quality, - or control variable, -

### *Greek letters*

$\alpha$	proportionality factor for the electro-mechanical losses, -
$\Delta$	difference, -
$\varepsilon$	effectiveness, -
$\eta$	efficiency, -
$\gamma$	isentropic exponent, -
$\kappa$	correction factor on the compressor displacement, -
$\mu$	viscosity, kg/m-s
$\omega$	min/max capacity flow rates ratio, -
$\rho$	density, kg/m <sup>3</sup>
$\theta$	fraction of time, -

### *Subscripts*

0	constant
a	air
amb	ambient
atm	atmospherical
aux	auxiliaries
c	contact
calc	calculated
cd	condenser, condensing
cp	compressor
dry	dry regime
env	enveloppe
ev	evaporator, evaporating
ex	exhaust
f	fictitious, fuel, fouling
g	gas
gw	gas-water
in	internal
lat	latent
leak	leakage
loss	(lectro-mechanical) loss
m	metal
man	manufacturer
meas	measured
n	nominal
p	isobaric
r	refrigerant
ref	reference
s	isentropic, swept volume
sens	sensible
set	set point
thr	throat (for a nozzle)
tot	total
tp	two phase
su	supply
w	water, wall
wb	wet bulb
wet	wet

### *Nomenclature used in the main report*

AFR	air flow rate, m <sup>3</sup> /h
BARP	barometric pressure, kPa
CHWFR	chilled water flow rate, l/s
CEP	Chiller electrical consumption, kW
CLT	Chiller or cooling coil cooling capacity, kW
CLS	Cooling coil sensible capacity, kW
CLL	Cooling coil latent capacity, kW

EArH	entering air relative humidity, %
EAT	entering air temperature, C
EAT	entering air humidity, -
HLT	total heating load, kW
HWFR	heating water flowrate, l/s
LArH	leaving air relative humidity, %
LAT	leaving air temperature, C
LAH	leaving air humidity, -
LWT	leaving water temperature, C
NGFR	natural gas flowrate, m <sup>3</sup> /h
UA	overall heat transfer coefficient, kW/K

## Introduction

This report presents models of different HVAC mechanical equipment components. These models have been developed with the help of EES (Engineering Equation Solver). This modeling tool allows an equation-based approach: each component is modeled by a set of equations which describe the main physical processes/peculiarities inherent to the component.

The proposed models involve a limited number of parameters, all of them having a physical meaning. The models do not require exhaustive information, such as the exact geometry of the component. This report aims at showing how the parameters of the models can be identified using only manufacturer submittal or commissioning information.

For each model, the distinction is made between the input variables, the output variables and the parameters. This modular approach makes easier the inter-connection between the different models: the outputs of one model become the inputs of another model.

The proposed models are very suitable for modeling global HVAC systems (an entire cooling or heating plant, which can be connected to a building model) in order to compute primary energy consumption.

For each HVAC component, a description of the model is first given. The parameters identification method is then presented. Encountered traps and proposed tricks are emphasized. A short analysis of the simulation results is finally carried out for each model.

The investigated HVAC components are, on the cooling side, the chiller and, on the heating side, the cooling coil and the other side the condensing boiler and the heating coil. For the chiller, a particular attention is paid to the hermetic scroll compressor.

## 1 Chiller

### 1.1 Description of the model

This paragraph presents a model of air-cooled water chiller. This model associates a scroll compressor, a condenser and an evaporator sub-models.

#### 1.1.1 Scroll compressor model

This model of a hermetic scroll compressor was proposed by Winandy et al. (2001). As shown in Figure 1-1, the modeling assumes that the refrigerant goes through the following consecutive processes:

1. heating-up ( $su \rightarrow su,1$ )
2. mixing with the internal leakage ( $su,1 \rightarrow su,2$ )
3. isentropic compression ( $su,2 \rightarrow in$ )
4. compression at a fixed volume ( $in \rightarrow ex,2$ )
5. cooling-down ( $ex,2 \rightarrow ex,1$ )
6. pressure drop ( $ex,1 \rightarrow ex$ )

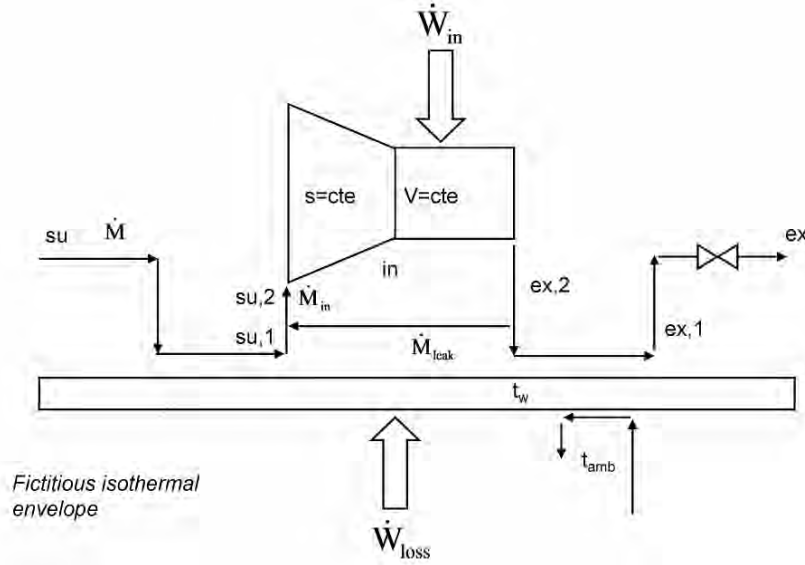


Figure 1-1 Schematic representation of the compression model

#### 1.1.1.1 Suction heating-up ( $su \Rightarrow su,1$ )

When entering the compressor, the refrigerant is heated-up in the suction pipe. This heat transfer is described by introducing a fictitious semi-isothermal heat exchanger, whose uniform temperature  $T_w$  is the wall temperature. As explained latter, this wall temperature will be computed by performing a heat balance across the fictitious wall. The resulting refrigerant temperature  $T_{su,1}$  is obtained by:

$$\dot{Q}_{su} = \dot{M} \cdot c_p \cdot (T_{su,1} - T_{su}) = \varepsilon_{su} \cdot \dot{M} \cdot c_p \cdot (T_w - T_{su}) = \left( 1 - e^{\left( \frac{-AU_{su}}{\dot{M} \cdot c_p} \right)} \right) \cdot \dot{M} \cdot c_p \cdot (T_w - T_{su}) \quad (1-1)$$

The supply heat transfer coefficient  $AU_{su}$  is assumed to vary with the flow rate according to

$$AU_{su} = AU_{su,n} \cdot \left( \frac{\dot{M}_{cp}}{\dot{M}_{cp,n}} \right)^{0.8} \quad (1-2)$$

Where  $AU_{su,n}$  is the nominal heat transfer coefficient corresponding to the nominal mass flow rate  $\dot{M}_n$ . This relationship can be justified by the Reynold's analogy for a turbulent flow through a pipe (Incropera and DeWitt, 2002).

#### 1.1.1.2 Mixing with the internal leakage ( $su,1 \Rightarrow su,2$ )

There are two different leakage paths in a scroll compressor. The radial leakage is due to a gap between the bottom or the top plate and the scrolls. The flank leakage results from a gap between the flanks of the scrolls (Halm, 1997). In the modeling presented here, all the different leakage paths are lumped into one unique fictitious leakage area  $A_{leak}$  which is a parameter of the model to identify.

The leakage flow rate can be computed by reference to the isentropic flow through a simply convergent nozzle, whose throat area is  $A_{leak}$ . The pressure at the inlet of the nozzle is the compressor discharge pressure (plus the pressure drop)  $P_{ex,2}$ . The flow is restricted by a critical low pressure for choked flow conditions:

$$P_{thr} = \mathbf{Max} ( P_{crit} , P_{su2,cp} ) \quad (1-3)$$

The critical pressure  $P_{crit}$  is computed by considering the refrigerant vapor as a perfect gas:

$$P_{crit} = P_{ex2,cp} \cdot \left[ \left( \frac{2}{\gamma + 1} \right)^{\left( \frac{\gamma}{\gamma - 1} \right)} \right] \quad (1-4)$$

The fictitious isentropic exponent  $\gamma$  is computed by:

$$P_{ex2,cp} \cdot v_{ex2,cp}^{\gamma} = P_{thr} \cdot v_{thr}^{\gamma} \quad (1-5)$$

Assuming that the flow through the nozzle is adiabatic, it follows that

$$h_{ex2,cp} = h_{thr} + 1 / 2 \cdot C_{thr}^2 \quad (1-6)$$

where  $C_{thr}$  is the speed of the fluid at the nozzle throat.

The specific enthalpy  $h_{thr}$  and the specific volume  $v_{thr}$  at the throat are functions of the pressure  $P_{thr}$  and of the specific entropy after the compression  $s_{ex,2}$  (since the flow through the nozzle is isentropic):

$$h_{thr} = \mathbf{h} ( \text{fluid\$} , s = s_{ex2,cp} , P = P_{thr} ) \quad (1-7)$$

$$v_{thr} = \mathbf{v} ( \text{fluid\$} , s = s_{ex2,cp} , P = P_{thr} ) \quad (1-8)$$

The system made up of the last six equations must be solved to determine, among others, the specific volume  $v_{thr}$  and the speed of the fluid  $C_{thr}$  at the throat.

Finally, using the equation of continuity, the leakage mass flow rate can be expressed at the nozzle throat by

$$\dot{M}_{leak,cp} = \frac{A_{leak} \cdot C_{thr}}{v_{thr}} \quad (1-9)$$

The modeling assumes that the internal leakage flow is mixed up with the flow entering the compressor before entering the suction chamber. This mixing process is described by equations of conservation of mass and energy.

$$\dot{M}_{cp} = \dot{M}_{in,cp} - \dot{M}_{leak,cp} \quad (1-10)$$

$$\dot{M}_{cp} \cdot h_{su1,cp} + \dot{M}_{leak,cp} \cdot h_{ex2,cp} = \dot{M}_{in,cp} \cdot h_{su1,cp} \quad (1-11)$$

The internal flow rate entering the compressor is imposed by the compressor displacement and the specific volume of the refrigerant in the suction chamber ( $v_{su,2,cp}$ ):

$$\dot{M}_{s,cp} = [1 + \kappa_{cp}] \cdot \frac{\dot{V}_{s,cp}}{v_{su2,cp}} \quad (1-12)$$

In the latter expression, a correction factor  $\kappa_{cp}$  on the compressor displacement is introduced and is an additional parameter of the model to identify. This fictitious increase of the displacement may be explained by the passive supercharging effect described by Nieter (1988) and mentioned later by Winandy (1999) in his work on hermetic scroll compressor modeling. The suction gas may start to be compressed before the end of the suction process, because of the decrease of the volume in the suction pockets near the end of the suction process.

### 1.1.1.3 Compression ( $su,2 \Rightarrow ex,2$ )

Two situations can occur: either the internal pressure in the compression chambers at the end of the compression (i.e. at the discharge angle) is higher than the discharge pressure (*over-compression*), or it is lower (*under-compression*). These two situations are illustrated in Figure 1-2.

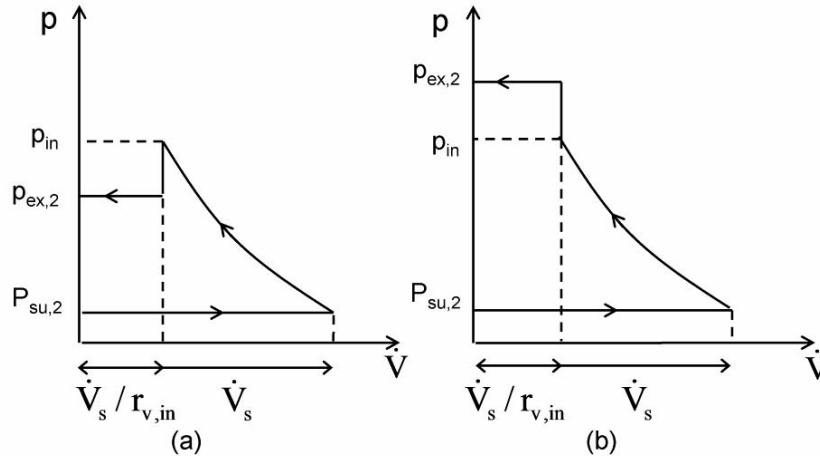


**Figure 1-2 Pressure – displaced volume diagram for the compression, (a): over-compression and (b): under-compression**

The compression is divided in two steps: an adiabatic and reversible compression from  $P_{su,2}$  to the internal pressure  $P_{in}$  followed by a compression at fixed volume and still adiabatic from  $P_{in}$  to the exhaust pressure  $P_{ex,2}$ . The work associated to the first part of the compression is

$$w_{in1,cp} = h_{in,cp} - h_{su2,cp} \quad (1-13)$$

With

$$h_{in,cp} = h(\text{fluid}, s_{su2,cp}, v_{in,cp}) \quad (1-14)$$

And

$$v_{in,cp} = \frac{v_{su2,cp}}{r_{v,in,cp}} \quad (1-15)$$

The work associated to the second part of the compression can be written as

$$w_{in2,cp} = v_{in,cp} \cdot (P_{ex2,cp} - p_{in,cp}) \quad (1-16)$$

With

$$p_{in,cp} = P(\text{fluid}, s_{in,cp}, v_{in,cp}) \quad (1-17)$$

The total work is then

$$w_{in,cp} = w_{in1,cp} + w_{in2,cp} \quad (1-18)$$

Since the entire process is assumed to be adiabatic, it follows that the enthalpy at the end of the compression process can be computed by:

$$h_{ex2,cp} = h_{su2,cp} + w_{in,cp} \quad (1-19)$$

#### 1.1.1.4 Exhaust cooling-down ( $ex,2 \Rightarrow ex,1$ )

The modeling of the exhaust cooling-down is similar to the one of the suction heating-up. A very similar set of equations is used.

#### 1.1.1.5 Electrical consumption of the compressor

The compressor electrical consumption can be split into the internal compressor power  $\dot{W}_{in}$  and the electro-mechanical loss  $\dot{W}_{loss}$ . The latter can be expressed as a constant electro-mechanical losses  $\dot{W}_{loss,0}$  and another loss proportional to the internal power ( $\alpha$  is the factor of proportionality):

$$\dot{W}_{el} = \dot{W}_{in} + \dot{W}_{loss} = (1 + \alpha)\dot{W}_{in} + \dot{W}_{loss,0} \quad (1-20)$$

The constant electro-mechanical loss and the factor of proportionality are 2 parameters to identify.

### 1.1.1.6 Heat balance over the compressor

As shown previously, a fictitious envelope of uniform temperature  $T_w$  is assumed to represent the three heat transfer processes: suction heating-up, exhaust cooling-down and ambient loss. Performing a steady state energy balance across this envelope yields the temperature of the envelope  $T_w$ .

$$0 = \dot{W}_{\text{loss,cp}} - \dot{Q}_{\text{su,cp}} - \dot{Q}_{\text{ex,cp}} - \dot{Q}_{\text{amb,cp}} \quad (1-21)$$

The ambient loss is computed in equation (1-22), on the basis of a global heat transfer coefficient  $AU_{\text{amb}}$  (between wall temperature and ambience temperature), which is a parameter to identify.

$$\dot{Q}_{\text{amb,cp}} = AU_{\text{amb,cp}} \cdot (t_{w,\text{cp}} - t_{\text{amb}}) \quad (1-22)$$

### 1.1.1.7 Discharge pressure drop

The pressure drop through the discharge port is described by the isentropic compressor flow through a converging nozzle, with similar equations than those introduced for the internal leakage modeling. The nozzle throat area  $A_{\text{ex}}$  is a parameter of the model to identify. This area can be much lower than the one of the discharge port (due, among others, to the vena contracta).

### 1.1.1.8 Information diagram of the model

The information diagram of the compressor model is given in Figure 1-3.

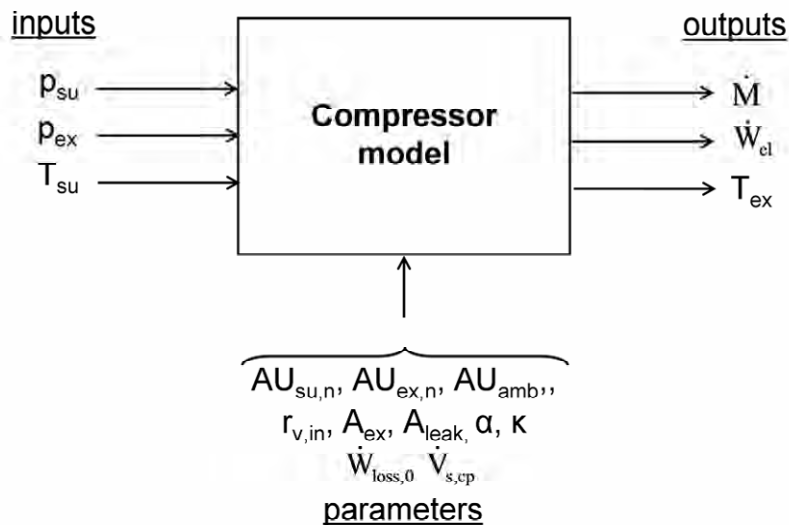


Figure 1-3 Information diagram of the compressor model

The displaced volume flow rate  $\dot{V}_{s,cp}$  (m<sup>3</sup>/s) of the compressor is here imposed. Alternatively, the swept volume of the compressor  $V_{s,cp}$  (m<sup>3</sup>) could have been imposed. In this case, the model would require the rotation speed  $N$  (rpm) as a input of the model since :

$$\dot{V}_{s,cp} = V_{s,cp} \cdot \frac{N_{rot}}{60}$$

### 1.1.2 Chiller global model

Both the condenser and the evaporator are modeled as semi-isothermal heat exchangers. In each case, the global heat transfer coefficient between the refrigerant and the secondary fluid is expressed by three resistances in series: a convective resistance on the refrigerant-side, the conduction resistance of the metal and a convective resistance on the secondary fluid side.

#### 1.1.2.1 *Air-cooled condenser*

In laminar regime, the convective resistance on the air-side is assumed to vary with the air mass flow rate according to:

$$R_{a,cd} = R_{a,cd,n} \cdot \left[ \frac{\dot{M}_{a,cd,n}}{\dot{M}_{a,cd}} \right]^{0.6} \quad (1-23)$$

In turbulent regime, the convective resistance on the refrigerant-side is assumed to vary with the refrigerant flow rate according to:

$$R_{r,cd} = R_{r,cd,n} \cdot \left[ \frac{\dot{M}_{r,cd,n}}{\dot{M}_{r,cd}} \right]^{0.8} \quad (1-24)$$

Hence, the global heat transfer coefficient can be computed by:

$$\frac{1}{AU_{cd}} = R_{a,cd} + R_{m,cd} + R_{r,cd} \quad (1-25)$$

Where  $R_{m,cd}$  is the metal conduction resistance.

The effectiveness of the heat exchanger is expressed by

$$\varepsilon_{cd} = 1 - \exp(-NTU_{cd}) \quad (1-26)$$

With the number of thermal units defined by

$$NTU_{cd} = \frac{AU_{cd}}{\dot{C}_{a,cd}} \quad (1-27)$$

A convenient approximation is to consider that the refrigerant is isothermal inside the coil. The condensing temperature can be defined as the weighted average of the actual refrigerant temperatures (in order to account for the effects of the condenser desuperheating and subcooling):

$$t_{cd} = \frac{(h_{r,su,cd} - h_{r,su,cd,tp}) \cdot \left[ \frac{T_{r,su,cd} + T_{cd}}{2} \right] + (h_{r,su,cd,tp} - h_{r,ex,cd,tp}) \cdot T_{cd} + (h_{r,ex,cd,tp} - h_{r,ex,cd}) \cdot \left[ \frac{t_{r,ex,cd} + T_{cd}}{2} \right]}{h_{r,su,cd} - h_{r,ex,cd}} \quad (1-28)$$

With the enthalpy of the refrigerant at the inlet of the two-phase zone:

$$h_{r,su,cd,tp} = h(\text{fluid}, P = p_{cd}, x = 1) \quad (1-29)$$

And the enthalpy of the refrigerant at the outlet of the two-phase zone:

$$h_{r,ex,cd,tp} = h(\text{fluid}, P = p_{cd}, x = 0) \quad (1-30)$$

The average condensing temperature can be expressed as a function of air inlet temperature, condensing power and condenser effectiveness by:

$$t_{cd} = t_{a,su,cd} + \frac{\dot{Q}_{cd}}{\varepsilon_{cd} \cdot \dot{C}_{a,cd}} \quad (1-31)$$

### 1.1.2.2 Evaporator

The description of the evaporator is similar to that of the condenser. Here, both regimes on the refrigerant side and the water side are assumed to be turbulent:

$$R_{w,ev} = R_{w,ev,n} \cdot \left[ \frac{\dot{M}_{w,ev,n}}{\dot{M}_{w,ev}} \right]^{0.8} \quad (1-32)$$

$$R_{r,ev} = R_{r,ev,n} \cdot \left[ \frac{\dot{M}_{r,ev,n}}{\dot{M}_{r,ev}} \right]^{0.8} \quad (1-33)$$

The average evaporating temperature is here defined by:

$$t_{ev} = \frac{(h_{r,ex,ev,tp} - h_{r,su,ev}) \cdot T_{ev} + (h_{r,ex,ev} - h_{r,ex,ev,tp}) \cdot \left[ \frac{T_{r,ex,ev} + T_{ev}}{2} \right]}{h_{r,ex,ev} - h_{r,su,ev}} \quad (1-34)$$

With:

$$h_{r,ex,ev,tp} = h(\text{fluid}, x = 1, P = p_{ev}) \quad (1-35)$$

### 1.1.2.3 Condenser fans and auxiliaries

The control of the condenser fans is described later. The consumption of the fan and the auxiliaries is taken into account when evaluating the COP of the chiller:

$$\text{COP} = \frac{\dot{Q}_{ev}}{\dot{W}} \quad (1-36)$$

$$\dot{W} = \dot{W}_{cp,tot} + \dot{W}_{fan} + \dot{W}_{aux} \quad (1-37)$$

$$\dot{W}_{cp,tot} = N_{cp} \cdot \dot{W}_{cp}$$

## 1.2 Parameters identification

### 1.2.1 Available information

#### 1.2.1.1 Information on the chiller

Chiller general data is given in Table 1-1.

**Table 1-1 Chiller general data**

Manufacturer	McQuay International
Chiller Model	AGZ 010AS
Chiller type	Air Cooled Liquid Chiller
Nominal Unit @ ARI Conditions	35°C Entering Air Temperature
Capacity	34.3 kW (9.8 tons)
Flow Rate	1.51 l/s (24.0 gpm)
Leaving Water Temperature	6.7°C (44.0°F)
Full Load COP	2.84
Integrated Part Load COP	3.58
Refrigerant Type	HCFC -22 (R22)
Refrigerant Circuits	1 Refrigerant Circuit
Heat Transfer Fluid	25% Propylene Glycol
Electrical Characteristics	460 Volt / 3 Phase / 60 Hz

**Thirty performance points are given by the manufacturer (**

Table 1-2). These performance data are given as a function of the leaving water temperature (evaporator exhaust temperature  $T_{w,ex,ev}$ ) and the ambient air temperature (condenser supply temperature  $T_{a,su,cd}$ ).

**Table 1-2 Chiller performance data (the red framed point is the closest to ARI standard)**

LWT (°C)	Ambient Air Temperature (°C)														
	25			30			35			40			45		
	Unit kW	PWR kW	Unit COP	Unit kW	PWR kW	Unit COP	Unit kW	PWR kW	Unit COP	Unit kW	PWR kW	Unit COP	Unit kW	PWR kW	Unit COP
5	35	8	3.4	33.7	8.8	3.03	32.3	9.7	2.7	30.9	10.7	2.38	29.4	11.8	2.09
6	36.2	8.1	3.49	34.9	8.9	3.12	33.5	9.8	2.78	32.1	10.8	2.46	30.5	11.9	2.15
7	37.5	8.2	3.59	36.2	9	3.21	34.8	9.9	2.86	33.3	10.9	2.53	31.7	12	2.22
8	38.9	8.3	3.68	37.5	9.1	3.3	36	9.9	2.94	34.5	10.9	2.61	32.8	12.1	2.29
9	40.2	8.4	3.78	38.8	9.1	3.39	37.3	10	3.02	35.7	11	2.68	34	12.2	2.35
10	41.6	8.4	3.87	40.1	9.2	3.48	38.6	10.1	3.11	36.9	11.1	2.75	35.2	12.3	2.42

These ratings are in accordance with ARI Standard 550/590-98. The electrical input is for the compressor only. The COP is for the entire unit (it accounts for fans electrical consumption).

The *part load performances* of the chiller are described by four points given in Table 1-3. These data are certified according to ARI Standard 550/590-98. The air temperature is missing for the 75%, 50% and 25% points. It has been assumed that this temperature is in accordance with the ARI Standard (26.7°C, 18.3°C and 12.8°C).

**Table 1-3 Chiller part load data**

<b>Chiller Performance (Water Application)</b>				
Percent of Rated Capacity	100 %	75 %	50 %	25 %
Capacity kW	34.5	25.7	17.2	8.4
Unit kW Input	12.1	7.4	4.6	2.4
COP	2.84	3.49	3.69	3.52
Entering Liquid Temp °C	12.22	10.83	9.44	8.06
Leaving Liquid Temp. °C	6.67			
Liquid Flow l/s	1.48			
Entering Air Temp. °C	35	26.7	18.3	12.8

Information on the *reduction in performances with the use of glycol* is given in Table 1-4 and Table 1-5.

**Table 1-4 Chiller Performance (25% Propylene Glycol Application)**

Percent of Rated Capacity	100%
Tons	33.8
Unit kW Input	12.0
COP	2.81
Entering Liquid Temp. °C	12.22
Leaving Liquid Temp. °C	6.67
Liquid Flow l/s	1.51
Entering Air Temp. °C	35

**Table 1-5 Adjustment factors for use of propylene glycol and anti-freeze fluids**

% P.G.	Freeze Point					
	°F	°C	Cap.	Power	Flow	PD
10	26	-3	0.987	0.992	1.01	1.068
20	19	-7	0.975	0.985	1.028	1.147
30	9	-13	0.962	0.978	1.05	1.248
40	-5	-21	0.946	0.971	1.078	1.366
50	-27	-33	0.929	0.965	1.116	1.481

### 1.2.1.2 Information on the compressors

The Copeland tandem compressor ZR136KC-TFD is made up of two ZR68KC-TFD scroll compressors. The swept volume of ZR68KC-TFD compressor is 93.013 cm<sup>3</sup> per revolution. This swept volume corresponds to a displacement of 16.183 m<sup>3</sup>/h at 50 Hz operation, and 19.533 m<sup>3</sup>/h at 60 Hz operation.

Performances of the compressor are presented in Table 1-6 and Table 1-7, giving the capacity and the power input of the compressor as a function of the evaporating and condensing temperatures. Rating conditions are:

- superheat at the compressor inlet: 20°F (11.11°C)
- subcooling at the condenser outlet: 15°F (8.33°C)
- ambient air temperature: 95 °F (35°C)
- 50Hz operation
- Refrigerant : HCFC R-22

The subcooling is defined as the difference between the compressor saturated discharge temperature (condensing temperature  $T_{cd}$ ) and the actual liquid temperature at the expansion device. The suction superheat is the difference between the actual gas temperature at the compressor supply and the saturated suction temperature (evaporating temperature  $T_{ev}$ ).

**Table 1-6 Capacity (W) of the compressor ZR68KC-TFD**

T <sub>cd</sub> [C]	T <sub>ev</sub> [C]									
		-23.3	-17.8	-12.2	-6.7	-1.1	4.4	7.2	10.0	12.8
26.7	5832	7884	10228	12983	16178	19841	21922	24120	26464	
32.2	5393	7385	9671	12309	15386	18932	20896	23035	25292	
37.8	4953	6916	9115	11664	14624	18053	19929	21980	24178	
43.3		6389	8528	11019	13862	17145	18962	20925	23035	
48.9			7884	10287	13042	16207	17965	19841	21863	
54.4				9466	12133	15181	16852	18669	20632	
60.0					11078	14009	15650	17408	19284	
65.6						12719	14302	15972	17789	

**Table 1-7 Power input (W) of the compressor ZR68KC-TFD**

T <sub>cd</sub> [C]	T <sub>ev</sub> [C]									
		-23.3	-17.8	-12.2	-6.7	-1.1	4.4	7.2	10.0	12.8
26.7	2560	2570	2580	2620	2660	2710	2740	2780	2810	
32.2	2970	2960	2960	2970	3000	3030	3060	3090	3120	
37.8	3430	3400	3380	3380	3390	3420	3430	3460	3480	
43.3		3900	3870	3850	3850	3860	3870	3890	3910	
48.9			4420	4390	4370	4370	4380	4390	4410	
54.4				4990	4960	4950	4960	4860	4980	
60.0					5630	5610	5610	5610	5620	
65.6						6350	6340	6340	6350	

The refrigerant mass flow rate swept by the compressor can be derived from the cooling capacity, the evaporating temperature, the compressor suction superheat and the condenser outlet subcooling. The cooling capacity is the enthalpy difference over the evaporator multiplied by the mass flow rate. The enthalpy at the evaporator inlet is equal to the one at the condenser outlet (including subcooling) and the enthalpy at the evaporator outlet is the one at the compressor suction.

**Table 1-8 Mass flow (g/s) of the compressor ZR68KC-TFD**

T <sub>cd</sub> [C]	T <sub>ev</sub> [C]									
		-23.3	-17.8	-12.2	-6.7	-1.1	4.4	7.2	10.0	12.8
26.7	32.27	43.01	55.05	68.97	84.88	102.87	113.01	123.66	134.95	
32.2	31.02	41.87	54.06	67.88	83.76	101.80	111.70	122.43	133.68	
37.8	29.69	40.83	53.02	66.91	82.77	100.88	110.68	121.35	132.71	
43.3		39.38	51.77	65.91	81.76	99.79	109.66	120.27	131.60	
48.9			50.06	64.33	80.37	98.50	108.46	119.01	130.32	
54.4				62.09	78.37	96.64	106.53	117.21	128.69	
60.0					75.26	93.72	103.93	114.79	126.28	
65.6						89.79	100.18	111.05	122.78	

### 1.2.2 Procedure for identifying the parameters (at full load)

The identification of the parameters of the model is achieved in two steps:

- The parameters of the compressor model are first identified, based on compressor performance points.
- The parameters of the evaporator and the condenser are finally identified, based on chiller performance points.

#### 1.2.2.1 First step: identification of the parameters of the compressor model

The parameters of the compressor model are tuned in order to bring the values (of the refrigerant mass flow rate, power consumption and cooling capacity) predicted by the model as close as possible to the values announced by the manufacturer. Identified parameters are given in the information diagram shown in Figure 1-4. This diagram shows that the evaporating and condensing temperatures as well as the suction superheat and the condenser subcooling are the inputs of the model, while the model calculates the mass flow, the power consumption, the cooling capacity and the heat rejection.

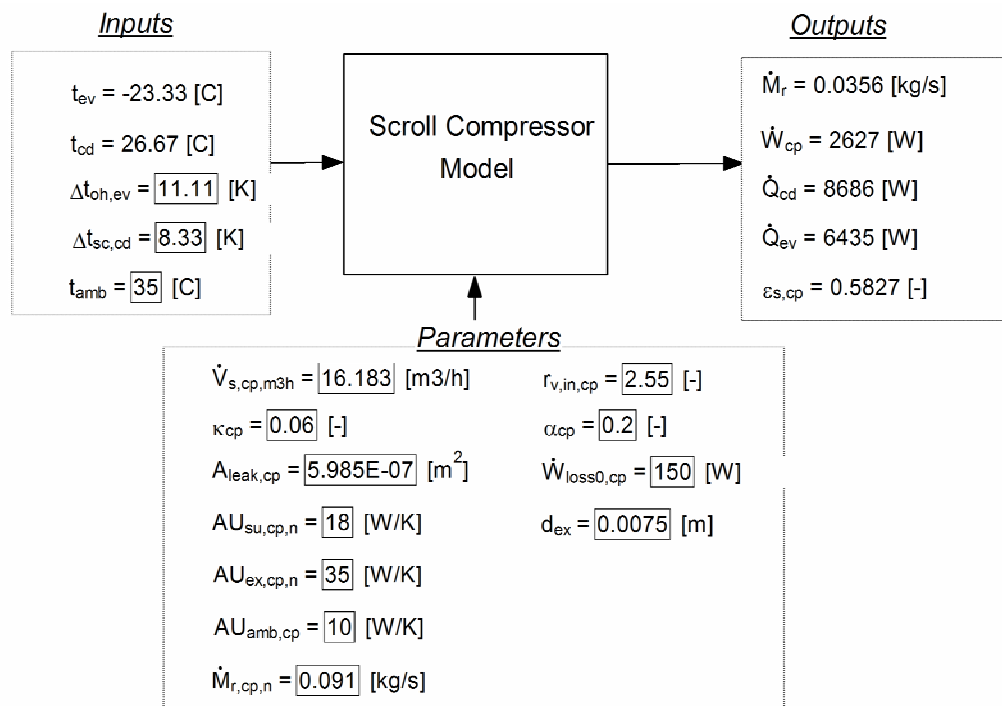


**Figure 1-4 Information diagram for the scroll compressor model (model ZR 68 KC-TFD)**

Prediction by the model of the refrigerant mass flow rate, power consumption and cooling capacity are compared to the values given by the manufacturer in Figure 1-5, Figure 1-6 and Figure 1-7. It can be observed that the agreement is fairly good. However, the model doesn't seem to predict correctly the mass flow rate for the low mass flows.

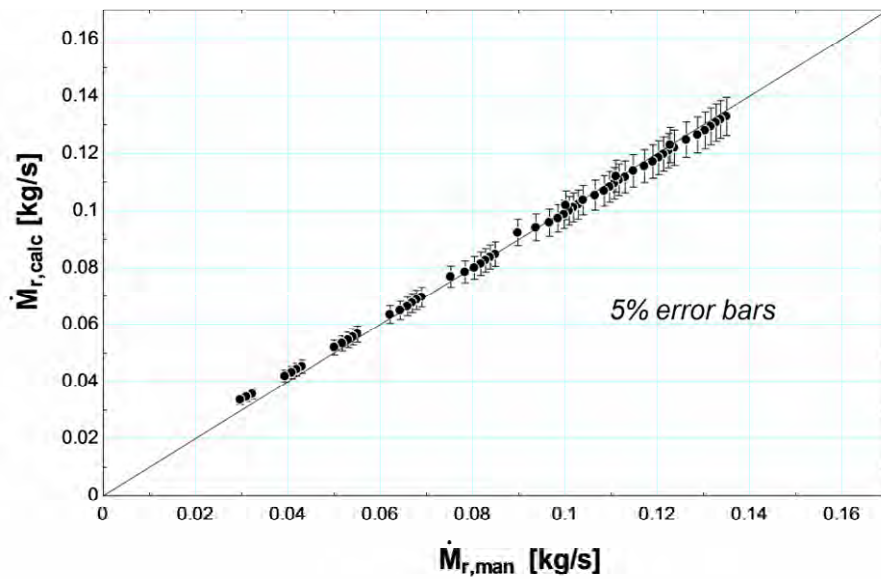


Figure 1-5 Prediction by the compressor model of the refrigerant mass flow rate

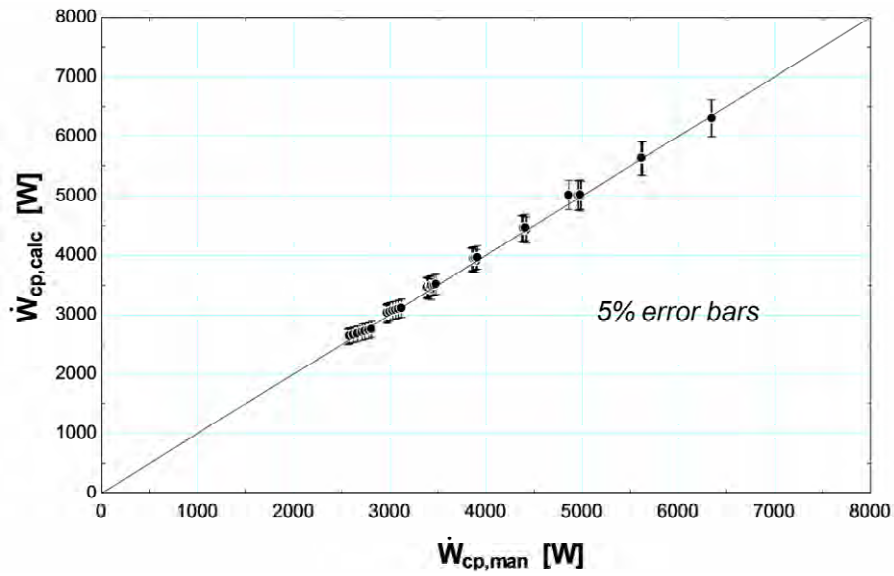


Figure 1-6 Prediction by the compressor model of the electrical power

Figure 1-7 shows that the low cooling capacities are over-predicted. This is due to the over-prediction of the refrigerant mass flow rate (see Figure 1-5).

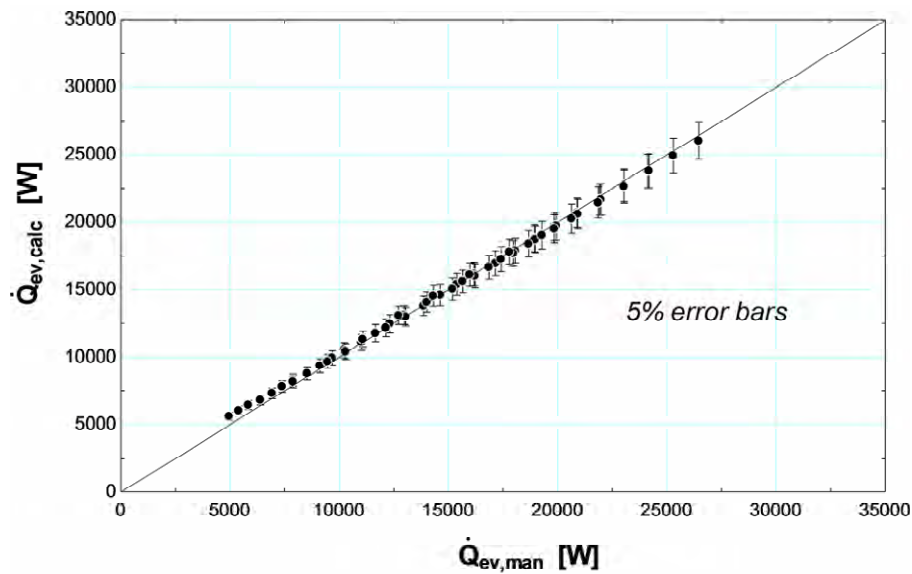


Figure 1-7 Prediction by the compressor model of the cooling capacity

Figure 1-8 compares the evolution of the global isentropic effectiveness predicted by the model and announced by the manufacturer with the pressure ratio imposed to the compressor. This global isentropic effectiveness is defined by

$$\varepsilon_{s,cp} = \frac{\dot{M}_r \cdot (h_{exs,cp} - h_{su,cp})}{\dot{W}_{cp}}$$

The disagreement between the values predicted by the model and announced by the manufacturer are due to the poor prediction of the refrigerant mass flow (which is under-predicted for the low values and over-predicted for the high values).

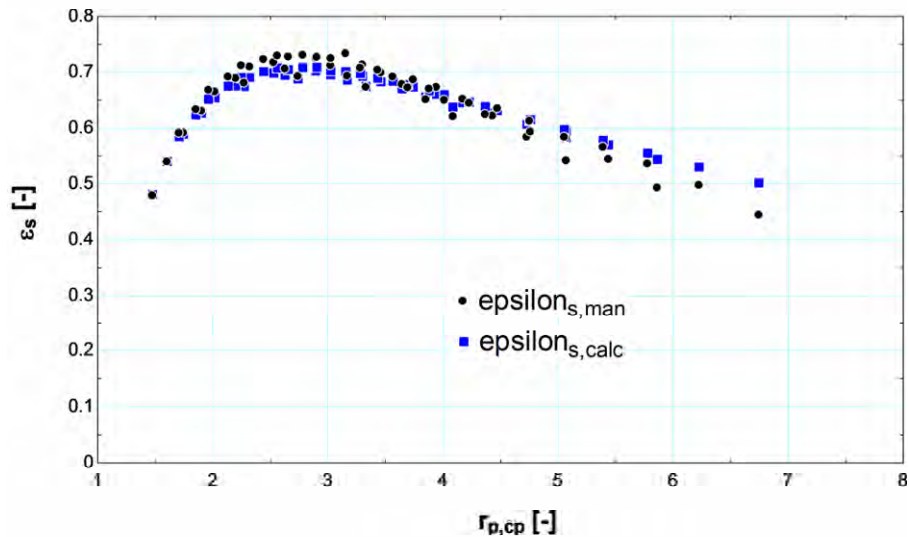
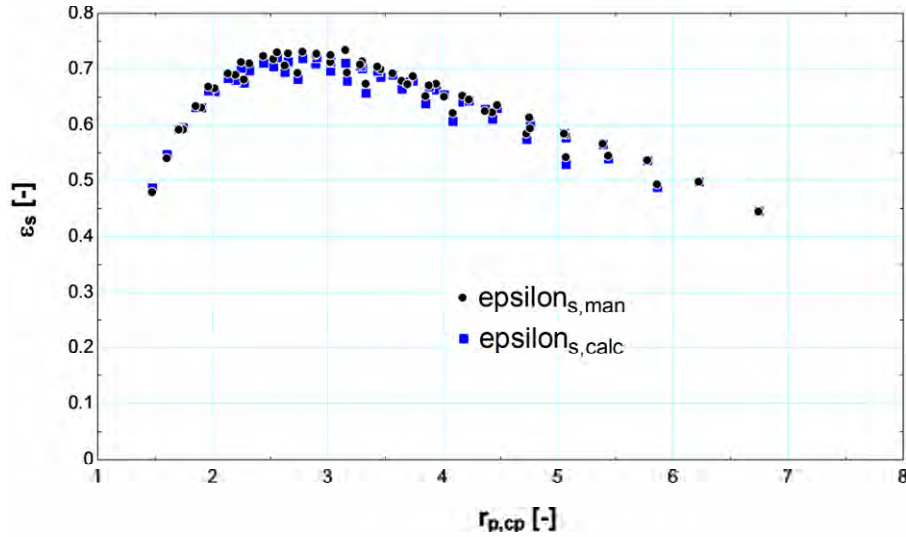


Figure 1-8 Prediction by the compressor model of isentropic effectiveness

The fictitious lumped leakage area of the model is re-identified for each performance point by imposing the mass flow rate to be equal to the value announced by the manufacturer. Figure 1-9 confirms that the disagreement in the prediction of the global isentropic effectiveness in Figure 1-8 was due to the flow rate prediction.



**Figure 1-9 Prediction by the compressor model of isentropic effectiveness (the mass flow rate is imposed equal to the mass flow rate given by the manufacturer)**

Figure 1-10 shows that the leakage area tends to increase when the supply pressure decrease and the pressure ratio decreases. This can be due to the axial compliance system inherent to this type of compressor.

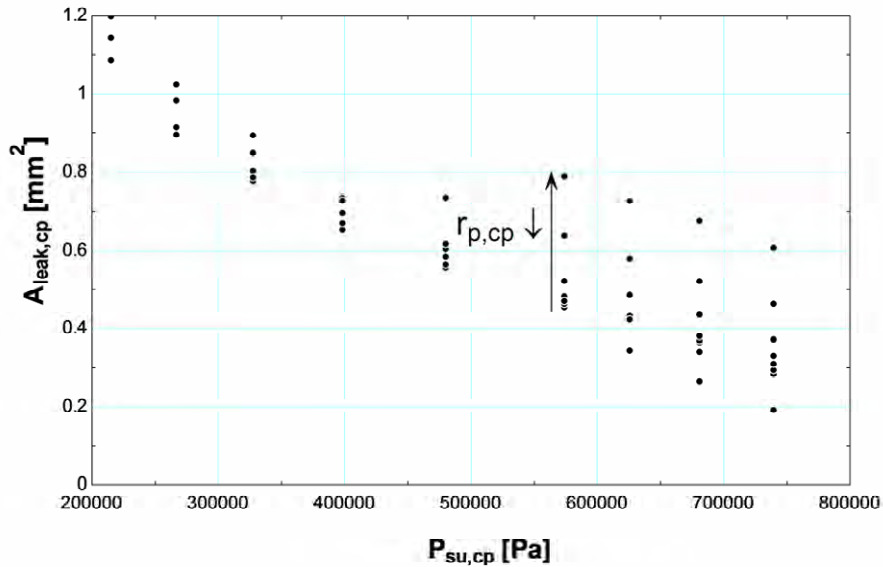


**Figure 1-10 Prediction by the compressor model of the leakage area (the mass flow rate is imposed equal to the mass flow rate given by the manufacturer)**

However, even with considering a constant leakage area, prediction by the model of the cooling capacity, power consumption and refrigerant mass flow rate are fairly good. The parameters of the models could be refined if the heat rejection (condensing power) was given

by the manufacturer. The exhaust gas temperature can actually be deduced from the value of the heat rejection. Knowing the exhaust temperature would allow to better identify the heat transfer coefficients in the model.

### 1.2.2.2 Second step: Identification of the parameters of the heat exchangers models

The parameters of the heat exchangers models are first identified on the basis of one unique point. From all the points, the one closest to ARI Standard (entering air dry and wet bulb temperature: 35°C and 23.9°C; leaving water temperature: 6.67°C; water flow rate: 0.043 L/s per kW) has been selected (red framed point in

Table 1-2).

The parameters of the condenser and the evaporator models (three resistances and two nominal flow rates) are identified by imposing the cooling capacity and the compressor consumption calculated by the model equal to the values announced by the manufacturer. The following relationships are also imposed:

- for the evaporator,

$$R_{w,ev,n} = R_{r,ev,n} \quad (\text{supposed to be optimal design}) \quad (1-38)$$

$$R_{m,ev} = 0.1 \cdot R_{w,ev,n} \quad (\text{good practice rule}) \quad (1-39)$$

$$\dot{M}_{w,ev,n} = \dot{M}_{w,ev} \quad (1-40)$$

$$\dot{M}_{r,ev,n} = \dot{M}_{r,ev} \quad (1-41)$$

- for the condenser,

$$R_{a,cd,n} = R_{r,cd,n} \quad (\text{supposed to be optimal design}) \quad (1-42)$$

$$R_{m,cd} = 0.1 \cdot R_{a,cd,n} \quad (\text{good practice rule}) \quad (1-43)$$

$$\dot{M}_{a,cd,n} = \dot{M}_{a,cd} \quad (1-44)$$

$$\dot{M}_{r,cd,n} = \dot{M}_{r,cd} \quad (1-45)$$

The latter ratios between the resistances are proposed here as a first guess (good practice rules). They can be tuned afterwards to get a better agreement between predictions by the model and measurements.

### Fans

The chiller investigated here comprises two fans. The condenser nominal airflow is given by the manufacturer (23700 m<sup>3</sup>/h for the two fans). It is assumed that the fans operate at their maximum flow rate for all the points given in

Table 1-2, since it gives the best agreement.

The identified parameters of the model are given in the information diagram of the chiller model shown in Figure 1-11. The identified fan consumption is 1100 W.

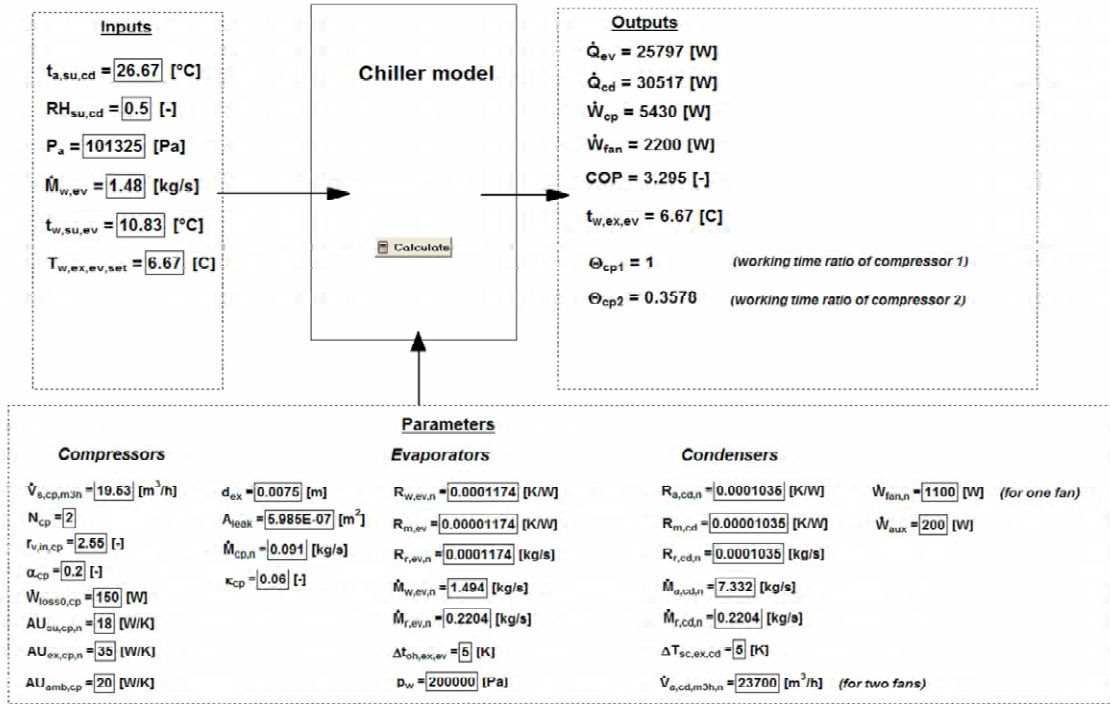


Figure 1-11 Information diagram of the chiller model

The agreement between predicted and measured performances is shown in Figure 1-12, Figure 1-13 and Figure 1-14. In these figures, the ratios between the resistances (for both the condenser and the evaporator) haven't been retuned and are those given in Equations (1-40) to (1-47).

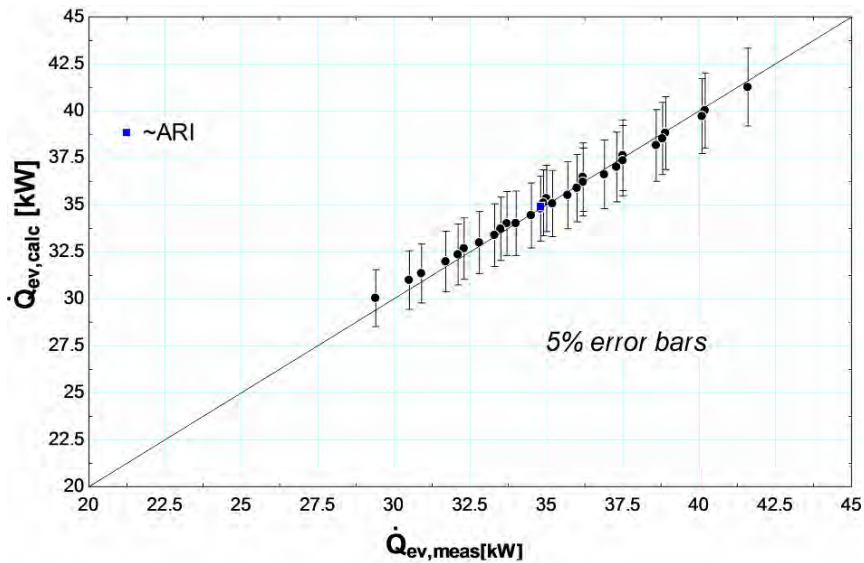


Figure 1-12 Prediction by the model of the chiller capacity

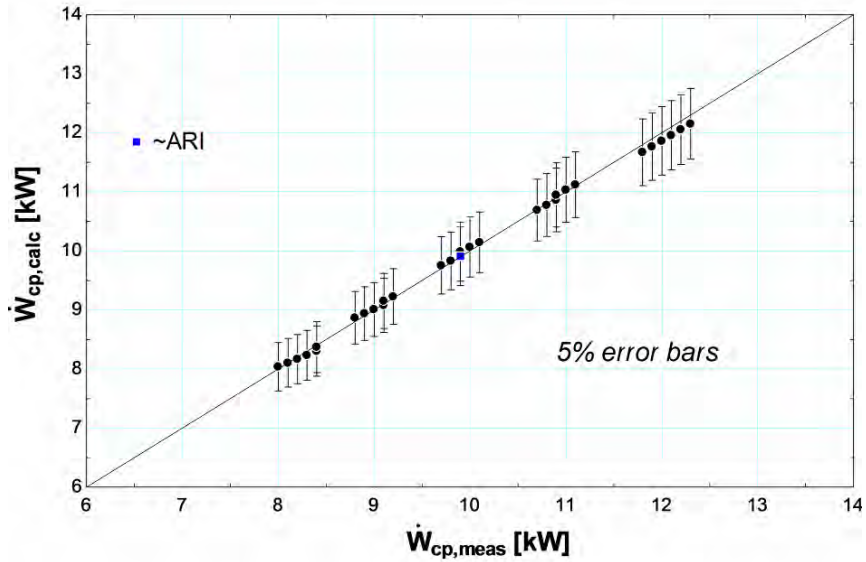


Figure 1-13 Prediction by the model of the compressors electrical consumption

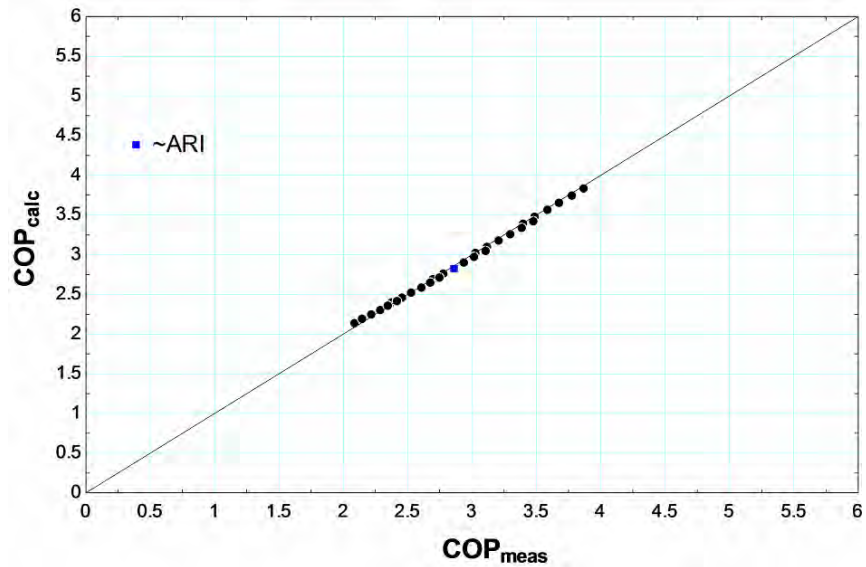


Figure 1-14 Prediction by the model of the chiller overall COP (including fan consumption)

### 1.2.3 Description of part load operation and condenser fans control

*Part load performances* are described by four points given in Table 1-3. The chiller is controlled by cycling its two compressors in order to maintain a set point on the leaving water temperature.

This control is simulated in the following way:

- when only one compressor is working, the leaving water temperature is  $t_{w,ex,ev,1}$

- when two compressors are working, this temperature is  $t_{w,ex,ev,12}$
- when no compressors are working, the water leaving temperature is the entering water temperature  $t_{w,su,ev}$ .

These three temperatures must be combined to reach (if there is enough available capacity) the water leaving temperature set point. The working time fractions  $\theta_{cp,1}$  and  $\theta_{cp,2}$  of the two compressors are calculated by solving successively the two following equations:

$$\Theta_{cp2} = \mathbf{Max} \left[ 0, \mathbf{Min} \left( 1, \frac{t_{w,ex,ev,set} - t_{w,ex,ev,1}}{t_{w,ex,ev,12} - t_{w,ex,ev,1}} \right) \right] \quad (1-46)$$

$$\Theta_{cp1} = \mathbf{Min} \left[ 1, \frac{t_{w,ex,ev,set} - t_{w,su,ev}}{t_{w,ex,ev,1} - t_{w,su,ev}} \right] \quad (1-47)$$

The achieved leaving water temperature is given by:

$$t_{w,ex,ev} = [1 - \Theta_{cp1}] \cdot t_{w,su,ev} + \Theta_{cp1} \cdot [(1 - \Theta_{cp2}) \cdot t_{w,ex,ev,1} + \Theta_{cp2} \cdot t_{w,ex,ev,12}] \quad (1-48)$$

The cooling capacity is given by:

$$\dot{Q}_{ev} = [1 - \Theta_{cp2}] \cdot \Theta_{cp1} \cdot \dot{Q}_{ev,1} + \Theta_{cp2} \cdot \dot{Q}_{ev,12} \quad (1-49)$$

The compressor consumption, the fan consumption, the total consumption and the COP are given by:

$$\dot{W}_{cp} = \Theta_{cp1} \cdot [(1 - \Theta_{cp2}) \cdot \dot{W}_{cp,1} + \Theta_{cp2} \cdot \dot{W}_{cp,12}] \quad (1-50)$$

$$\dot{W}_{fan} = \Theta_{cp1} \cdot [(1 - \Theta_{cp2}) \cdot \dot{W}_{fan,1} + \Theta_{cp2} \cdot \dot{W}_{fan,12}] \quad (1-51)$$

$$\dot{W} = \dot{W}_{cp} + \dot{W}_{fan} + \dot{W}_{aux} \quad (1-52)$$

$$COP = \frac{\dot{Q}_{ev}}{\dot{W}} \quad (1-53)$$

*Condenser fan motors* are automatically cycled in response to condenser pressure by a standard method of head pressure control. The second fan cycles in order to maintain the head pressure, which allows the unit to run at low ambient air temperature down to 1.7°C. The first fan modulates its motor speed in response to condenser pressure, which allows the unit to operate down to -18°C. This control can be described by the following equations:

$$X_{set,fan} = gain \cdot (t_{cd} - t_{cd,set}) \quad (1-54)$$

$$X_{contr,fan} = \mathbf{Max} (0, X_{set,fan}) \quad (1-55)$$

$$\dot{V}_{a,cd,set} = \dot{V}_{a,cd,min} + (\dot{V}_{a,cd,max} - \dot{V}_{a,cd,min}) \cdot X_{contr,fan} \quad (1-56)$$

$$\dot{V}_{a,cd,min} = 0.2 \cdot \dot{V}_{a,cd,max} \quad (1-57)$$

$$\dot{V}_{a,cd,max} = \dot{V}_{a,cd,n} \quad (1-58)$$

$$\dot{V}_{a,cd} = \text{Min} (\dot{V}_{a,cd,set}, \dot{V}_{a,cd,max}) \quad (1-59)$$

The fan control variable is defined as:

$$x_{fan} = \frac{\dot{V}_{a,cd}}{\dot{V}_{a,cd,n}} \quad (1-60)$$

The total fan consumption is the summation of the consumption of each fan:

$$\dot{W}_{fan} = \dot{W}_{fan1} + \dot{W}_{fan2} \quad (1-61)$$

Since the first one is a variable speed fan, its consumption varies with its control variable  $x_{fan,1}$  according to

$$\dot{W}_{fan1} = x_{fan1}^3 \cdot \dot{W}_{fan,n} \quad (1-62)$$

The control variable of the first fan is defined by

$$x_{fan1} = \text{If} (2 \cdot x_{fan,1}, 2 \cdot x_{fan,2} \cdot x_{fan,1}) \quad (1-63)$$

This control variable is the ratio between the actual volume flow rate delivered by the fan and its maximum volume flow rate. This ratio is very close the one between the actual rotational speed and the maximal rotational speed of the fan.

Since the second fan cycles, its consumption can be expressed as a function of its control variable  $x_{fan,2}$  (here defined as the working time fraction of the fan).

$$\dot{W}_{fan2} = x_{fan2} \cdot \dot{W}_{fan,n} \quad (1-64)$$

With

$$x_{fan2} = \text{If} (2 \cdot x_{fan,1}, 0, 0, 2 \cdot x_{fan} - 1) \quad (1-65)$$

The prediction by the model of the electrical consumption at part load is shown in Figure 1-15. It appeared that the best agreement was found for a fan operating all the time at its nominal volume flow rate ( $x_{fan}=1$ ), i.e. without control. However, we don't know how these points have been defined by the manufacturer.

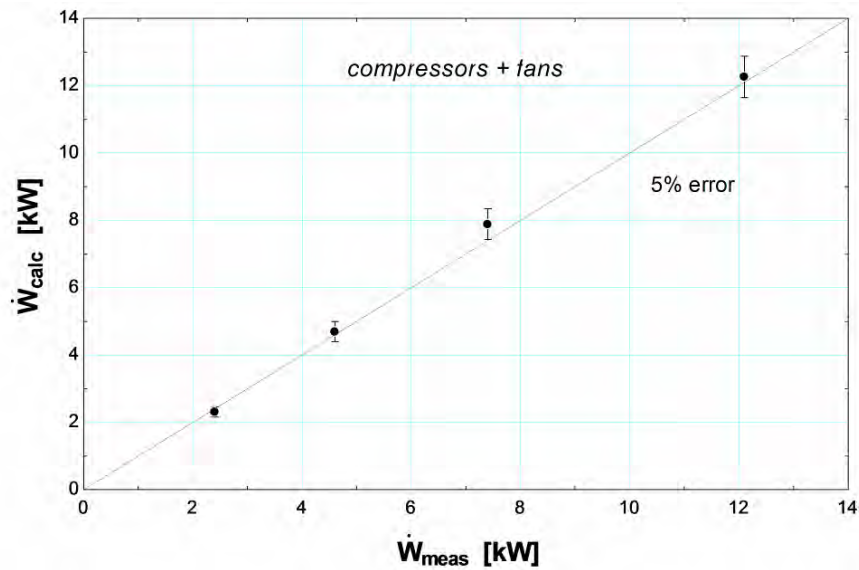


**Figure 1-15 Prediction by the model of the chiller total consumption (compressors + fans) at part load**

#### 1.2.4 Influence of glycol concentration on the performances

Chiller capacity is reduced when glycol is added in the water. This is taken into account in the model by re-identifying the water-side nominal resistance in the evaporator model, in order to get the capacity reduction given in Table 1-5. The model is not able to reproduce the power increase given in this table. The information diagram associated to the re-identification process is given in Figure 1-16.

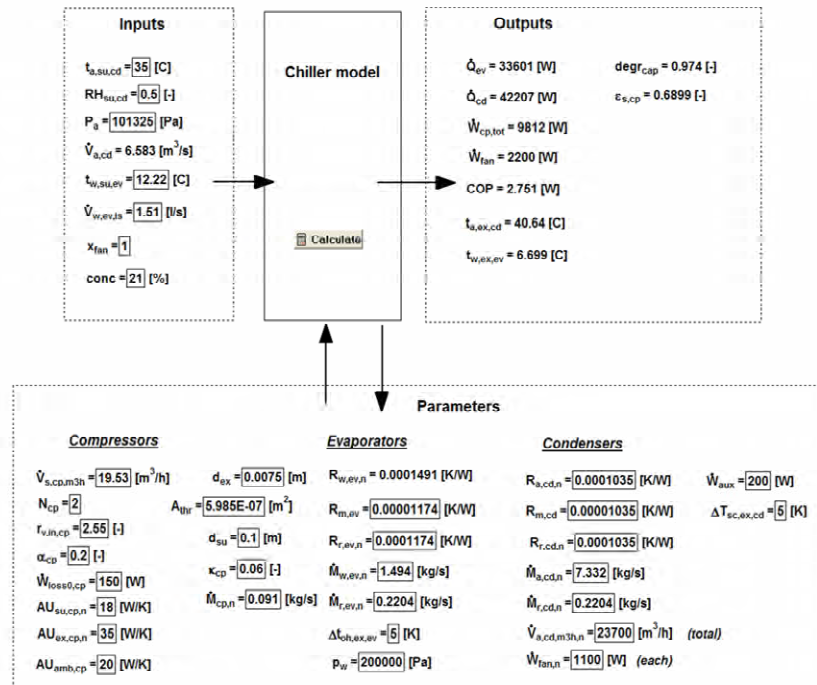


Figure 1-16 Information diagram of the chiller model for the re-identification of the water-side nominal resistance

### 1.3 Simulation results analysis

No comparative tests were done for the chiller exercise, but only two empirical tests. The analysis presented here is conducted in a chronological way: improvements of the modeling have been proposed following a first analysis of the results, what has lead to new simulations and new analyses.

First of all, results related to the *empirical test I* (and presented in the main report) are analyzed. Then, a thorough inspection of all available *measurements* is carried out in order to better understand the behavior of the chiller and improve its modeling.

#### 1.3.1 Analysis of empirical test I

##### 1.3.1.1 Perfect control of the chiller, but without fan control

The chiller model presented hereunder assumes that the control is perfect and doesn't account for any dynamics. Accordingly, the set point on the leaving water temperature is always achieved (provided that the chiller has enough capacity). As shown in the main report, the measured leaving water temperature differs widely from the set point. This is not a good frame of comparison for evaluating the capacity of the model to predict the chiller electrical consumption. The simulation is rerun with the measured leaving water temperature as an input of the model (instead of the set point of 5.56°C), which means that the capacity of the chiller is imposed. Here also, the control of the fans is not introduced, which means they are working at their maximum volume flow rate (23700 m<sup>3</sup>/h, i.e.  $x_{fan} = 1$ ).

The time evolution (over seven days) of the chiller total electrical consumption (CEP) is shown in Figure 1-17. It can be observed that the model is able to detect when one or two

compressors are working. However, the highest electrical consumptions (where two compressors are working) are still widely underestimated. This could be due to a bad prediction of the condensing pressure.

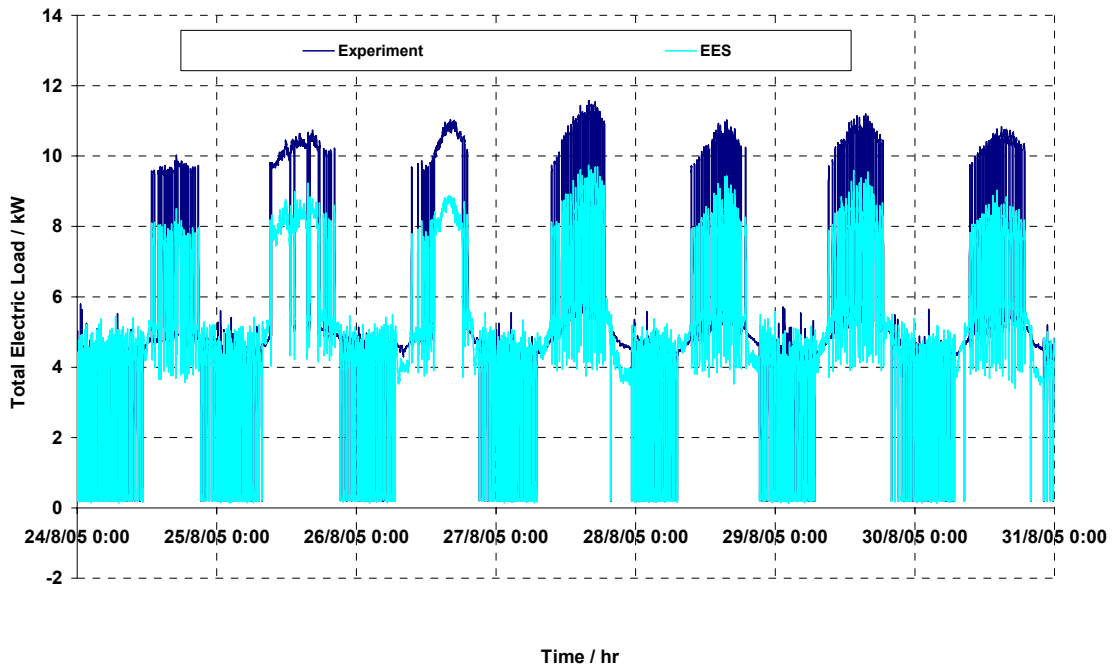


**Figure 1-17 Chiller Empirical Test I –Chiller Electric Load (the leaving water temperature is imposed)**

The averaged daily chiller electrical consumption is shown in Figure 1-18. As shown in Figure 1-17, the model is not able to predict the highest electrical consumptions.

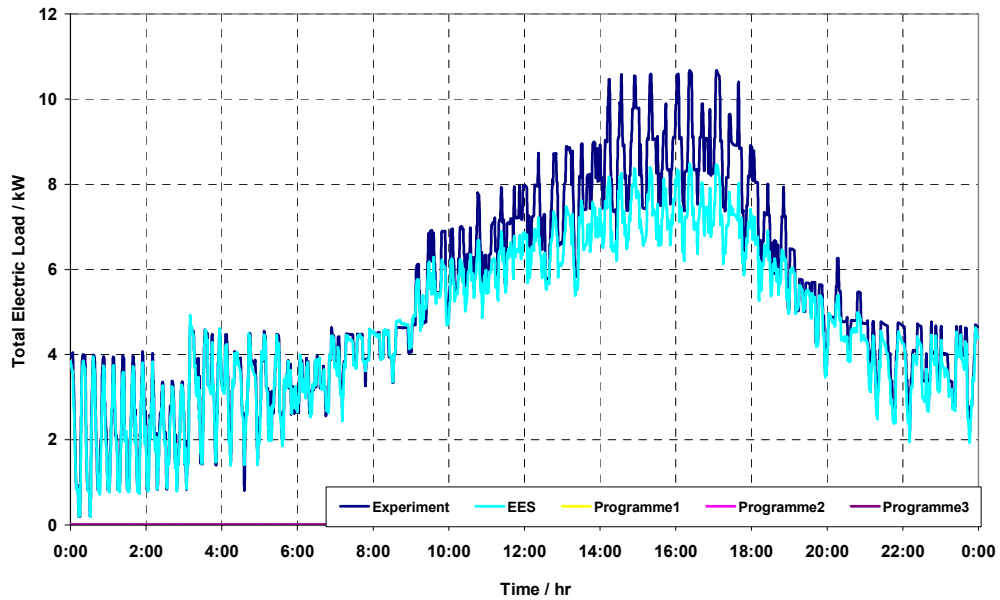


**Figure 1-18 Chiller Empirical Test I – Averaged Daily Chiller Electric Load (the leaving water temperature is imposed)**

However, this doesn't seem to be critical for long-term simulation: Figure 1-19 shows that the chillers energy consumption (integration of the chiller power consumption over the seven days of the simulation) predicted by the model only differs by 9% from the measured one (0.80 MWh against 0.88 MWh). In this figure, the small difference between the thermal energy predicted by the model and the measured one is only due to the fact that the two calculations are not based on the same entering water temperature (difference of 0.025K).

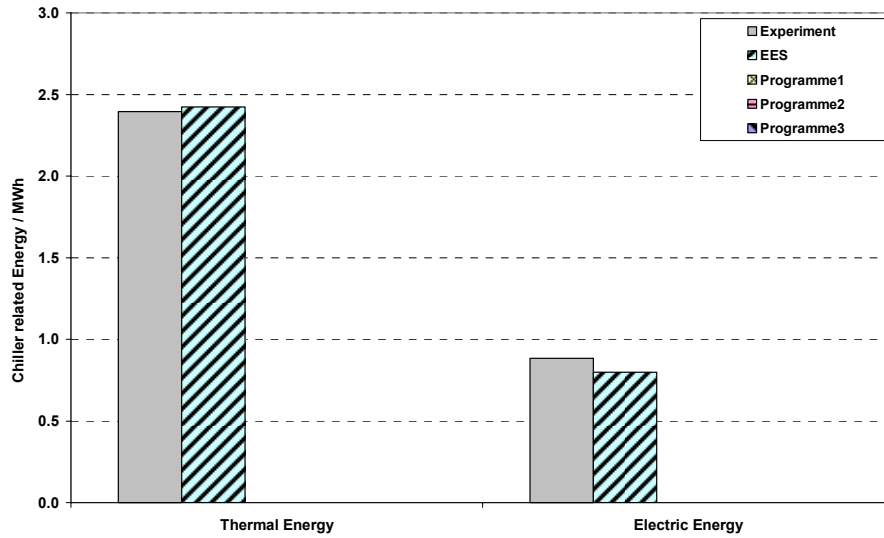


**Figure 1-19 Empirical Test I – Chiller Total Thermal and Electric Energy (the leaving water temperature is imposed)**

The time evolution of the condenser air leaving temperature is shown in Figure 1-20. Having imposed the measured leaving water temperature as an input of the model hasn't strongly modified the calculated temperature profile: the model still under-predicts the leaving air temperature.

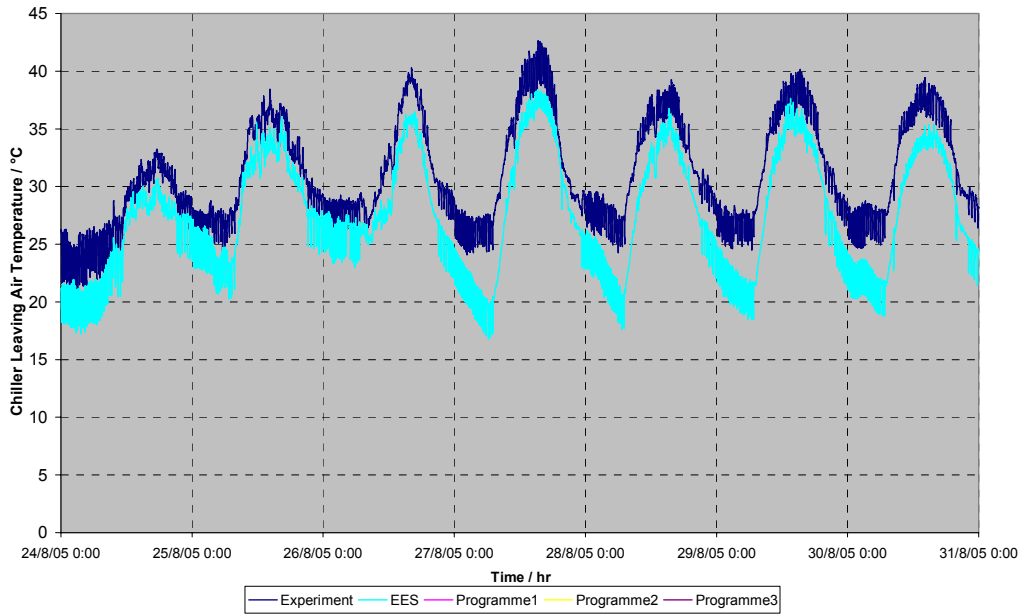


**Figure 1-20 Chiller Empirical Test I –Leaving Air Temperature (Condenser side) (the leaving water temperature is imposed)**

Figure 1-21 shows the error on the prediction of the condenser air leaving temperature as a function of the condenser entering air temperature. One general trend appears: the absolute error increases as the entering temperature decreases. In this simulation, the control of the fan was not represented (the air volume low rate at the condenser exhaust is constant and equal to the nominal value, i.e. 23700 m<sup>3</sup>/h for the two fans). However, Figure 1-21 makes appear that the control of the fans should probably have been introduced, since this control imposes a decrease in the air flow rate when the entering air temperature decreases. This conclusion could seem contradictory with what was said regarding Figure 1-15 (§1.3). However, performance points in Figure 1-15 are given by the manufacturer without any indication on the fan control.

Fan control is introduced hereafter (§1.3.1.2).

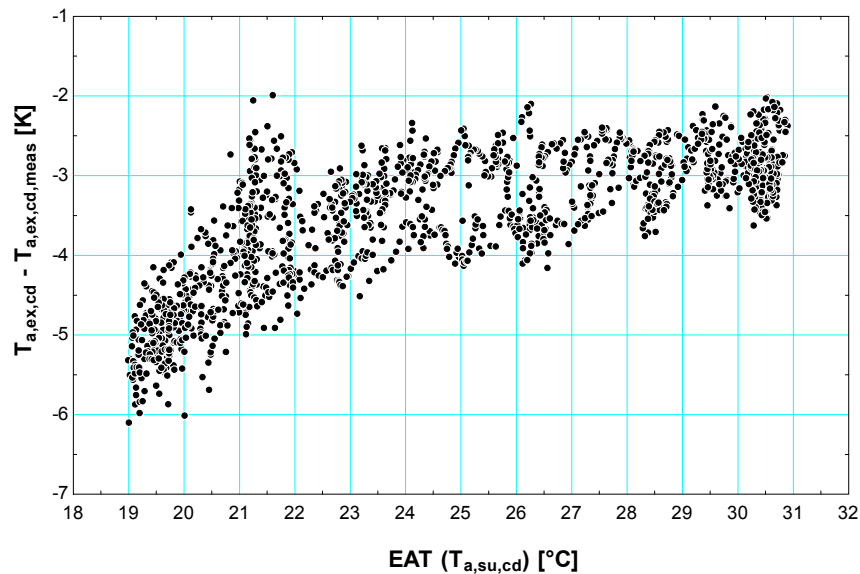


**Figure 1-21 Error on the prediction of the condenser leaving temperature as a function of the condenser entering temperature**

### 1.3.1.2 Perfect control of the chiller with fan control

In this simulation, the control of the fan described by equations (1-54) to (1-60) is introduced. Hypothetical values of the gain and the condensing temperature set point are roughly identified by comparing prediction by the model and measurements for the leaving air temperatures for a few points.

$$\text{gain} = \frac{1}{28}$$

$$t_{\text{cd,set}} = 26$$

The time evolution of the condenser air leaving temperature is shown in Figure 1-22. By introducing the control, higher leaving air temperatures are better predicted. However, large discrepancies appear for the low temperatures. These large oscillations correspond to the chiller working with only one cycling compressor: when the latter is OFF, the model assumes that the condenser exhaust air temperature is equal to the supply air temperature. Hence, the oscillations would be damped if a thermal mass was introduced in the condenser model. Not considering the oscillations, the agreement has been improved by introducing the fan control (compared to Figure 1-20). However, parameters of the control model (gain, condensing temperature set point, nominal volume flow rate or number of working fans) may certainly be refined.

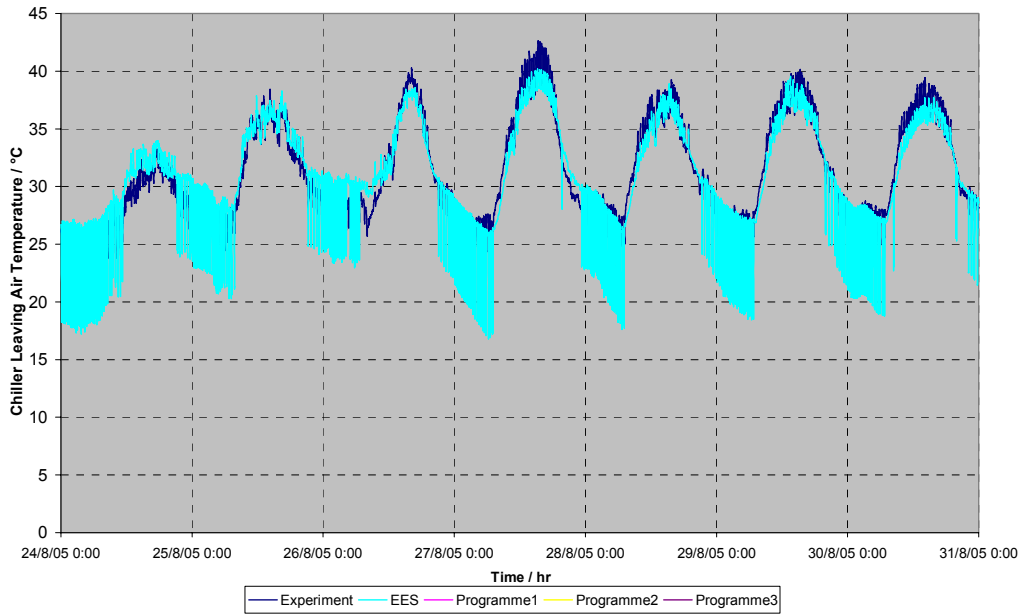


**Figure 1-22 Chiller Empirical Test I –Leaving Air Temperature (Condenser side) (the leaving water temperature is imposed and the control of the fan is introduced)**

Total chiller thermal and electrical energies associated to this simulation are shown in Figure 1-23. The model is unable to predict correctly the electrical consumption. This may be linked to a bad prediction of the condensing pressure and thus of the compressors consumption. This will be discussed in §1.3.2.

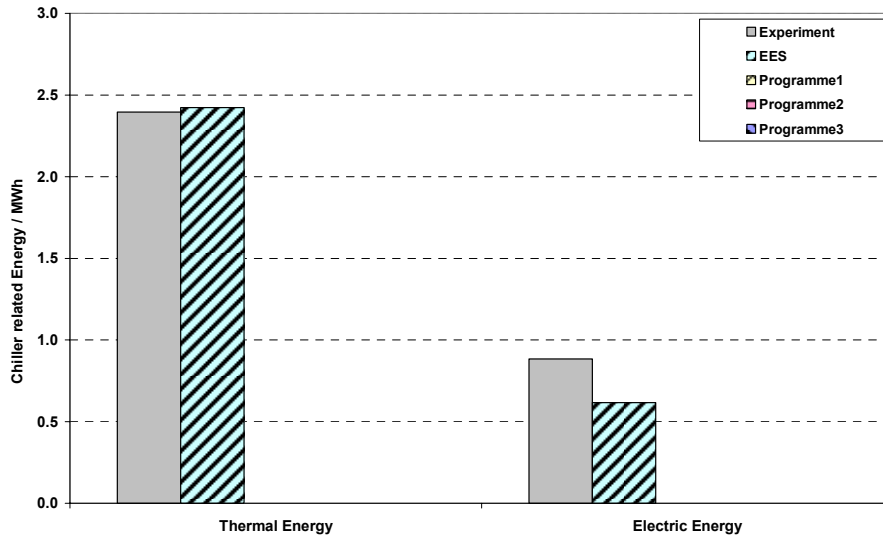


**Figure 1-23 Empirical Test I – Chiller Total Thermal and Electric Energy (the leaving water temperature is imposed and the control of the fan is introduced)**

### 1.3.1.3 Perfect control of the chiller without fan control but reduced air flow rate

In the simulation presented here, the leaving water temperature is still imposed as an input of the model. The fan control is not introduced, but the air flow rate is reduced from 23700 m<sup>3</sup>/h to 11850m<sup>3</sup>/h, as if only one fan was working ( $x_{fan}=0.5$ ). The comparison between the measured and calculated condenser exhaust air temperature is given in Figure 1-24. Not considering the large oscillations, it can be observed that the two curves diverge for the low temperatures (thus, the fan control should be re-introduced). However, the highest air temperatures are better predicted.

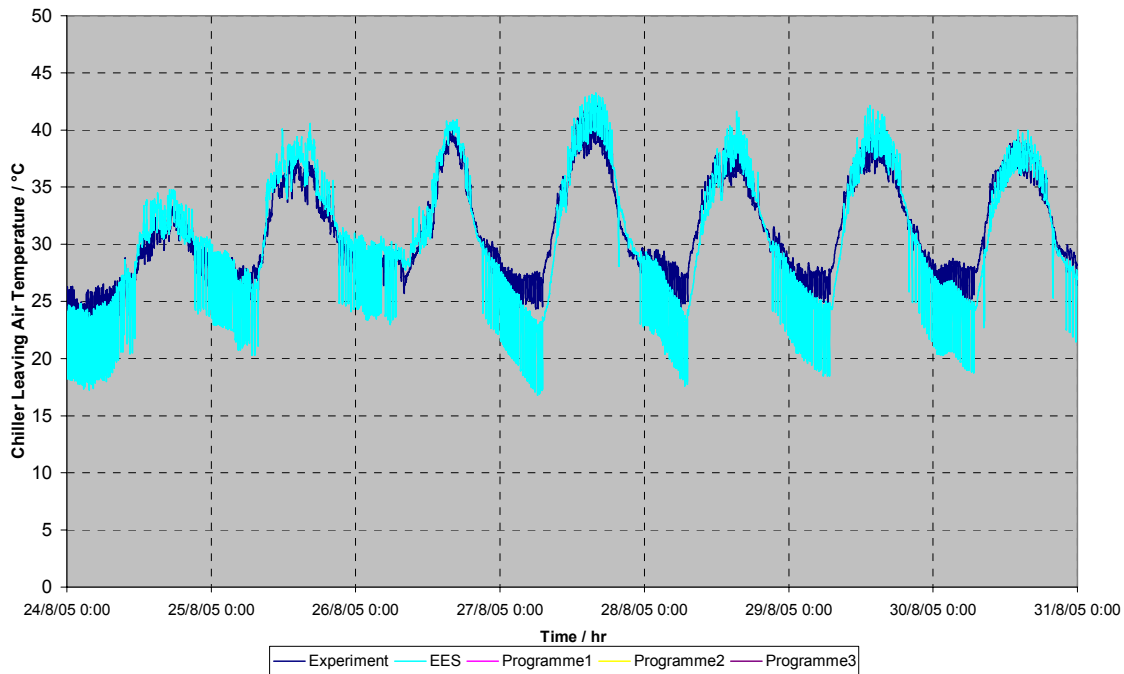


**Figure 1-24 Chiller Empirical Test I –Leaving Air Temperature (Condenser side) (the leaving water temperature is imposed and only one fan is working)**

Two remarks/assumptions can be drawn from the comparison of the results in § 1.3.1.1, 1.3.1.2 and 1.3.1.3:

1. the control of the fan should be introduced, and the parameters of the control modeling correctly refined;
2. it seems that only the varying-speed controlled fan is working, its rotation speed being reduced for lower entering air temperatures.

### 1.3.2 Analysis of the measurements

The philosophy of this exercise is to evaluate in which extent the model can predict the chiller performance when its parameters are identified only on the basis of manufacturer catalog data. However, detailed available measurements are here used as inputs of the chiller model in order to better understand its behavior and improve its modeling.

The following paragraphs are organized as follows:

- 1) From the measurements related to *Empirical Test I*, the *compressor model* is validated (§1.3.2.1).
- 2) From 18 almost stabilized points from *Empirical Test II*, some *parameters* of the chiller model are *refined* (§1.3.2.2).
- 3) The simulation of *Empirical Test I* is re-run with the refined parameters in order to validate the *chiller model* (§1.3.2.3).

### 1.3.2.1 Points from Empirical Test I

#### Compressor consumption

The compressors are “dissociated” from the heat exchangers by imposing the evaporating pressure, the condensing pressure and the number of working compressors as input of the simulation. The number of working compressors can be easily determined from the measurement of the chiller power consumption CEP (Figure 1-25).

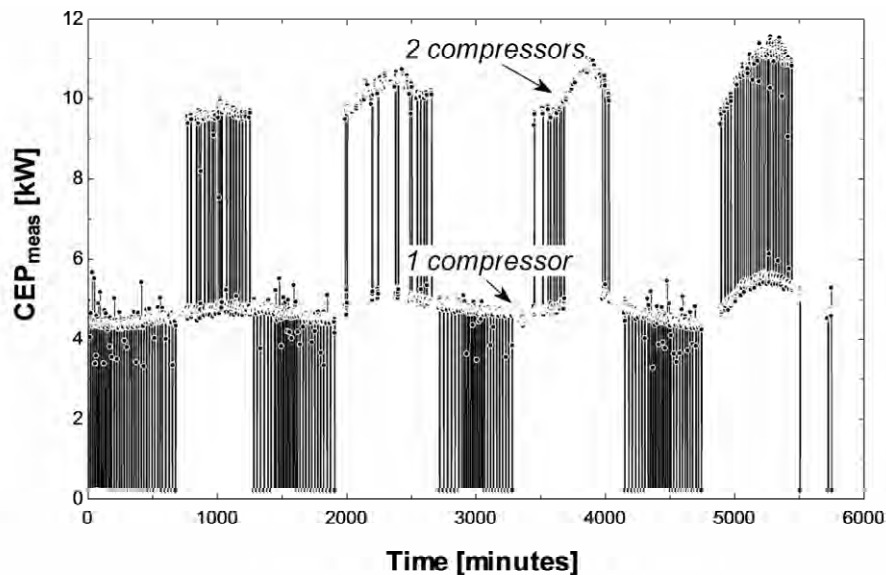


**Figure 1-25 Empirical Test I – Time evolution (minute by minute) of the measured chiller power consumption**

Figure 1-26 compares the time evolution of the computed and measured chiller power consumption (CEP). Figure 1-27 is a zoom on a detail of Figure 1-26. The chiller power consumption accounts for the auxiliaries, the fan and the compressors. The auxiliaries consumption can be identified from the experimental points where no compressors are working and is close to 200 W (what can be observed in the bottom of Figure 1-26). The fan consumption is imposed (equal to the measured value) (Figure 1-28). Accordingly, Figure 1-26 and Figure 1-27 indirectly show the capability of the model to predict the compressors’ consumption. It can be observed that the latter is predicted within 5%, and is slightly under-predicted. It can be due to pressures drops in the evaporator and the condenser (the supply pressure is lower than the evaporating pressure and the exhaust pressure is higher than the condensing pressure).

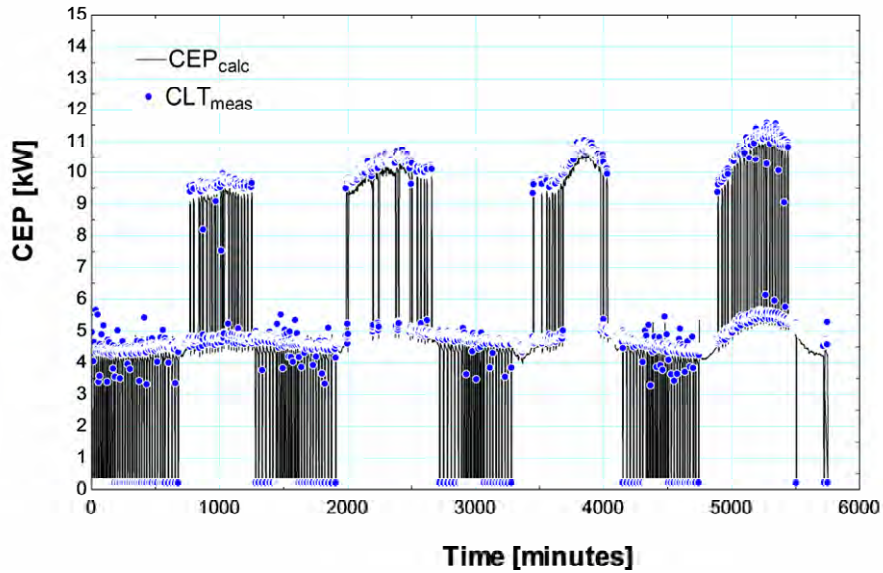


Figure 1-26 Empirical Test I – Time evolution (minute by minute) of the measured and calculated chiller power consumption

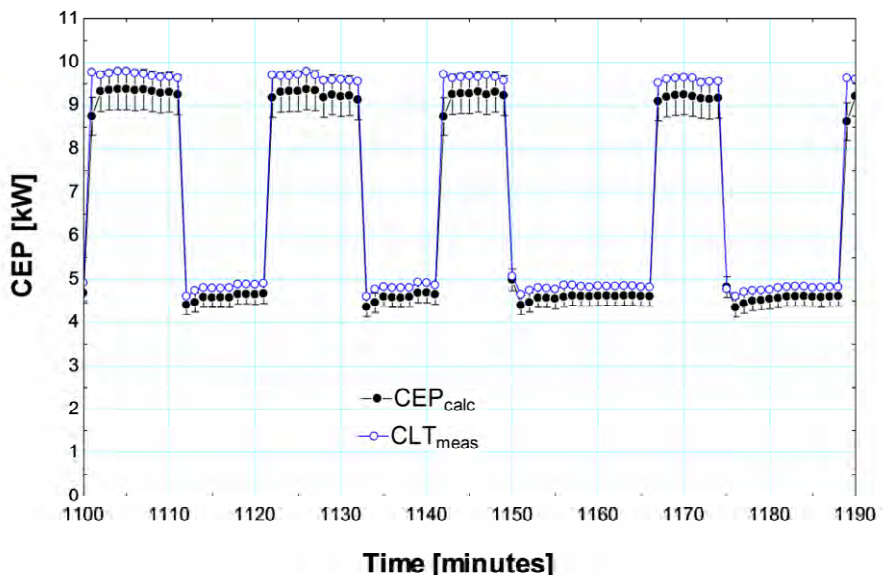


Figure 1-27 Empirical Test I – Time evolution (minute by minute) of the measured and calculated chiller power consumption (zoom): the error bars correspond to an error of 5%

In summary, the model of the compressor, with its parameters identified solely with catalogue data, is able to predict with a very good agreement the compressor consumption when the latter is integrated into a chiller model.

*Fan consumption*

In the *empirical test I*, only one fan is working (the one with the varying speed control). Its measured electrical consumption is given in Figure 1-28. This figure shows the fan

consumption as a function of the condensing pressure. For pressures higher than 1650 kPa, the fan seems to work at its maxing rotation speed, what corresponds to a consumption close to 1000 W (this value is close to the one identified in §1.2.2.2). For pressures lower than 1650 kPa, the fan reduces its speed, what yields a reduction of the electrical consumption.

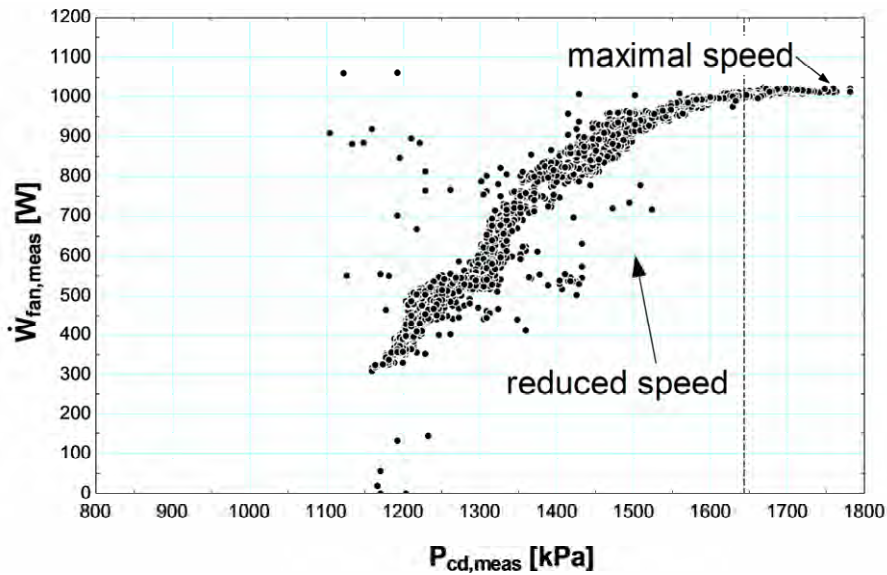


**Figure 1-28 Empirical Test I – Measured fan consumption versus measured condensing pressure**

### *Cooling capacity*

Figure 1-29 shows the time evolution of the measured supply (EWT) and exhaust (LWT) evaporator water temperatures. It can be observed that the cycling of the compressors creates very strong transient temperature profiles. Accordingly, the internal energy variation of the evaporator (associated to the combined thermal mass of the heat exchanger metal, refrigerant and water) cannot be neglected. The cooling capacity calculated on water side (on the basis of the water mass flow rate, evaporator supply and exhaust water temperatures) may diverge strongly from the cooling capacity calculated on the refrigerant side (on the basis of refrigerant flow rate, evaporating and condensing pressures and hypothetical subcooling and superheat). This is illustrated in Figure 1-30, which gives the calculated cooling capacity as a function of the measured cooling capacity.

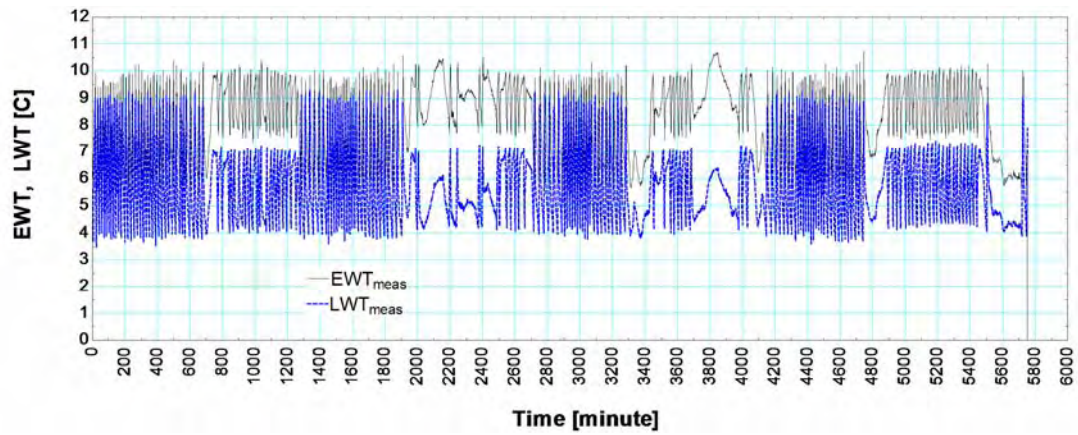


Figure 1-29 Empirical Test I – Time evolution of the measured entering and leaving water temperatures

From the temperature profile given in Figure 1-29, three points (average over a few minutes) in almost steady-state regime (such as period around time 2310) have been extracted and superposed on Figure 1-30. As expected, for these three points, the agreement between measured and predicted value of CLT is better, but not fully satisfactory.

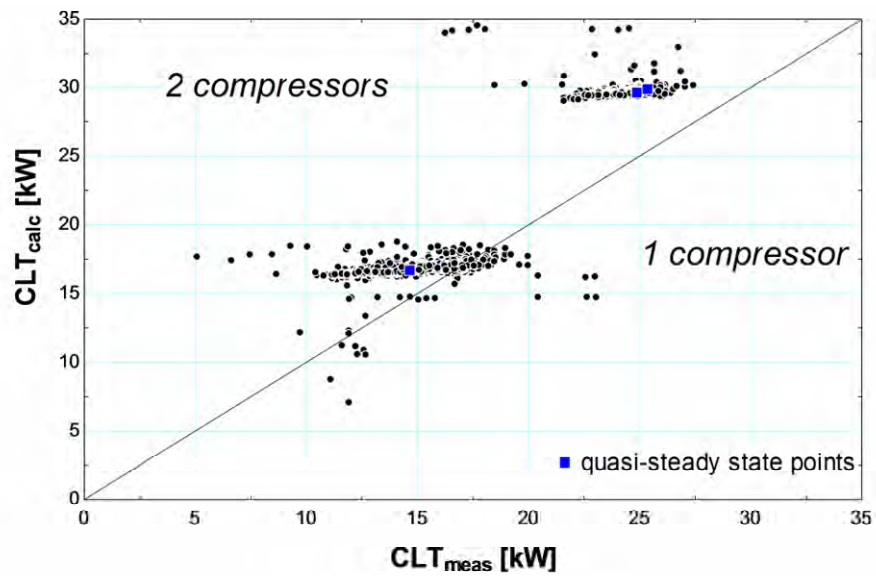


Figure 1-30 Empirical Test I – Prediction by the model of the cooling capacity

### 1.3.2.2 Quasi-steady state points extracted from Empirical Test II

Eighteen points in (assumed) almost reached steady-state regime have been extracted from the *Empirical Test II* measurement data.

#### Identification of the model parameters

Since the air flow rate through the condenser is not given, it has roughly been estimated on the basis of the heat balance on the condenser. The condensing power is the one predicted by

the model. The supply and exhaust air temperatures are part of the available measurements. The heat balance doesn't account for any internal energy variation term. From the estimated air mass flow rate, the volume flow rate and finally the fan control variable  $x_{fan}$  have been calculated. The evolution of the fan control variable with the difference between the condensing temperature and condensing temperature set point (arbitrarily set to 25°C) is shown in Figure 1-31. The general trend is the following: the fan control variable increases as the temperature difference increases and seems to be limited to a maximal value.

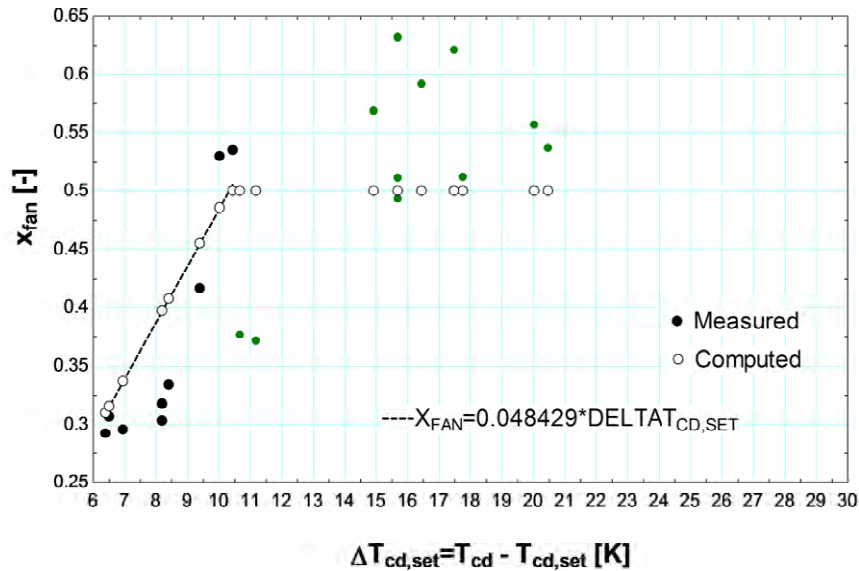


**Figure 1-31 Selection of points from Empirical Test II – Evolution of the fan control variable with the difference between the condensing temperature and condensing temperature set point (arbitrarily set to 25°C)**

This trend is the one described by the fan control model introduced previously (Equations (1-54) to (1-60)). From the points in the ascending part of the curve, a gain of 0.04829 1/K is identified. Prediction by the fan control model of the  $x_{fan}$  can be compared to measured  $x_{fan}$  in the same figure. (Remark: the nominal volume flow rate has been increased from 23700 m<sup>3</sup>/h to 28000 m<sup>3</sup>/h so that the maximal value of  $x_{fan}$  is 0.5, since, in this simulation, only one fan is in operation).

The resistances of the condenser and evaporator models are re-identified, using the Wilson Plot method (Wilson, 1915). This method is described in detail in § 4.2.2.2 (heating coils). Identified resistances are only roughly identified, because of the uncertainty on the evaporating and condensing powers. For example, the Wilson plot method applied to the evaporator is shown in Figure 1-32. This figure shows the evolution of the identified overall heat transfer resistance with the refrigerant mass flow rate exponent (-0.8). The water mass flow rate is constant. From the shift and the slope of the linear curve fit, the refrigerant side resistance and the combined water/metal resistance can be estimated.

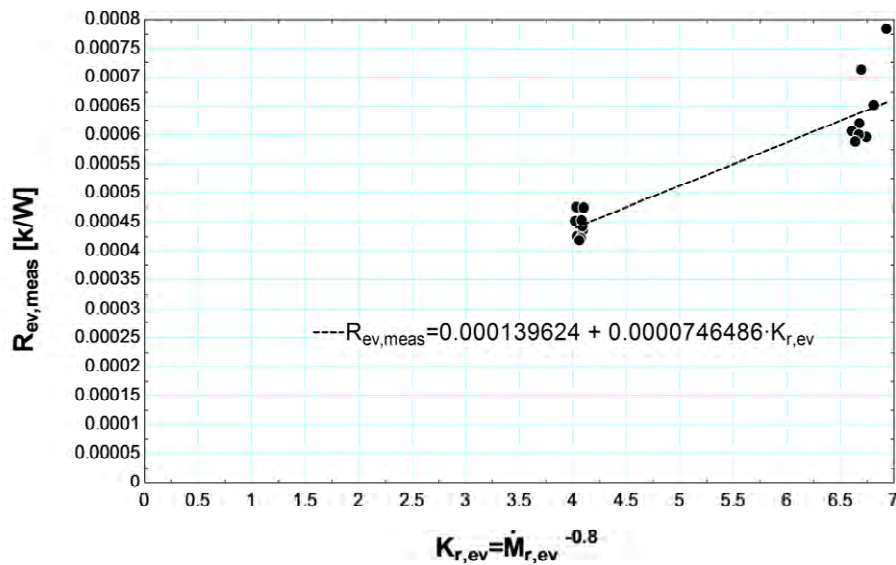


**Figure 1-32 Selection of points from Empirical Test II – Wilson plot method applied to the evaporator**

A relationship between the measured fan electrical consumption and the evaluated air volume flow rate should be identified. As shown in Figure 1-33, the fan consumption seems to vary linearly with the air volume flow rate. Two groups of points can be distinguished, according to the number of working compressors (1 or 2). This doesn't make any sense and is probably due to inaccuracy inherent to the air flow rate identification method. However, a linear relationship is introduced in the modeling to compute the fan consumption. The constant term and the slope of this relationship are the mean values from the two curve fits in Figure 1-33:

$$\begin{aligned} \dot{W}_{fan} &= \dot{W}_{fan,0} + \alpha_{fan} \cdot \dot{V}_{a,cd} \\ \dot{W}_{fan,0} &= 306 \\ \alpha_{fan} &= 132.5 \end{aligned}$$

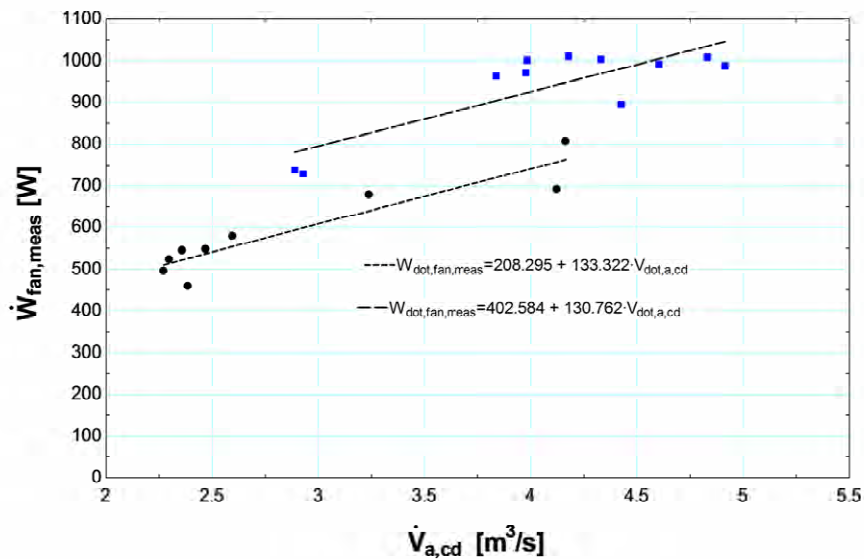


Figure 1-33 Selection of points from Empirical Test II – Evolution of the measured fan consumption with the evaluated (not measured!) air volume flow rate

### Simulation

The model is here run over the 18 points, with the parameters identified in the previous section. All the identified parameters are summarized in Figure 1-34.

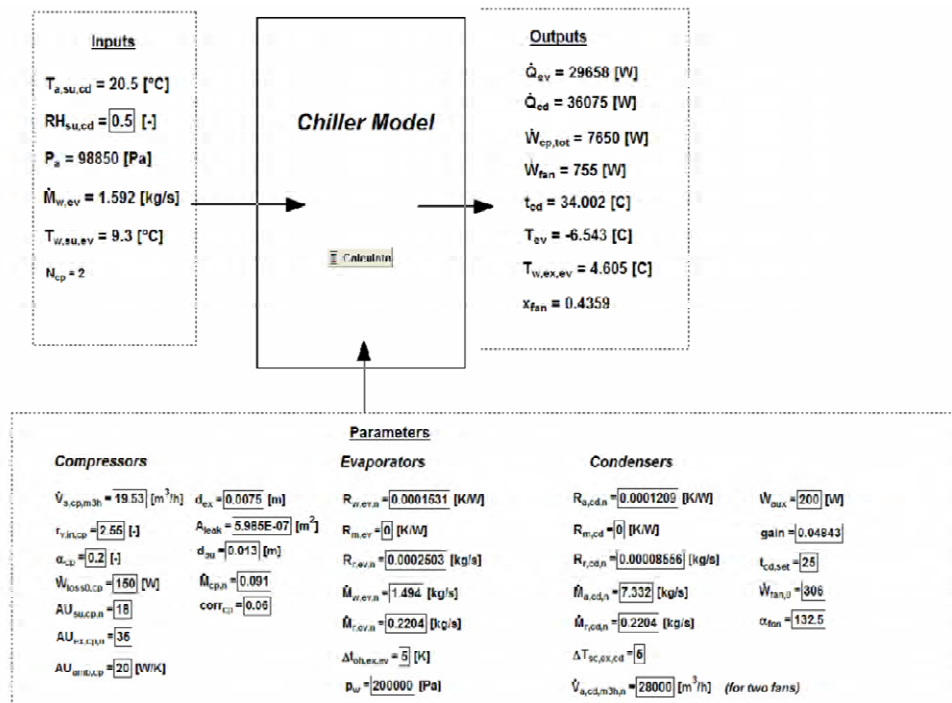


Figure 1-34 Selection of points from Empirical Test II – Information diagram of the chiller model: parameters identified in the previous section

Figure 1-35 and Figure 1-36 show that the evaporating and condensing pressure are predicted within 5%.

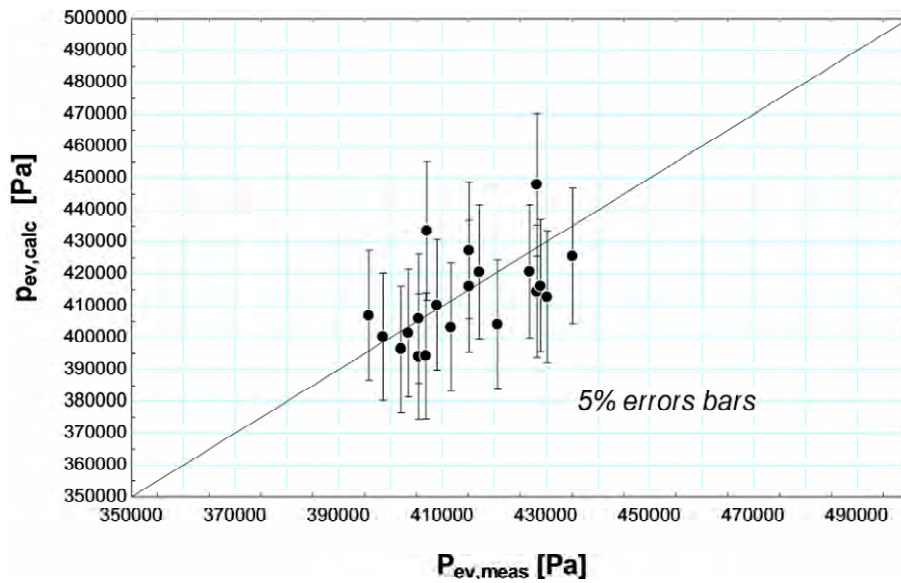


Figure 1-35 Selection of points from Empirical Test II – Prediction by the model of the evaporating pressure

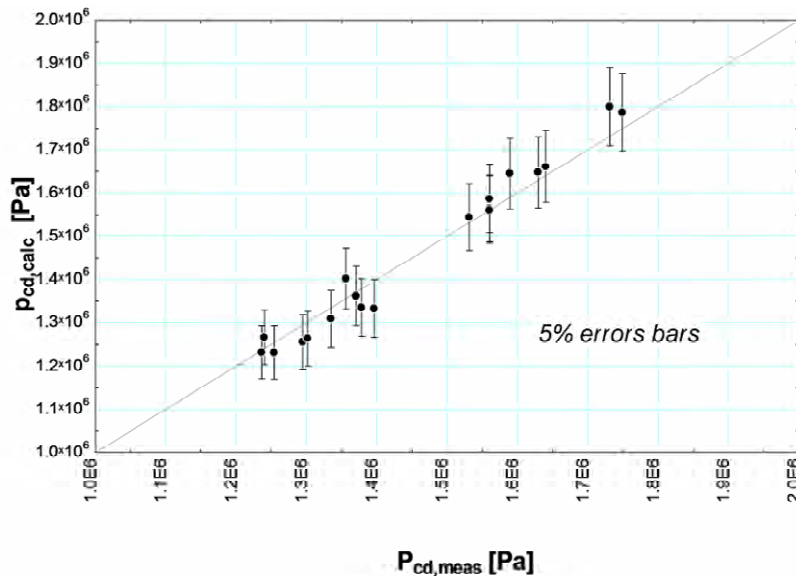
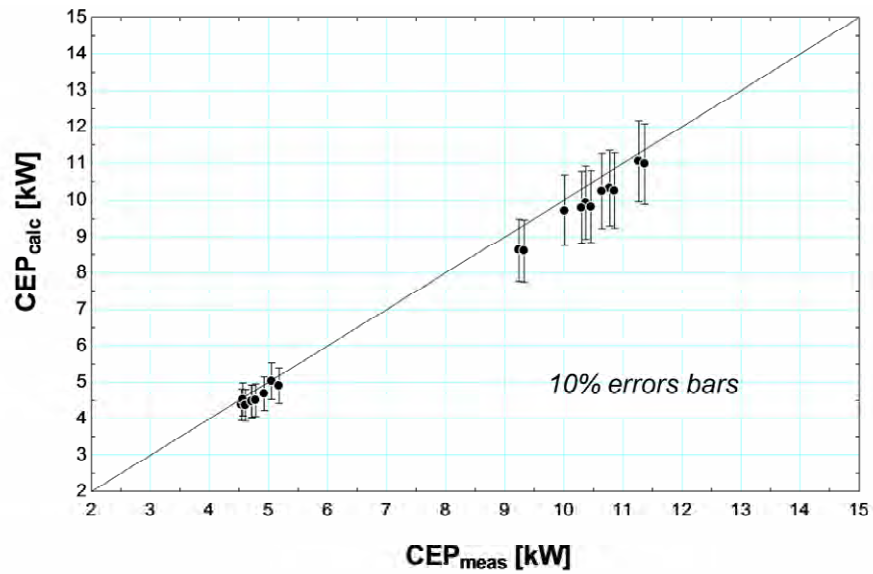


Figure 1-36 Selection of points from Empirical Test II – Prediction by the model of the condensing pressure

Figure 1-37 shows that the chiller total electrical consumption is predicted within 10%.



**Figure 1-37 Selection of points from Empirical Test II – Prediction by the model of the chiller electrical consumption**

*1.3.2.3 Simulation of Empirical Test I with parameters identified in §1.3.2.2*

The Empirical Test I simulation is rerun with parameters identified in §1.3.2.2. Main results are presented hereunder. The number of working compressors is imposed, instead of imposing the temperature set point at the chiller exhaust.

*Leaving air temperature*

Figure 1-38 and Figure 1-39 compare the time-evolutions of the predicted and measured condenser exhaust air temperature. Compared to previous simulations, it can be observed that the agreement is much better. For the lower air temperatures (1 compressor is working), the large oscillations are still due to the fact that the condenser model does not include any thermal mass. Hence, in the simulation, the exhaust condenser air temperature is equal to the supply air temperature when the compressor is OFF.

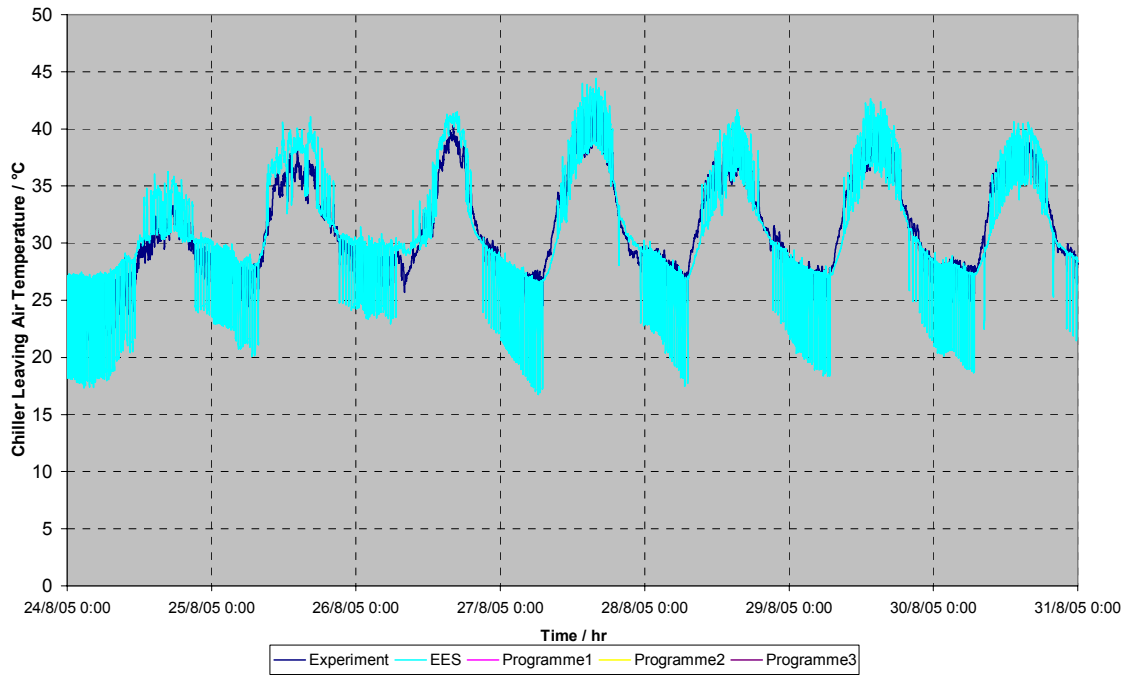


**Figure 1-38 Chiller Empirical Test I –Leaving Air Temperature (Condenser side) (the number of working compressors is imposed)**

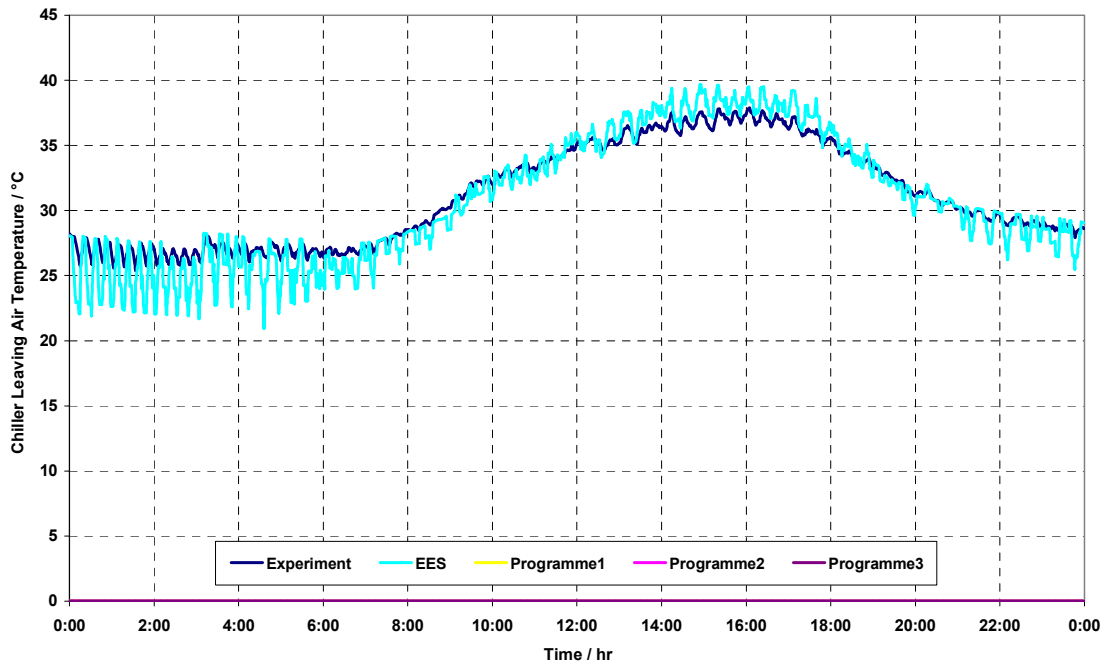


**Figure 1-39 Chiller Empirical Test I – Averaged Daily Leaving Air Temperature (the number of working compressors is imposed)**

The time evolutions of the predicted and measured averaged daily evaporator exhaust water temperature are compared in Figure 1-40. Here also, the bigger oscillations are due to the fact the evaporator model does not include any thermal mass. However, it seems that the model

systematically under-predicts the exhaust temperature. The evaporator model should probably be made more accurate by better identifying its parameters (the three thermal resistances).

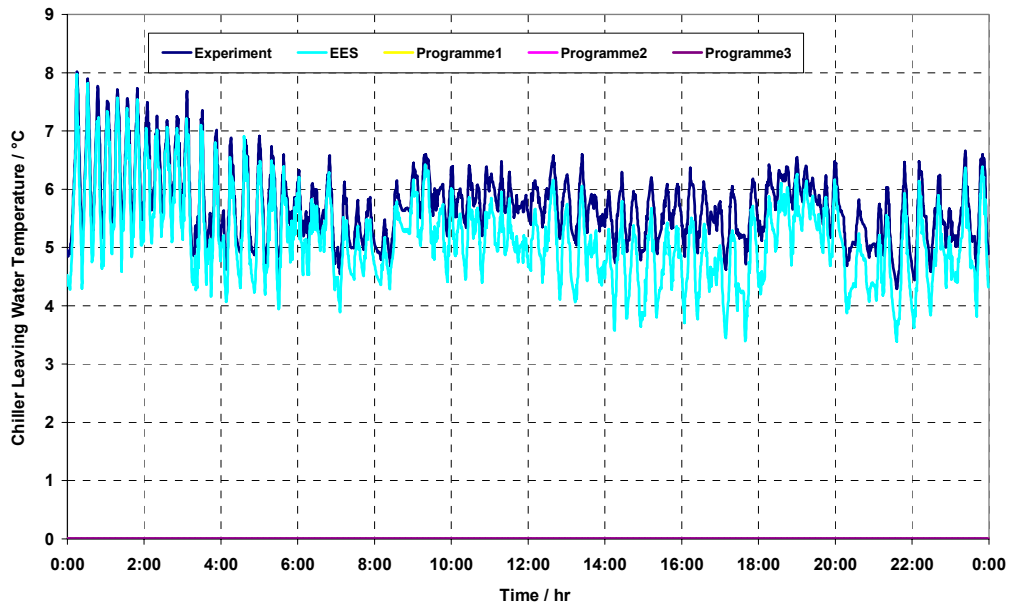


**Figure 1-40 Chiller Empirical Test I – Averaged Daily Leaving Water Temperature (the number of working compressors is imposed)**

The time-evolutions of the predicted and measured total electrical consumptions are compared in Figure 1-41 and Figure 1-42. It can be observed that agreement is very good.

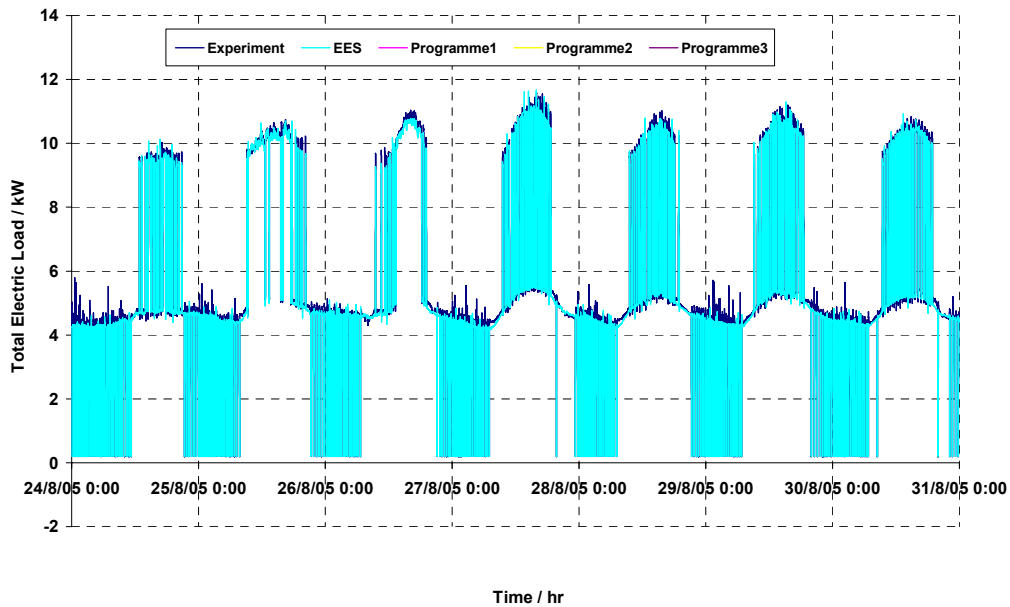


**Figure 1-41 Chiller Empirical Test I – Total chiller electrical consumption (the number of working compressors is imposed)**

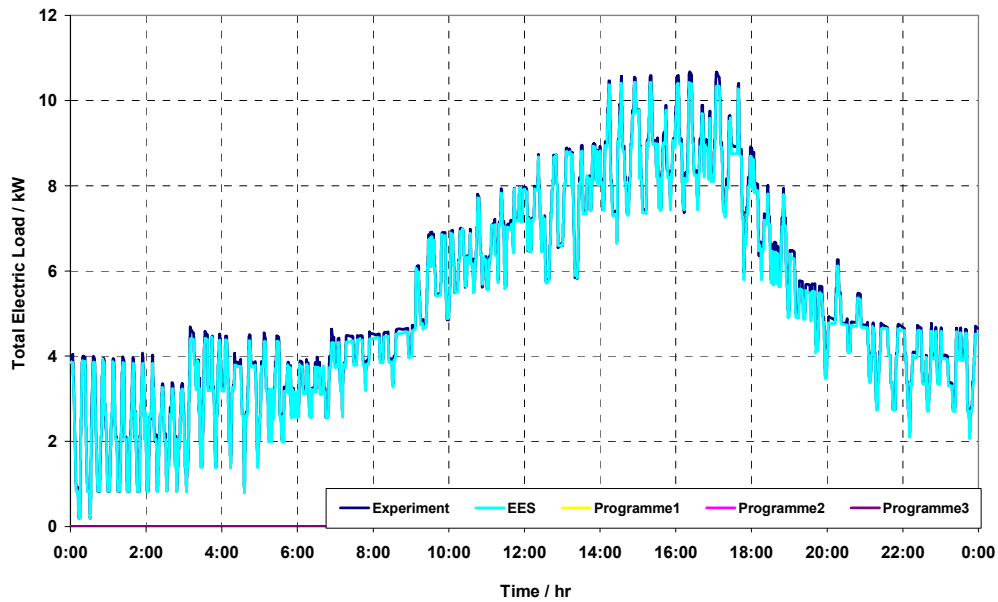


**Figure 1-42 Chiller Empirical Test I – Averaged daily total electrical consumption (the number of working compressors is imposed)**

The thermal and electrical total energies (integration of the cooling capacity and chiller consumption over the entire simulation period) predicted and measured are compared in Figure 1-43. The total electrical energy is predicted within 1.1% (0.87 MWh against 0.88 MWh). However, the predicted thermal energy is 21% higher than the measured one (2.98MWh against 2.40 MWh). As mentioned previously, the evaporator model should probably be largely improved by identifying better the thermal resistances.

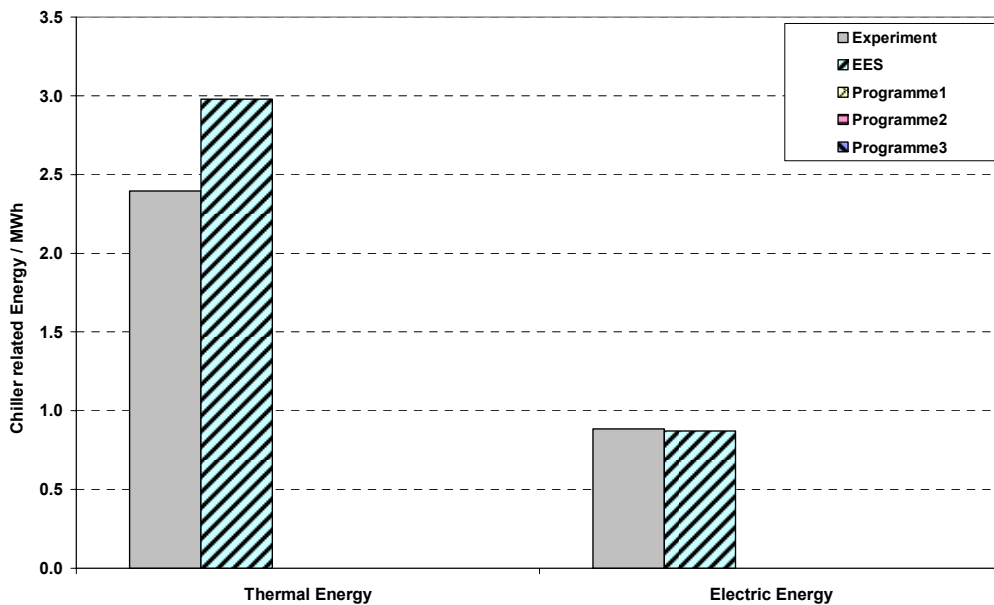


**Figure 1-43 Empirical Test I – Chiller Total Thermal and Electrical Energies (the number of working compressors is imposed)**

## 2 Cooling coil

### 2.1 Description of the model

This cooling coil model is based on a model previously proposed and partially validated by Lebrun et al. (1990). This model treats the cooling coil as a one-zone counter-flow heat exchanger. Fully dry and fully wet regimes are described simultaneously and the regime to be considered is the one leading to the maximal cooling capacity (Braun et al. 1989).

$$\dot{Q}_{\text{coil}} = \mathbf{Max} (\dot{Q}_{\text{coil,dry}}, \dot{Q}_{\text{coil,wet}}) \quad (2-1)$$

In both regimes, the overall heat transfer coefficient is calculated by considering three resistances in series: the convective resistance on the air side, the conduction resistance of the metal and the convective resistance on the refrigerant side. In dry regime, this gives:

$$\frac{1}{AU_{\text{coil,dry}}} = R_{\text{a,coil}} + R_{\text{m,coil}} + R_{\text{r,coil}} \quad (2-2)$$

The influence of the cooling coil geometry, which is not known “a priori”, is lumped into the thermal resistances on the refrigerant and on the air sides. The model accounts for the influence of the refrigerant properties on the refrigerant-side resistance. The approach is similar to the one introduced by Jin and Spitler (2002) in their water-water heat pump.

By assuming, on each side, a correlation of the type

$$Nu = C Re^m Pr^n \quad (2-3)$$

the heat transfer coefficient can be expressed by

$$h = C^* \dot{M}^m K^* \quad (2-4)$$

where

$$K^* = \mu^{n-m} k^{1-n} c^n \quad (2-5)$$

To define the exponent  $m$ , the internal and external flows are assumed to be turbulent and laminar respectively. For the exponent  $n$ , a value of 0.3 is used. Figure 2-1 shows the values of the coefficient  $K^*$  for pure water and different aqueous solutions of ethylene glycol. According to these results, it is concluded that the thermal resistance on the refrigerant side must take into account the effect of the fluid properties, since the coefficient  $K^*$  varies significantly. Figure 2-1 shows also that the heat transfer coefficient is largely degraded when high ethylene glycol concentrations are used (by 70 % for an ethylene glycol concentration of 50% in mass).

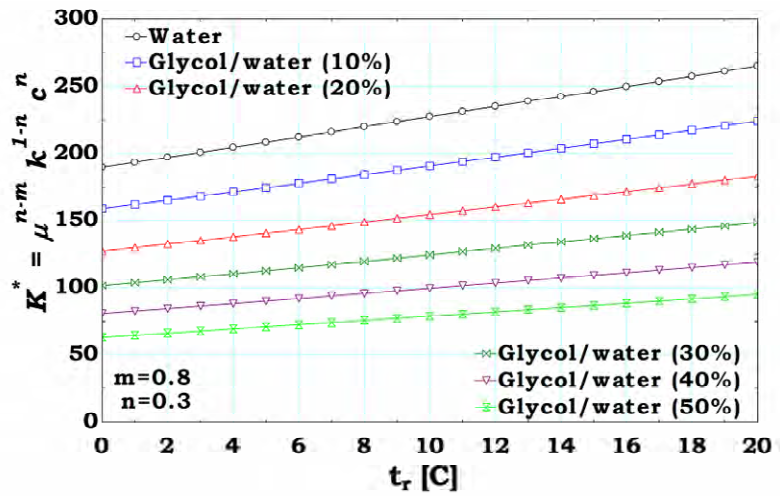


Figure 2-1 Variation of the coefficient  $K^*$  with the refrigerant temperature (Lemort et al., 2008)

Figure 2-2 shows that, on the air side, the thermal resistance could be calculated by taking only into account the effect of the air mass flow rate. The coefficient  $K^*$  is not very sensitive, neither to the air temperature nor to the air pressure.

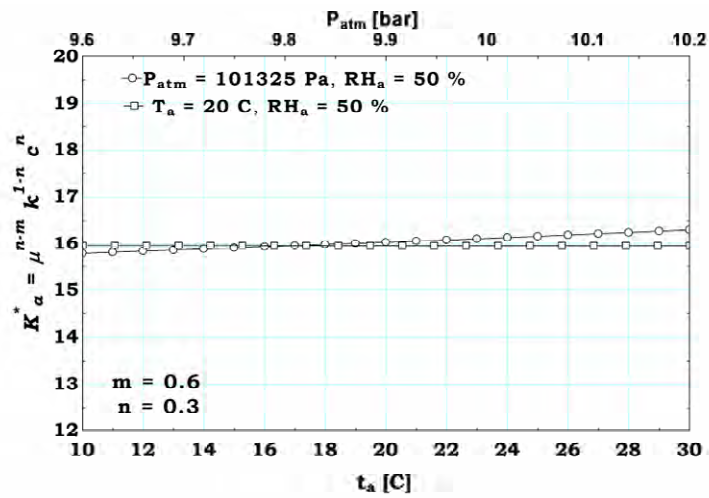


Figure 2-2 Variation of the coefficient  $K^*$  with the air temperature and pressure

Both thermal resistances are consequently defined as

$$R_{a,coil} = R_{a,coil,n} \cdot \left[ \frac{\dot{M}_{a,coil,n}}{\dot{M}_{a,coil}} \right]^{0.6} \quad (2-6)$$

$$R_{r,coil} = R_{r,coil,n} \cdot \frac{K_{r,n}^*}{K_r^*} \cdot \left[ \frac{\dot{M}_{r,coil,n}}{\dot{M}_{r,coil}} \right]^{0.8} \quad (2-7)$$

Where  $R_{a,coil,n}$  and  $R_{r,coil,n}$  are the parameters of the model, which must be identified on the basis of experimental results or of catalogue data.  $\dot{M}_{a,coil,n}$ ,  $\dot{M}_{r,coil,n}$ ,  $K_{r,n}^*$  are constant parameters, imposed by the choice of the nominal point.

In dry regime, the cooling coil capacity is given by Equation (2-8), involving the humid inlet air and refrigerant temperatures. The cooling coil effectiveness  $\varepsilon_{coil,dry}$  is expressed as a function of the heat transfer coefficient  $AU_{coil,dry}$  by means of the classical  $\varepsilon$ -NTU method,

$$\dot{Q}_{coil,dry} = \varepsilon_{coil,dry} \cdot \dot{C}_{min,coil,dry} \cdot (t_{a,su,coil} - T_{r,su,coil}) \quad (2-8)$$

When the cooling coil works in wet regime, the air can be replaced by a fictitious perfect gas, whose enthalpy is fully defined by the actual wet bulb temperature. The air side thermal resistance and the total cooling power are defined by Equations (2-9) and (2-11) (Lebrun et al. 1990).

$$R_{af,coil} = R_{a,coil} \cdot \frac{C_{p,a,coil}}{C_{p,af,coil}} \quad (2-9)$$

with:

$$C_{p,a,f,coil} = \frac{h_{a,su,coil} - h_{a,ex,coil,wet}}{T_{wb,su,coil} - T_{wb,ex,coil,wet}} \quad (2-10)$$

$$\dot{Q}_{coil,wet} = \varepsilon_{coil,wet} \cdot \dot{C}_{min,coil,wet} \cdot (t_{wb,su,coil} - T_{r,su,coil}) \quad (2-11)$$

To determine the air state at the cooling coil exhaust in wet regime, a fictitious semi-isothermal heat exchanger is defined, according to the ASHRAE classical procedure (ASHRAE 2000). One of the two fluids supplying this heat exchanger is the air; the other one is a fictitious fluid of infinite capacity flow rate, whose uniform temperature is supposed to correspond to the average temperature of the external surface of the coil, also called “contact” temperature  $T_{c,coil,wet}$ . The “contact” effectiveness is defined by:

$$\varepsilon_{c,coil,wet} = 1 - \exp(-NTU_{c,coil,wet}) \quad (2-12)$$

$$NTU_{c,coil,wet} = \frac{1}{R_{a,coil} \cdot \dot{C}_{a,coil}} \quad (2-13)$$

Enthalpy and specific humidity of the air at the cooling coil exhaust can easily be defined through the following relationships:

$$h_{a,su,coil} - h_{a,ex,coil,wet} = \varepsilon_{c,coil,wet} \cdot (h_{a,su,coil} - h_{c,coil,wet}) \quad (2-14)$$

$$W_{su,coil} - W_{ex,coil,wet} = \varepsilon_{c,coil,wet} \cdot (W_{su,coil} - W_{c,coil,wet}) \quad (2-15)$$

where  $h_{c,coil,wet}$  and  $W_{c,coil,wet}$  correspond to the enthalpy and the specific humidity of saturated air at the coil contact temperature.

An information flow diagram of this cooling coil model is given in Figure 2-3. Some variables are considered as input values, whereas the output values are calculated by the model. Only three parameters have to be identified: the nominal values of the three thermal resistances. As mentioned before, the two nominal flow rates and the nominal coefficient  $K_{r,n}^*$  are imposed by the choice of the nominal point. Some other parameters have to be added in order to characterize the refrigerant: its density, its specific heat, its dynamic viscosity and its thermal conductivity.

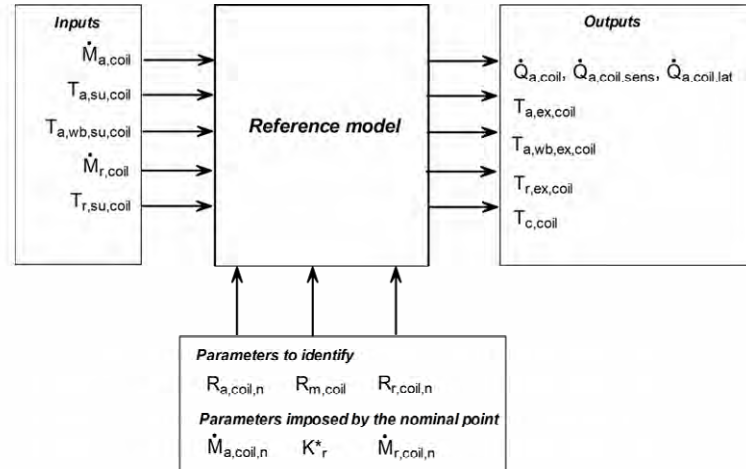


Figure 2-3 Information flow diagram of the cooling coil reference model

## 2.2 Parameters identification

### 2.2.1 “Nominal” point given by the manufacturer (*Comparative Test*)

#### 2.2.1.1 Consistency of the point

For the comparative test, only the nominal performance point given by the manufacturer can be used to identify the parameters of the model. This point is given in Table 2-1. In this table, data marked with \*) are calculated and are not part of the equipment data. This operating point is defined according to ARI-410. It is assumed that the cooling coil is fed with an aqueous solution of ethylene glycol 35% in mass (mean value of the range given by the ARI standard).

Table 2-1 Cooling coil performance data (Data marked with \* were calculated and are not part of the equipment submittal)

Cooling Coil Performance		
Barometric pressure*	kPa	101.3
Supply Air Temperature	°C Dry bulb	27.8

	°C Wet bulb	19.2
Supply Air Relative Humidity*	%	44.4
Supply Air Moisture*	kg/kg	0.0104
Exhaust Air Temperature	°C Dry bulb	12.5
	°C Wet bulb	12.2
Leaving Air Relative Humidity*	%	96.9
Leaving Air Moisture*	kg/kg	0.0087
Leaving Air Density	kg/m <sup>3</sup>	1.23
Volume Air Flow Rate at leaving air conditions *	m <sup>3</sup> /h	5430
Air Pressure Drop	kPa	0.194
Entering Liquid Temp.	°C	6.7
Leaving Liquid Temp.	°C	12.1
Liquid Flow	l/s	1.8
Liquid Pressure Drop	kPa	22.4
Total Cooling Power	kW	35.8
Latent Cooling Power*	kW	7.3

The *total cooling capacity* is calculated on the refrigerant side on the basis of the refrigerant flow rate and of the supply and exhaust temperatures:

$$\dot{Q}_{\text{coil}} = \dot{C}_{r,\text{coil}} \cdot (t_{r,\text{ex,coil}} - t_{r,\text{su,coil}}) \quad (2-16)$$

The refrigerant capacity flow rate is given by:

$$\dot{C}_{r,\text{coil}} = \dot{M}_{r,\text{coil}} \cdot c_{p,r,\text{coil}} \quad (2-17)$$

The refrigerant mass flow rate is expressed as a function of the refrigerant volume flow rate and refrigerant density (calculated at the inlet temperature) by:

$$\dot{M}_{r,\text{coil}} = \dot{V}_{r,\text{coil}} \cdot \rho_{r,\text{coil}} \quad (2-18)$$

A total capacity of 35813 W is calculated, which corresponds to the value given in Table 2-1. The values of the variables involved in this calculation are listed in Table 2-2.

**Table 2-2 Values of the variables involved in the total cooling capacity calculation**

---


$$\begin{aligned}
 M_{\dot{r}_{coil}} &= 1.866 \text{ [kg/s]} \\
 Q_{\dot{coil}} &= 35813 \text{ [W]} \\
 \rho_{r_{coil}} &= 1054 \text{ [kg/m}^3\text{]} \\
 t_{r_{ex}_{coil}} &= 12.1 \text{ [C]} \\
 t_{r_{su}_{coil}} &= 6.7 \text{ [C]} \\
 V_{\dot{r}_{coil}} &= 0.00177 \text{ [m}^3\text{/s]}
 \end{aligned}$$


---

The *air mass flow rate* is not given by the manufacturer. It is calculated on the basis of an air-side energy balance:

$$\dot{Q}_{a,coil,meas} = \dot{Q}_{coil} \quad (2-19)$$

$$\dot{Q}_{a,coil,meas} = \dot{M}_{a,coil} \cdot (h_{a,su,coil} - h_{a,ex,coil,meas}) \quad (2-20)$$

The supply and exhaust air specific enthalpies are calculated for humid air, with the pressure, and the dry- and wet-bulb temperatures:

$$h_{a,su,coil} = h('AirH2O', T_{a,su,coil}, P=P_{atm}, B_{a,wb,su,coil}) \quad (2-21)$$

$$h_{a,ex,coil,meas} = h('AirH2O', P=P_{atm}, B_{a,wb,ex,coil,meas}, T_{a,ex,coil,meas}) \quad (2-22)$$

The air mass flow rate is converted into exhaust volume flow rate by:

$$\dot{M}_{a,coil} = \dot{V}_{a,coil} \cdot \rho_{a,ex,coil,meas} \quad (2-23)$$

$$\rho_{a,ex,coil,meas} = \rho('AirH2O', T_{a,ex,coil}, P=P_{atm}, B_{a,wb,ex,coil,meas}) \quad (2-24)$$

$$\dot{V}_{a,coil,m3h} = \dot{V}_{a,coil} \cdot 3600 \quad (2-25)$$

The calculated air volume flow rate (5326 m<sup>3</sup>/h) only slightly differs from the value given in Table 2-1 (difference of 1.9%). This is probably due to differences in evaluation of humid air properties.

**Table 2-3 Values of the variables involved in the air flow rate calculation**

---


$$\begin{aligned}
 h_{a_{ex}_{coil}_{meas}} &= 34608 \text{ [J/kg]} \\
 h_{a_{su}_{coil}} &= 54474 \text{ [J/kg]} \\
 Q_{\dot{coil}} &= 35813 \text{ [W]} \\
 Q_{\dot{a}_{coil}_{meas}} &= 35813 \text{ [W]} \\
 \rho_{a_{ex}_{coil}_{meas}} &= 1.218 \text{ [kg/m}^3\text{]} \\
 t_{a_{ex}_{coil}_{meas}} &= 12.5 \text{ [C]} \\
 t_{a_{su}_{coil}} &= 27.8 \text{ [C]} \\
 t_{wb_{ex}_{coil}_{meas}} &= 12.2 \text{ [C]}
 \end{aligned}$$


---

---


$$\begin{aligned}
t_{wb,su,coil} &= 19.2 \text{ [C]} \\
\dot{V}_{a,coil} &= 1.48 \text{ [m}^3\text{/s]} \\
\dot{V}_{a,coil,m3h} &= 5326 \text{ [m}^3\text{/h]}
\end{aligned}$$


---

The *sensible* and *latent cooling powers* are calculated by:

$$\dot{Q}_{sens,coil,meas} = \dot{C}_{a,coil} \cdot (t_{a,su,coil} - t_{a,ex,coil,meas}) \quad (2-26)$$

$$\dot{Q}_{lat,coil,meas} = \dot{Q}_{a,coil,meas} - \dot{Q}_{sens,coil,meas} \quad (2-27)$$

The air capacity flow rate is given by:

$$\dot{C}_{a,coil} = \dot{M}_{a,coil} \cdot c_{p,a,coil} \quad (2-28)$$

$$c_{p,a,coil} = \mathbf{Cp} ('AirH2O', T = t_{a,su,coil}, P = P_{atm}, B = t_{wb,su,coil}) \quad (2-29)$$

A sensible cooling power of 28300 W and a latent cooling capacity of 7512 W are calculated. The latent power differs from 2.9% from the value given in Table 2-1. Values of the variables associated to this calculation are listed in Table 2-4.

**Table 2-4 Values of the variables involved in the sensible and latent cooling capacities calculation**

---


$$\begin{aligned}
c_{p,a,coil} &= 1026 \text{ [J/kg-K]} \\
\dot{C}_{a,coil} &= 1850 \text{ [W/K]} \\
P_{atm} &= 101300 \text{ [Pa]} \\
\dot{Q}_{a,coil,meas} &= 35813 \text{ [W]} \\
\dot{Q}_{lat,coil,meas} &= 7512 \text{ [W]} \\
\dot{Q}_{sens,coil,meas} &= 28300 \text{ [W]} \\
t_{a,ex,coil,meas} &= 12.5 \text{ [C]} \\
t_{a,su,coil} &= 27.8 \text{ [C]} \\
t_{wb,su,coil} &= 19.2 \text{ [C]}
\end{aligned}$$


---

Before attempting to identify the parameters of the model, it is recommended to *estimate the uncertainties* on the “measured” total, sensible and latent cooling capacities. No information is given about the accuracy of the values given in Table 2-1. With RTD temperature sensors, an absolute accuracy of  $\pm 0.1\text{K}$  can be expected. With a calibrated flow meter, an accuracy of 1% on the refrigerant flow rate measurement can be estimated. Results of the uncertainty propagation calculation are given in Table 2-5.

**Table 2-5 Estimated uncertainties on the measured total, sensible and latent cooling capacities**

$\dot{Q}_{coil}$ [W]	$35813 \pm 1003$	2.8%
$\dot{Q}_{sens,coil,meas}$ [W]	$28300 \pm 1022$	3.6%

$\dot{Q}_{lat,coil,meas}$ [W]	7512 ±679	9.0%
-------------------------------	-----------	------

### 2.2.1.2 Procedure for identifying the parameters

Since only one performance point is available, it is chosen to identify the parameters by imposing both the ratio between the air- and refrigerant-side resistances and the ratio between the metal and the air-side resistances. These two ratios are chosen according to good practice rules:

- The air-side resistance is supposed to be 10% higher than the refrigerant-side resistance. Actually, following a simple design rule, the resistances on both sides should be equal. The air-side resistance is usually reduced by using fins, so that it is closer to the refrigerant-side resistance.
- The metal resistance is fixed at 5% of the air-side resistance. Actually, the metal resistance is usually small. However, nominal performances of the coil sometimes account for some fouling in the refrigerant piping. This fouling fictitiously results in a higher (fictitious) metal resistance.

Results obtained by imposing these two resistances ratios are shown in Figure 2-4. The total cooling capacity is implicitly imposed since, the refrigerant flow rate, inlet and outlet temperature are imposed (“inputs”). The model calculates the outlet air dry-bulb and wet-bulb temperatures, and consequently the sensible and latent cooling capacities.

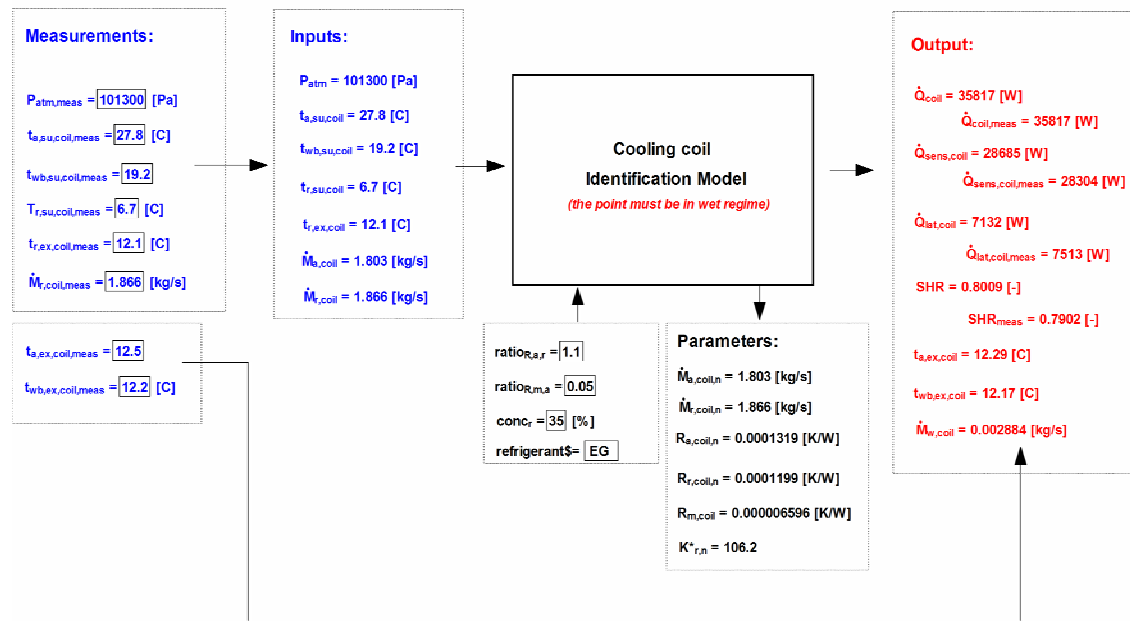


Figure 2-4 Identification of the parameters of the model on the basis of the nominal point (parameters used for the comparative tests)

The comparison between the values announced by the manufacturer and the values predicted by the model is detailed in Table 2-6. The agreement is within 1.3 % for the sensible cooling capacity. The exhaust air dry bulb temperature is predicted within 0.21K.

**Table 2-6 Agreement between measured and calculated values for the first identification process**

	<i>Manufacturer data</i>	<i>Prediction by the model</i>	<i>Error</i>
$t_{a,ex,coil}$ [°C]	12.5	12.29	0.21 K
$\dot{Q}_{sens,coil}$ [W]	28682	28300	1.3%

The sensitivity of the model to the air-refrigerant resistance ratio is also investigated. Figure 2-5 shows the evolutions of the calculated exhaust air temperature and the air-side resistance with the resistance ratio.

In order to reach the outlet air temperature announced by the manufacturer (12.5 C), a resistance ratio of 1.674 should be imposed; which corresponds to an air side resistance of 0.0001726 K/W and a refrigerant-side resistance of 0.0001031 K/W. This ratio is found to be high, with respect to values commonly identified.

However, this figure makes also appear that the values of the identified resistances are very sensitive to the exhaust air temperature; which means that the high identified resistance ratio of 1.674 could be due to inaccuracy of temperature measurements.

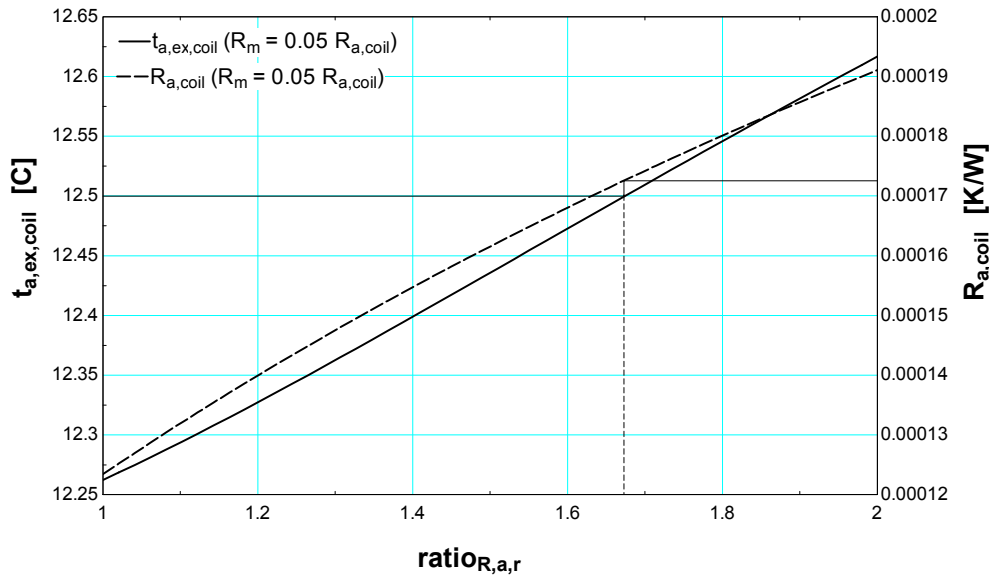


**Figure 2-5 Evolution of the calculated air outlet temperature and air-side convective resistance with the ratio of the air-side and refrigerant side resistances (the metal resistance is 5% of the air-side resistance)**

### 2.2.1.3 Concluding remarks

In conclusion, *theoretically*, there should be enough information for identifying the air side and the water side convective resistances provided that:

- the point corresponds to a wet regime,
- a guess value for the metal resistance is imposed.

*Practically*, such a tuning of the resistance can be very inaccurate, since it strongly depends on the accuracy of the temperature measurement.

If only *one* point is available to tune the model (as it is often the case in current practice), it is recommended:

- to keep an air-side resistance 5% to 10% higher than the refrigerant-side resistance,
- to fix the metal resistance at 5 to 10% of the air-side resistance.

This rule can be considered as a “good practice rule”, provided the sensible power is predicted within 5% of the value announced by the manufacturer.

Parameters identified with an air-refrigerant resistances ratio of 1.1 (see Figure 2-4) are considered for the comparatives tests.

### 2.2.2 Quasi steady-state points extracted from experimental data (empirical tests)

In addition to the nominal performance data of Table 2-1, which are from the manufacturer submittal, quasi-steady state points are extracted from the experimental data and can be used to calibrate the cooling coil model. Four points are extracted for the empirical test I and ten others for the empirical test II. These points are respectively given in Table 2-7 and Table 2-8.

For both empirical tests, experimental data of relative air humidity had to be compensated whereas air and water temperatures underlay small changes only. Compensation rules were found manually with regard to: air and water side energy balances, amount of condensation that was re-calculated from experimental data and compared to the measurements, accuracy of sensors.

**Table 2-7 Quasi-steady state points based on experimental data for empirical test I (Data marked with \* have been calculated and are not part of the recorded experimental data)**

Cooling Coil Performance I		#1	#2	#3	#4
Barometric pressure*	kPa	97.8	98.1	98.4	98.4
Entering Air Temp.	°C	22.2	22.5	22.9	23.4
Entering Air Relative Humidity*	%	51.2	50.3	68.5	65.0
Entering Air Moisture*	kg/kg	0.0088	0.0088	0.0120	0.0121

Leaving Air Temp.	°C	11.8	11.7	12.6	11.7
Leaving Air Relative Humidity*	%	96.3	96.3	100	100
Leaving Air Moisture*	kg/kg	0.0086	0.0085	0.0093	0.0088
Air Flow Rate at coil leaving air conditions*	m <sup>3</sup> /h	2910	3786	2834	3200
Entering Liquid Temp.	°C	4.60	6.27	7.15	4.74
Leaving Liquid Temp.	°C	12.14	10.95	11.05	9.10
Mixing Liquid Temp.	°C	6.34	8.72	9.81	8.44
Liquid Flow*	l/s	0.36	0.79	1.04	1.28
Total Cooling Capacity*	kW	10.91	15.02	16.32	22.24
Latent Cooling Capacity*	kW	0.55	0.92	6.61	9.25

### 2.2.2.1 Consistency of the points

Before attempting to use the points given in Table 2-7 and Table 2-8 for identifying the parameters of the cooling coil model, it is necessary to check their consistency. This is done here, by comparing the cooling capacities calculated on both sides (refrigerant- and air-sides). This comparison is shown in Figure 2-6. The agreement between the two heat balances is within 5%.

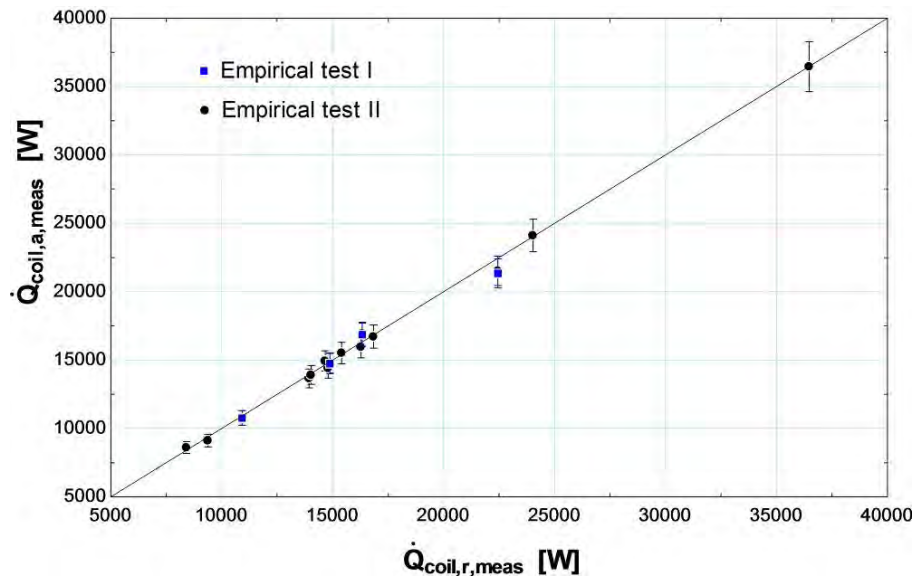


Figure 2-6 Comparison between the cooling capacities calculated on the air-side (y-axis) and on the refrigerant side (x-axis).

**Table 2-8 Quasi-steady state points based on experimental data for test II (Data marked with \*) have been calculated and are not part of the recorded experimental data)**

Cooling Coil Performance II		#1	#2	#3	#4	#5	#6	#7	#8	#9	#10
Barometric pressure*)	kPa	98.5	98.5	98.5	98.7	98.9	98.9	98.4	98.8	98.9	98.8
Entering Air Temp.	°C	22.9	22.9	26.4	27.5	23.2	19.0	27.9	28.0	23.6	23.5
Entering Air Relative Humidity*)	%	46.9	46.8	39.9	35.8	56.1	80.3	49.6	48.8	51.3	56.0
Entering Air Moisture*)	kg/kg	0.0084	0.0084	0.0088	0.0084	0.0102	0.0113	0.0120	0.0118	0.0095	0.0104
Leaving Air Temp.	°C	11.6	11.8	11.1	11.7	11.9	11.8	11.8	11.5	11.3	11.8
Leaving Air Relative Humidity*)	%	95.1	95.0	97.1	95	99.6	99.7	99.1	99.1	99.1	99.1
Leaving Air Moisture*)	kg/kg	0.0083	0.0084	0.0082	0.0084	0.0088	0.0088	0.0087	0.0086	0.0084	0.0087
Air Flow Rate at coil leaving air	m³/h	3997	3882	1513	1689	3211	3008	1709	1790	4725	3136

conditions*)											
Entering Liquid Temp.	°C	5.40	5.07	3.46	5.04	4.96	2.69	4.41	4.89	3.09	4.98
Leaving Liquid Temp.	°C	11.64	12.10	13.85	15.11	11.24	11.09	12.86	12.43	9.21	11.38
Mixing Liquid Temp.	°C	7.80	7.35	4.74	6.41	7.51	4.83	6.56	7.14	6.86	7.58
Liquid Flow*)	l/s	0.61	0.52	0.20	0.23	0.64	0.41	0.41	0.48	0.97	0.65
Total Cooling Capacity*)	kW	15.4	14.6	8.4	9.0	16.2	13.7	14.1	14.8	24.0	16.9
Latent Cooling Capacity*)	kW	0.3	0.1	0.7	0.0	3.9	6.4	4.7	4.8	4.3	4.4

### 2.2.2.2 Identified parameters

First of all, the cooling power predicted by the model, with the parameters identified on the basis of the nominal point (see Figure 2-4), is compared to the measured cooling capacity. This comparison is shown in Figure 2-7. It appears that the model is not able to predict the cooling capacity (for the considered parameters). The discrepancy between the calculated and the measured values increase as the cooling capacity increase.

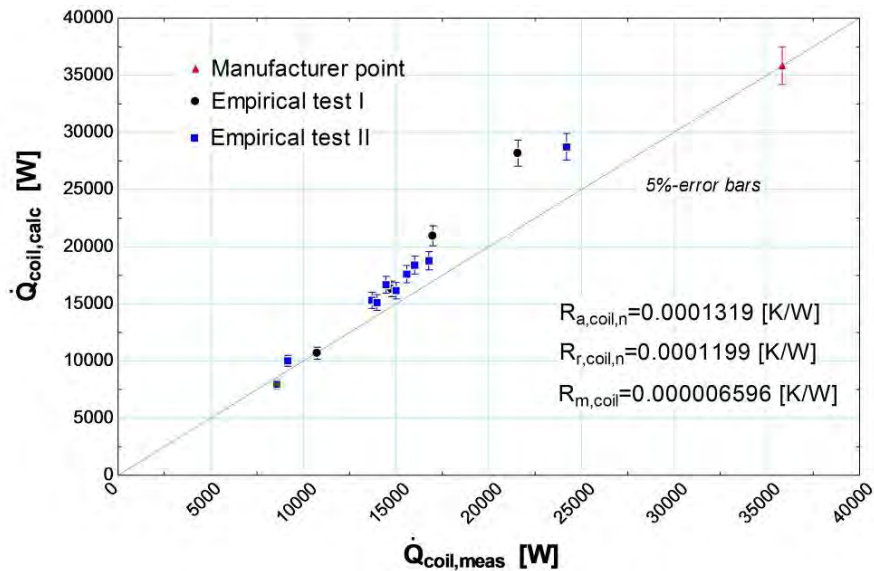


**Figure 2-7 Prediction by the model of the cooling capacity (the parameters of the model are those identified with the nominal point only, for a resistance ratio of 1.1 (comparative test))**

The same comparison is carried out for an air-refrigerant resistance ratio of 1.674, since this ratio was found to predict correctly the air outlet dry-bulb temperature. As mentioned previously, this resistance ratio yields an air-side resistance of 0.001726 K/W, a refrigerant-side resistance of 0.0001031 K/W and a metal resistance of 0.000008632 K/W (the metal resistance is fixed at 5% of the air-side resistance). As shown in Figure 2-8, the agreement between the cooling capacity predicted by the model and the measured cooling capacity is not better with these new parameters.

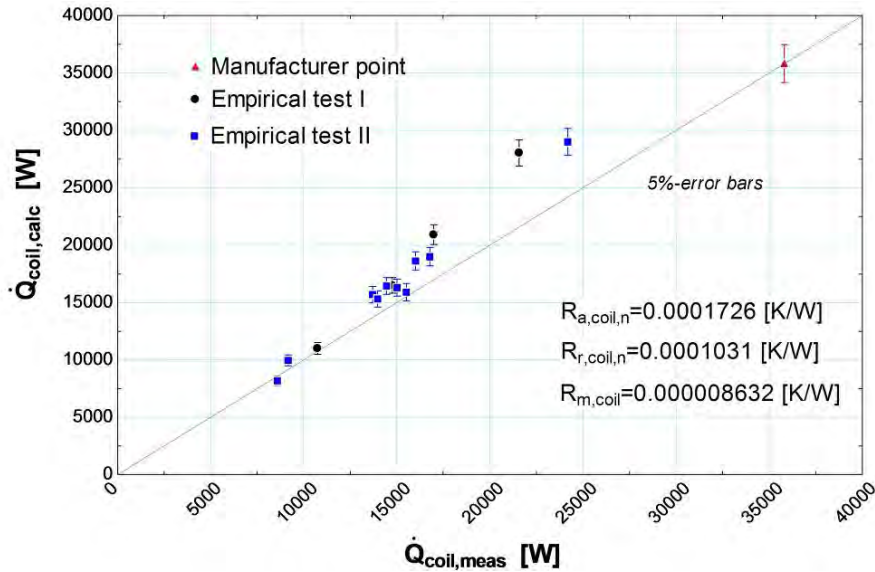


**Figure 2-8 Prediction by the model of the cooling capacity (the parameters of the model are those identified with the nominal point only, for a resistance ratio of 1.674 (comparative test))**

One explanation for this discrepancy could be that the coil is fouled up. The model can account for this fouling by introducing a fouling resistance  $R_{f,coil}$  in series with the three other resistances:

$$\frac{1}{AU_{coil}} = R_{a,coil} + R_{m,coil} + R_{r,coil} + R_{f,coil} \quad (2-30)$$

It was found that a fouling resistance of

- 0.000165 K/W for the points relative to the empirical test I and
- 0.000105 k/W for the points relative to the empirical test II

gave the best agreements between the predicted and measured total, sensible and cooling capacities. These agreements are shown in Figure 2-9, Figure 2-10 and Figure 2-11. The agreement is within 5% for the total and sensible cooling capacities and within 10% for the latent capacity.

The fact that the identified fouling resistance for empirical test I is higher than the one for empirical test II could be explained by the history of the cooling coil. Actually, empirical test I was carried out one year before empirical test II, with a slightly different refrigerant (an

aqueous solution of propylene glycol 21% in mass for test I and 18% in mass for test II). The system could have been flushed out between the two tests, which would have (at least partially) cleaned the coil.

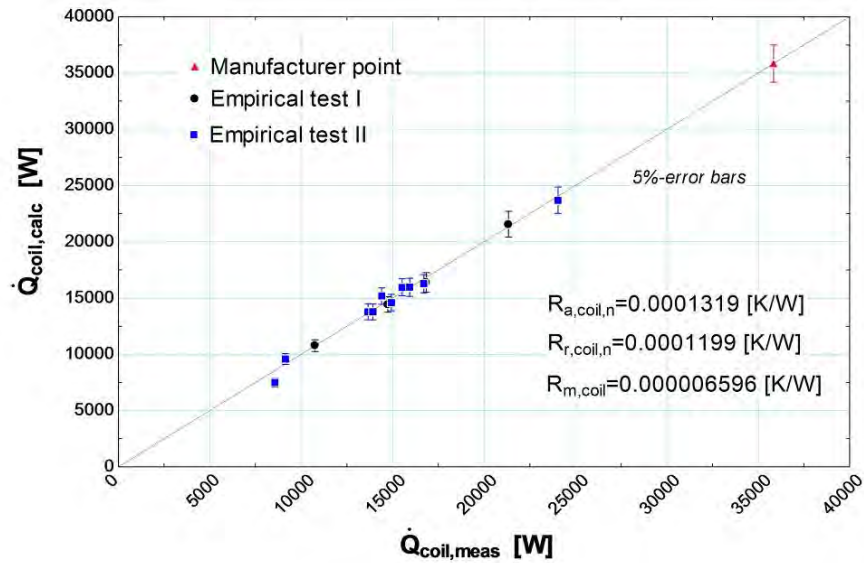


Figure 2-9 Prediction by the model of the total cooling capacity (the parameters of the model are those identified with the nominal point only, for a resistance ratio of 1.1 (comparative test))

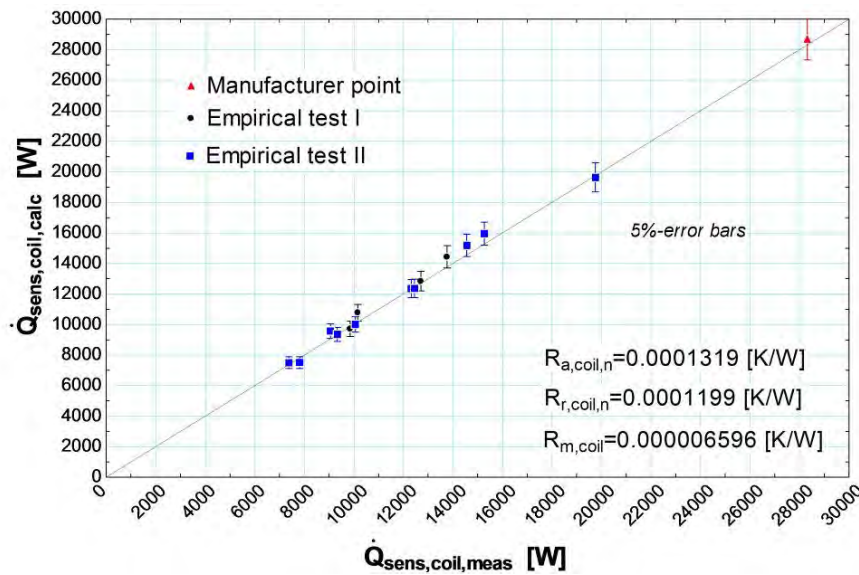


Figure 2-10 Prediction by the model of the sensible cooling capacity (the parameters of the model are those identified with the nominal point only, for a resistance ratio of 1.1 (comparative test))

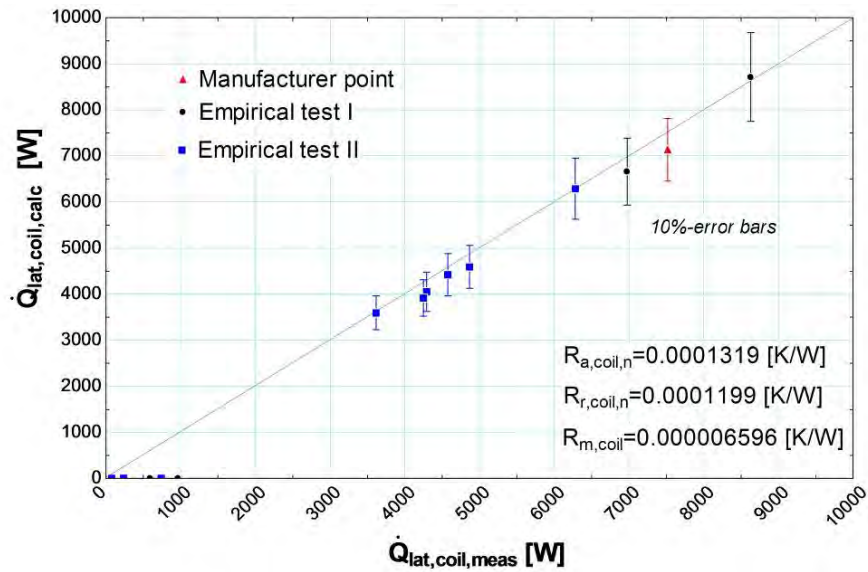


Figure 2-11 Prediction by the model of the latent cooling capacity (the parameters of the model are those identified with the nominal point only, for a resistance ratio of 1.1 (comparative test))

The same comparison is carried out with parameters of the model on the basis of an air-refrigerant resistance ratio of 1.674. The comparison between the predicted and measured cooling capacities is shown in Figure 2-12, Figure 2-13 and Figure 2-14. The agreement is even better here.

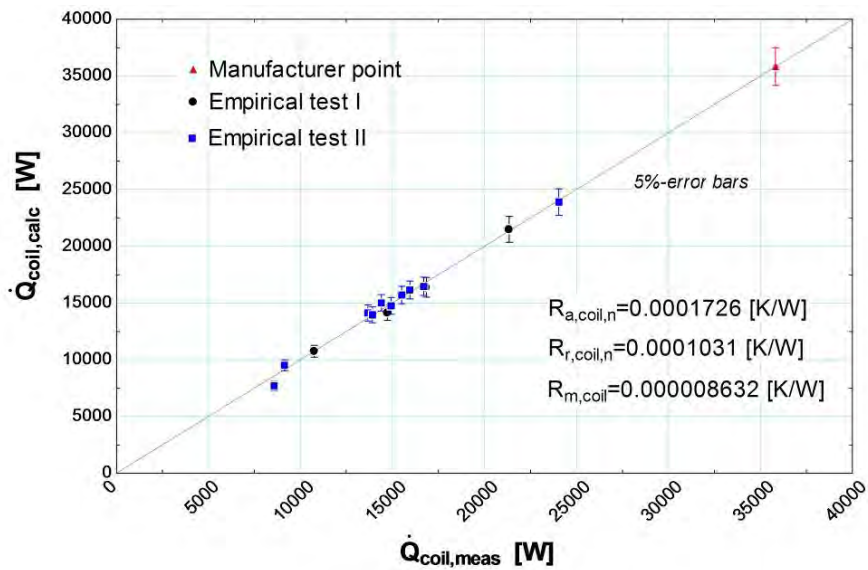
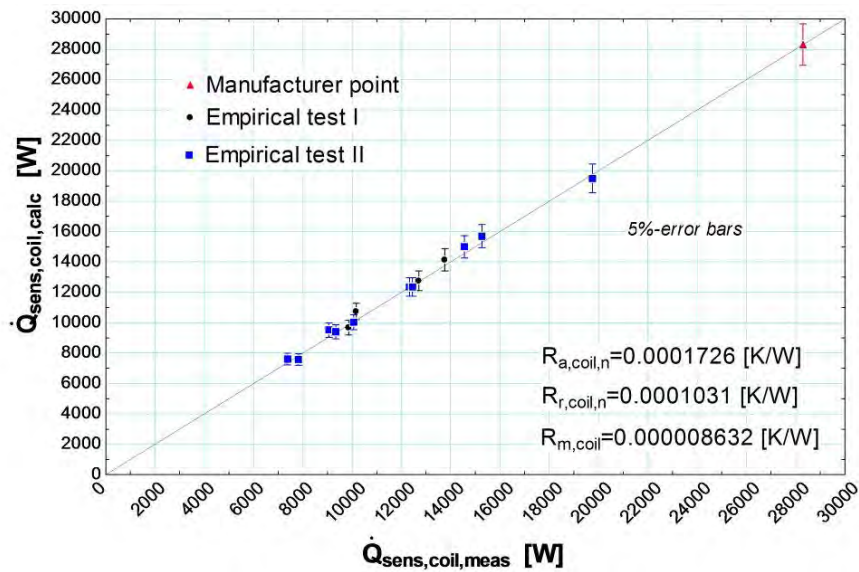
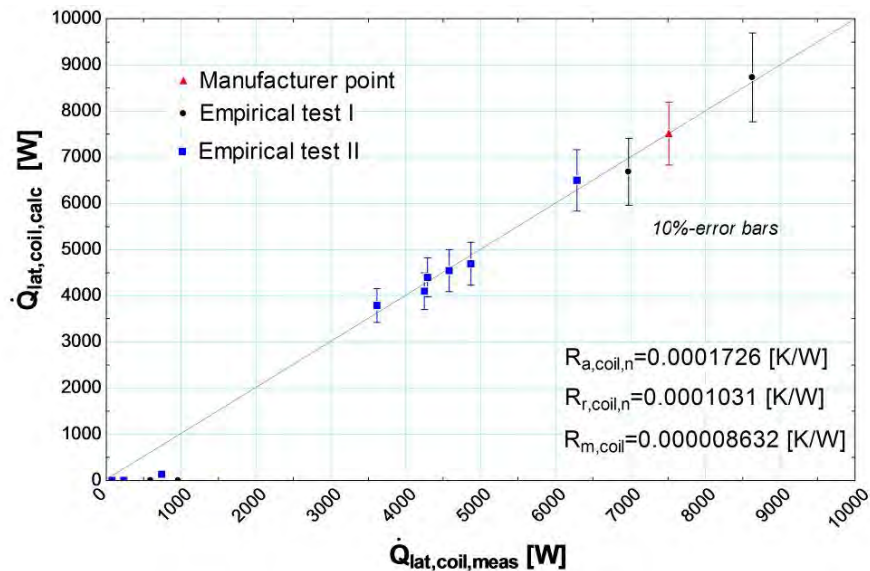


Figure 2-12 Prediction by the model of the total cooling capacity (the parameters of the model are those identified with the nominal point only, for a resistance ratio of 1.1 (comparative test))



**Figure 2-13 Prediction by the model of the sensible cooling capacity (the parameters of the model are those identified with the nominal point only, for a resistance ratio of 1.1 (comparative test))**



**Figure 2-14 Prediction by the model of the latent cooling capacity (the parameters of the model are those identified with the nominal point only, for a resistance ratio of 1.1 (comparative test))**

Both Figure 2-11 and Figure 2-14 show that the model is not able to predict the latent cooling capacity, when the latter is small. The following explanations are proposed:

1. Most of the contentious points are actually characterized by low refrigerant flow rates, as shown in Table 2-9. Turbulators are nestled inside the refrigerant tubes, in order to enhance the heat transfer. However, for very low refrigerant flow rates, the flow regime may not be turbulent anymore. The refrigerant flow could be a combination of laminar flow in some zones of the coil and turbulent in others (as for instances, in the elbows). If the flow is not purely turbulent, the assumption of a refrigerant-side resistance varying with the mass flow rate power 0.8 (Equation 2-7) is not valid anymore.

2. It is always difficult to determine accurately low latent cooling powers by difference between the total and sensible cooling powers. Discrepancies between the measured values and the calculated values could be due to inaccuracy of the measurements.
3. Experimental data have been compensated with regards to the accuracy of the sensors (mainly the relative air humidity) so that
  - air and refrigerant sides energy balances correspond to each other,
  - the amount of condensation recalculated from experimental data corresponds to measurements

This data compensation could have introduced a slight source of error for some points.

**Table 2-9 Comparison between the predicted and measured values for the total, latent and sensible cooling capacities (in regard to the Reynolds number)**

	$\dot{Q}_{coil,meas}$	$\dot{Q}_{coil,calc}$	$\dot{Q}_{sens,coil,meas}$	$\dot{Q}_{sens,coil,calc}$	$\dot{Q}_{lat,coil,meas}$	$\dot{Q}_{lat,coil,calc}$	$Re_{r,coil}$
I #1	10753	10737	10162	10737	591.5	0	475
I # 2	14725	14140	13762	14140	962.9	0	1113
I #3	16836	16361	9860	9673	6976	6688	1515
I # 4	21335	21482	12705	12751	8630	8731	1698
II #1	15503	15699	15269	15699	234.4	0	951
II # 2	14393	15002	14558	15002	-164.8	0	801
II #3	8559	7708	7820	7575	739.6	132.8	290
II # 4	9130	9524	9053	9524	76.96	0	354
I # 5	15938	16142	12324	12354	3614	3788	982
II #6	13664	14108	7379	7607	6285	6502	577
II # 7	13914	13953	9336	9409	4578	4544	616
II #8	14933	14733	10065	10038	4868	4695	734
II # 9	24044	23893	19755	19495	4289	4397	1387
II # 10	16701	16460	12452	12357	4249	4102	998

However, this lack of accuracy in the prediction of the low latent capacities is probably not critical on a long-term simulation of the cooling coil.

### 2.2.2.3 Concluding remarks

In conclusion, it appears that the nominal point doesn't constitute a sufficient information for identifying the parameters of the cooling coil model.

Moreover, aging of the cooling coil may make the parameters identification process more difficult. For the cooling coil under investigation, actual performances seem to differ from nominal performances due to, among other, fouling of the refrigerant pipes.

A higher resistance ratio seems to give a better agreement between predicted and calculated cooling capacities.

For the empirical tests, the fouling resistance is introduced in the model and the resistance ratio is increased (to 1.674).

## 2.3 Simulation results analysis

### 2.3.1 Analysis of the comparative tests

A summarized description of the cooling coil comparative tests is given in Table 2-10. More information can be found in the main report. The cooling coil is either controlled by varying the glycol water flow rate (for a constant glycol water temperature at the coil supply) or by varying the supply glycol temperature (for a constant glycol water flow rate) in order to achieve an air temperature set point at the exhaust of the coil (13°C or 18°C). The glycol water can be either an aqueous solution of ethylene glycol 35% in mass or an aqueous solution of propylene glycol 21% in volume. On the air side, Constant Air Volume and Variable Air Volume are compared.

**Table 2-10 Cooling coil comparative test matrix**

Test Case	Configuration	Air Flow	Fluid	DCA-ST
CC100	m <sub>var</sub>	CAV	35%	13
CC120			Ethylene Glycol	18
CC140			18%	13
CC160			Propylene Glycol	18
CC200		VAV	35%	13
CC220			Ethylene Glycol	18
CC240			18%	13
CC260			Propylene Glycol	18
CC300	T <sub>var</sub>	CAV	35%	13
CC320			Ethylene Glycol	18
CC340			18%	13
CC360			Propylene Glycol	18
CC400		VAV	35%	13
CC420			Ethylene Glycol	18
CC440			18%	13
CC460			Propylene Glycol	18

The input of the simulation are the entering water temperature, the entering air temperature and humidity, the air flow rate, either the water flow rate or the water entering temperature. Since the exhaust air temperature is imposed (provided the set point can be reached), the cooling coil sensible capacity is indirectly an input of the simulation. The air temperature set point may not be achieved, since the water flow rate is limited to a maximal value and the

entering water temperature to a minimal value. The simulation must determine either the water flow rate (CC100 to CC260) or the entering water temperature (CC3000 to CC460). Results will differ from one simulation codes to another because of the way the overall heat transfer coefficient is defined. Moreover, for a given sensible capacity, the simulation codes are likely to predict different latent capacities. Consequently, the results must be compared in terms of overall heat transfer coefficient  $AU$  and Sensible Heat Ratio  $SHR$ . As mentioned in the main report, the overall  $AU$  (or  $UA$ ) value can be calculated either from the sensible cooling load or from the total cooling load:

$$UA_{\text{sens}} = \frac{CLS}{\Delta T_m} \quad (2-31)$$

$$UA_{\text{tot}} = \frac{CLT}{\Delta T_m} \quad (2-32)$$

Where the mean logarithmic temperature difference is defined as:

$$\Delta T_m = \frac{(LWT - EAT) - (EWT - LAT)}{\ln \frac{LWT - EAT}{EWT - LAT}} \quad (2-33)$$

The Sensible Heat Ratio is defined as:

$$SHR = \frac{CLS}{CLT} \quad (2-34)$$

Numerous inter-program comparisons of the simulations results are presented in the main report (Felsmann, 2008). Only a few of them are analyzed here.

### 2.3.1.1 Variable chilled water flow rate control

Figure 2-15 compares the evolutions of the sensible overall heat transfer coefficients predicted by the different models with the water flow rate. Among others, it can be observed that the VABI and MATLAB models predict lower heat transfer coefficient for the higher flow rates than EES or TRNSYS. The latter present similar overall heat transfer coefficients.

Figure 2-16 and Figure 2-17 present the time evolution of the chilled water flow rate computed by the different models for two specific days extracted from CC100 (one hot-dry day and one hot-humid day). Because of his lower heat transfer coefficient, MATLAB predicts a higher chilled water flow rate. The latter is however limited to its maximal value (1.77), what can be seen in Figure 2-17.

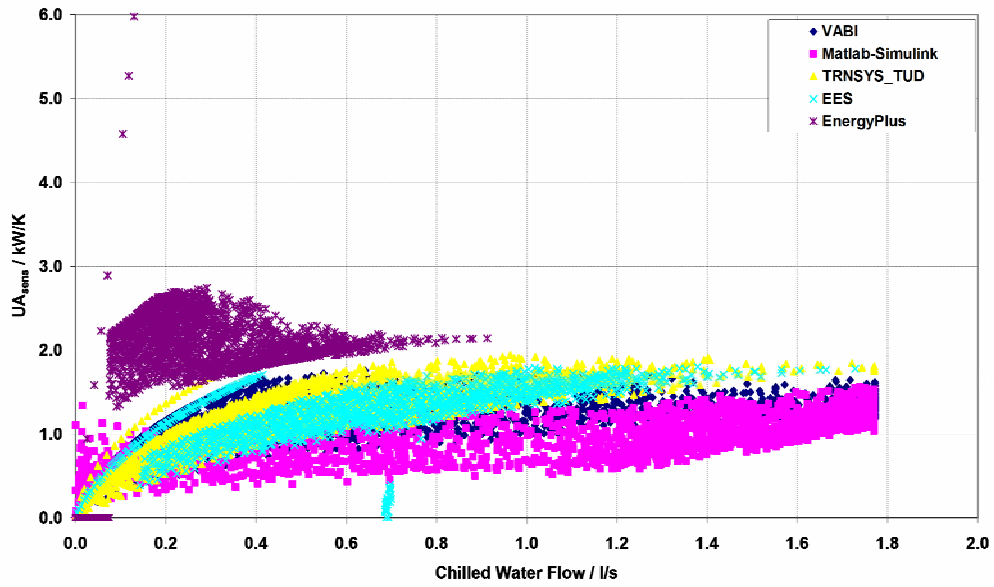


Figure 2-15 Evolution of the sensible overall heat transfer coefficient with the water flow rate

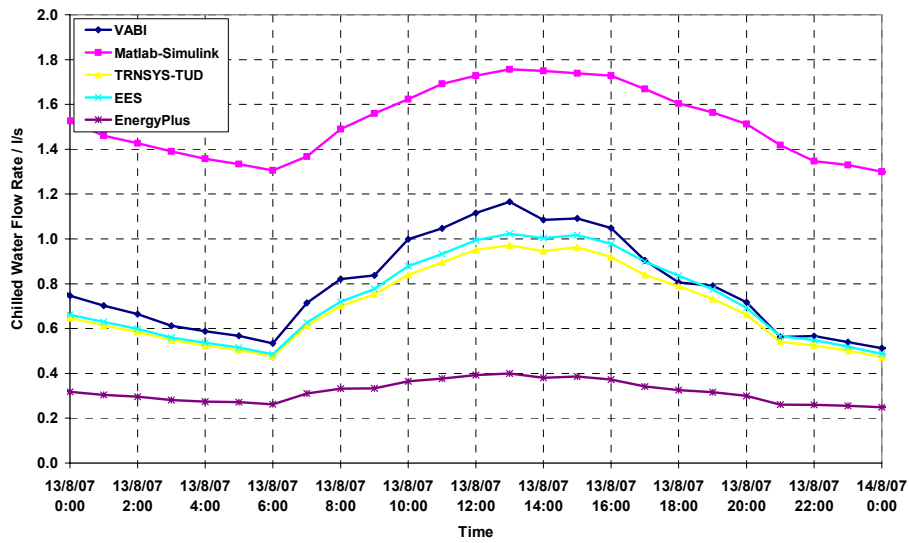


Figure 2-16 Time evolution of the chilled water flow rate (CC100- hot & dry)

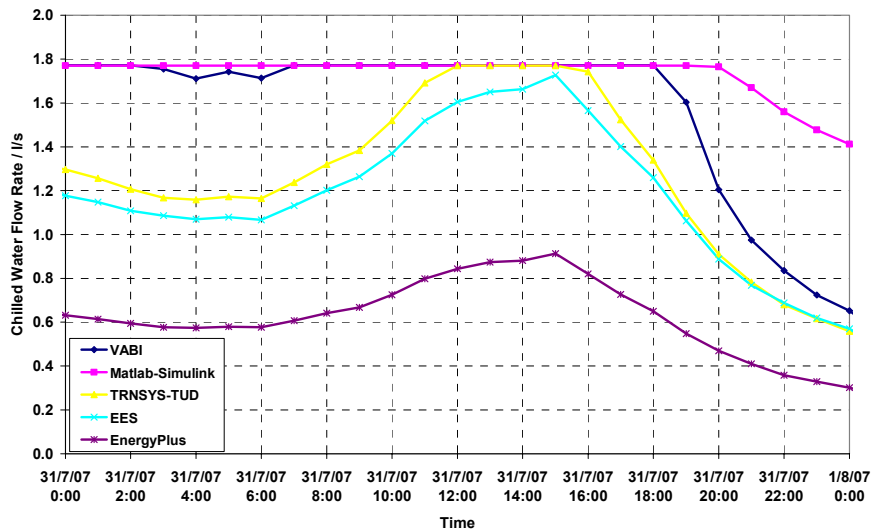


Figure 2-17 Time evolution of the chilled water flow rate (CC100- hot & humid)

Figure 2-18 shows the time-evolution of the chilled water flow rate for a hot humid day and a VAV operation. At hour 8, the air flow rate switches from 2000 m<sup>3</sup>/h to 5000 m<sup>3</sup>/h. Since the air temperature set point at the coil outlet is maintained, the water flow rate increases. All the models respect the limitation in the water flow rate.

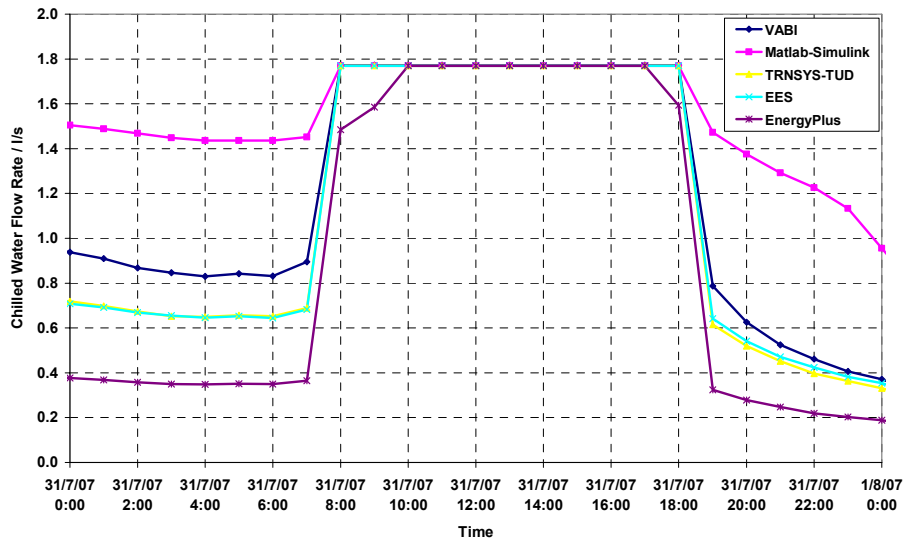


Figure 2-18 Time evolution of the chilled water flow rate (CC200- hot & humid)

Figure 2-19 and Figure 2-20 show the time evolution of the predicted total and latent cooling capacities for one hot-humid day extracted from test CC100. Due to their higher heat transfer coefficient, these capacities predicted by EES and TRNSYS are higher than those predicted by MATLAB and VABI. Remark: if there was no maximal limitation on the chilled water flow rate and if the models were assuming a perfect control of the coil (what is the case for the EES model), the sensible cooling capacity would be the same.

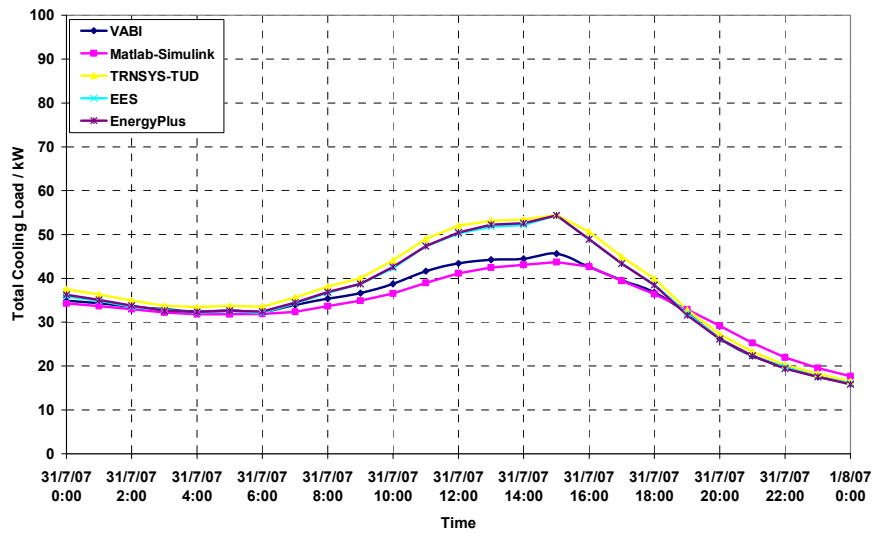


Figure 2-19 Time evolution of the total cooling capacity (CC100- hot & humid)

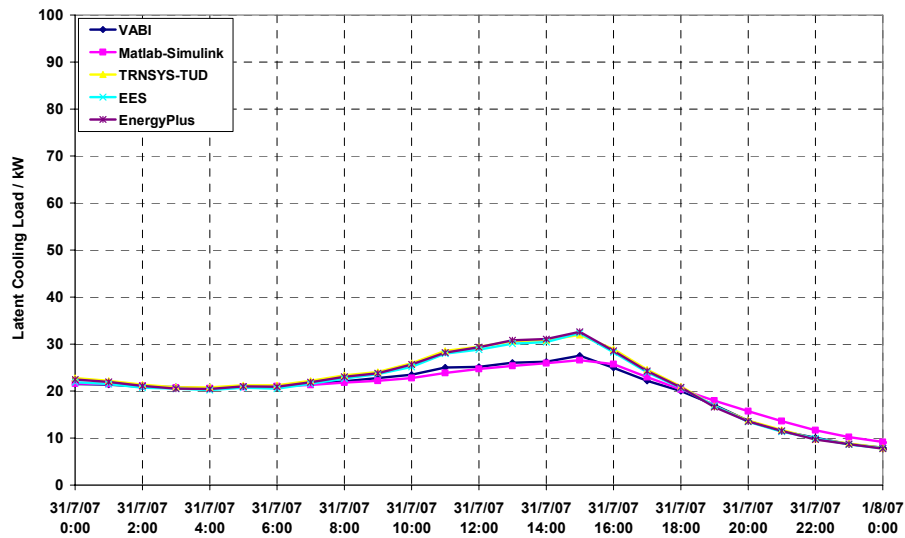


Figure 2-20 Time evolution of the latent cooling capacity (CC100- hot & humid)

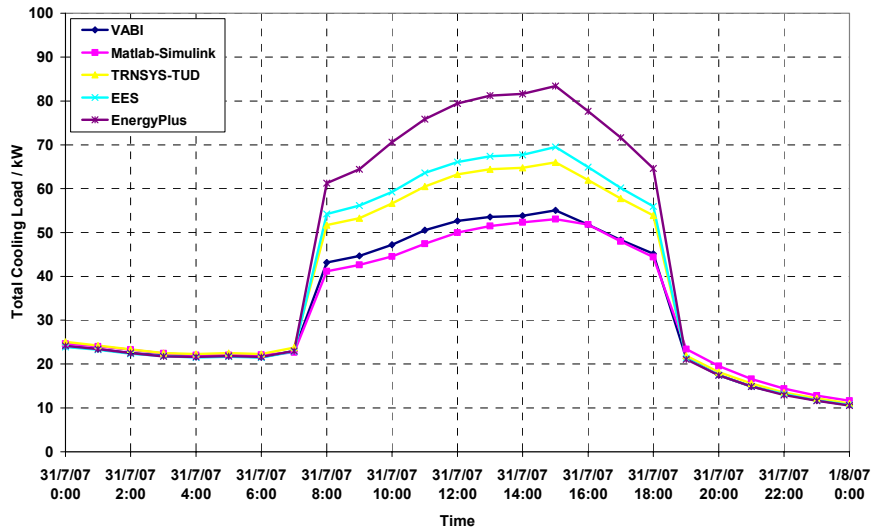


Figure 2-21 Time evolution of the total cooling capacity (CC200- hot & humid)

The total chilled water volumes passing the coil (integration over all the simulation period) for each test and each model are given in Figure 2-22. For the tests CC300 to CC460, these volumes are the same since the coil is controlled at constant water flow rate by varying the supply water temperature. For the test CC100, the volumes predicted by EES and TRNSYS are similar. However, for the test CC140, the volume predicted by EES is lower. EES seems not to account for the nature of the refrigerant (glycol water) in the same way than TRNSYS. The way EES accounts for the nature of the refrigerant was presented in §2.1.

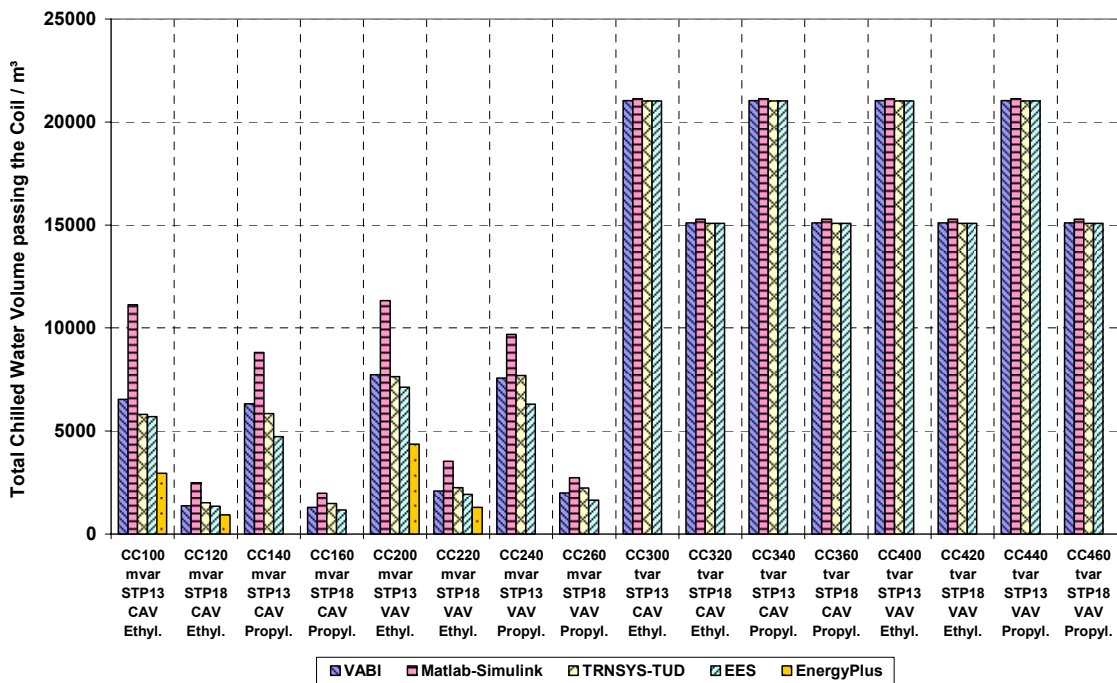


Figure 2-22 Total chilled water volume passing the coil [m3]

### 2.3.1.2 Variable chilled water temperature control

The mean entering water temperature for each test and each model is given in Figure 2-23. For tests CC100 to CC260, this temperature is constant since the coil is controlled with a constant entering water temperature and a varying water flow rate. For tests CC300 to CC460, the coil is controlled with a constant water flow rate (1.77 l/s) and a varying inlet water temperature. As for the coil controlled by the water flow rate, the results can be explained by the coil overall heat transfer coefficient. For example, in the test CC300, both TRNSYS and EES predict the higher inlet water temperature. The underlying reason is that they present larger heat transfer coefficient (see Figure 2-15).

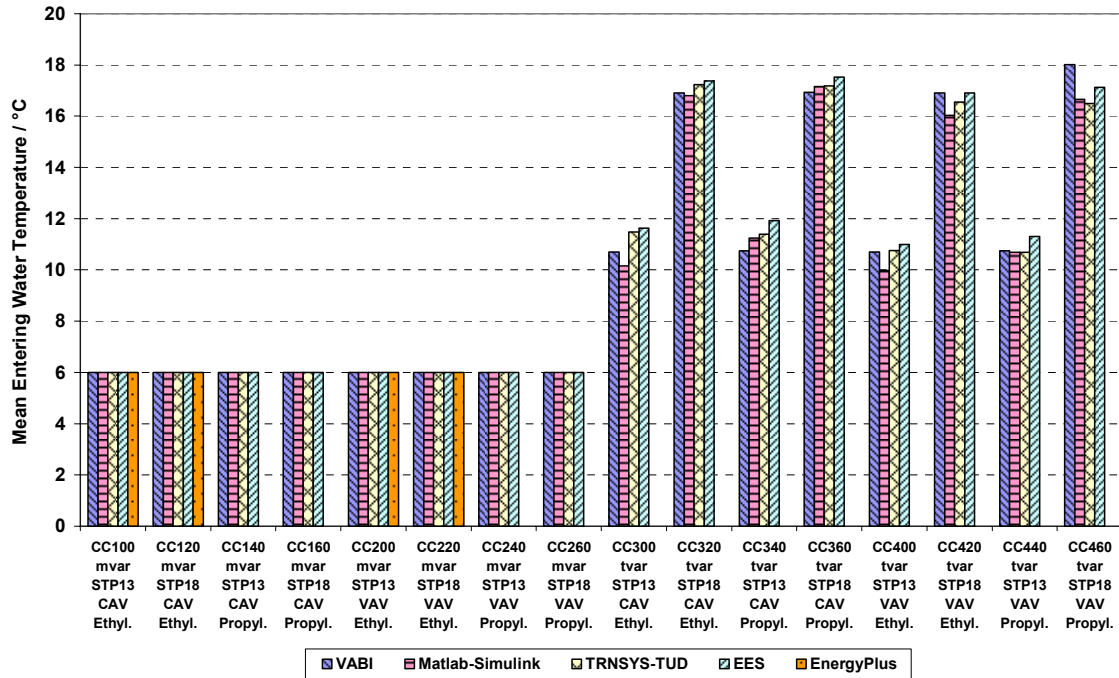
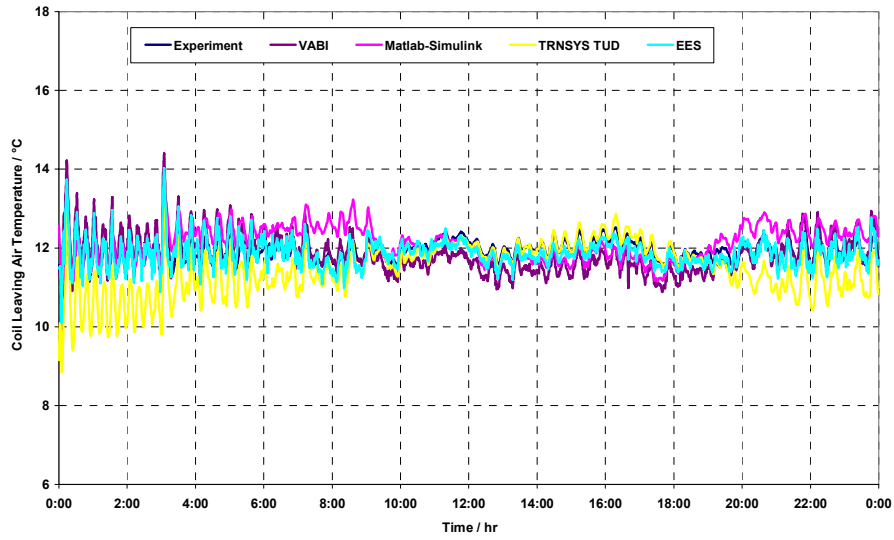


Figure 2-23 Mean entering water temperature

### 2.3.2 Analysis of the empirical tests

Only results from the *Empirical Test I* are presented here. Results related to *Empirical Test II* are shown in the main report. For the empirical tests, the inputs are the entering air temperature, the entering air relative humidity, the entering water temperature and the air and water flow rates.

Figure 2-24 and Figure 2-25 show the averaged daily time evolution of respectively the leaving air and leaving water temperature. It can be observed that the EES model predicts pretty well these two temperatures.



**Figure 2-24 Cooling Coil Empirical Test I – Averaged Daily Leaving Air Temperature**

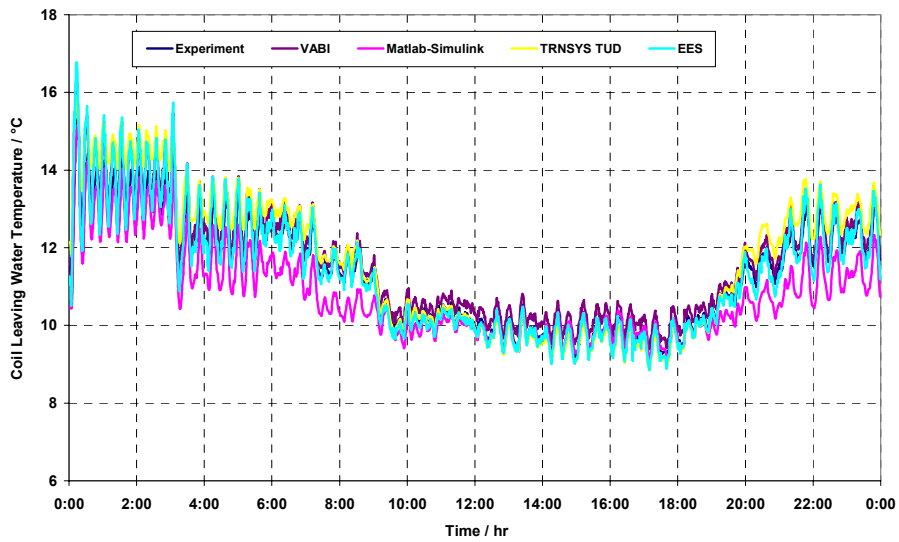


**Figure 2-25 Cooling Coil Empirical Test I – Averaged Daily Leaving Water Temperature**

The averaged daily time evolutions of the total cooling load, measured and predicted by the different models, are given in Figure 2-26. Here also, it can be observed that the agreement between prediction by the EES model and the measurements is good.

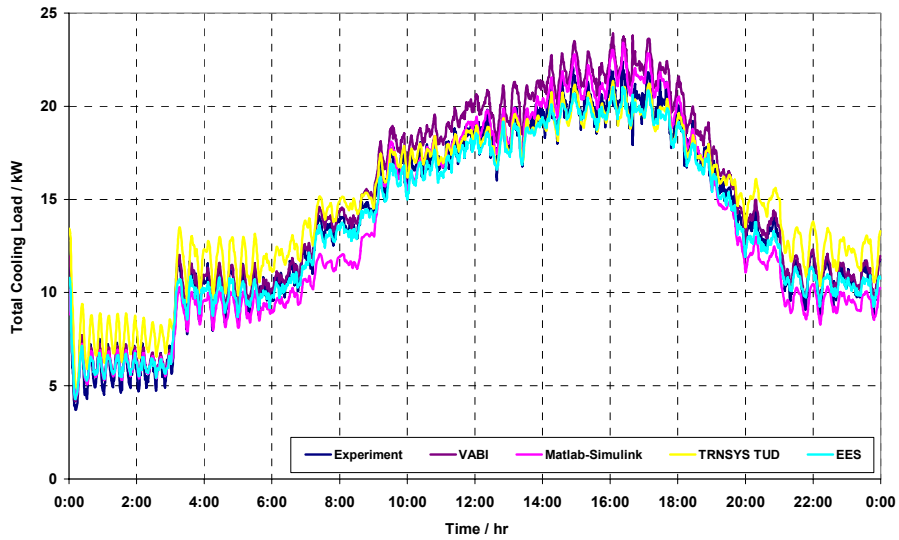


**Figure 2-26 Cooling Coil Empirical Test I – Averaged Daily Total Cooling Load**

Figure 2-27 shows the time evolution of the condensate accumulation. During the three first days, the model “follows” well the measurements. After that, the accumulated condensate predicted by the model starts to diverge from the measurements. This is due to the fact that in the modeling, the coil can be described in completely dry regime, while in the reality the coil is partly wet and partly dry.

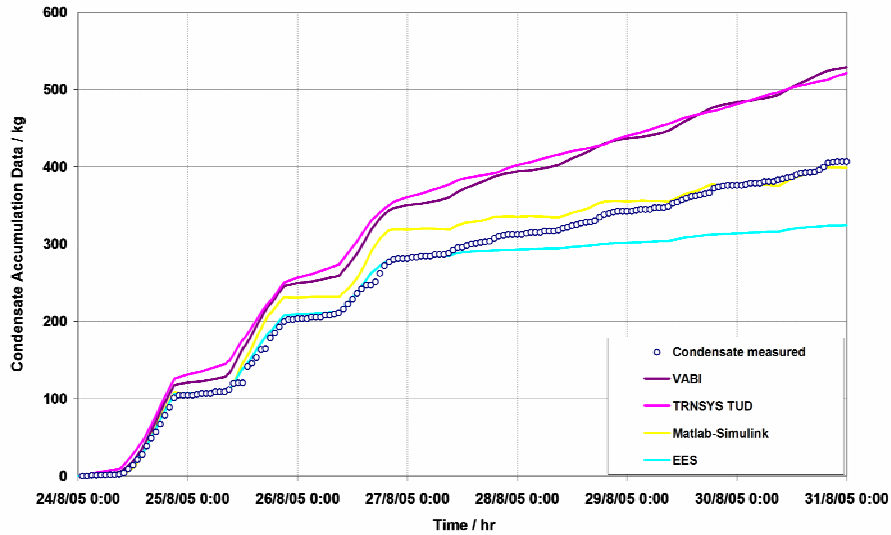


**Figure 2-27 Cooling Coil Empirical Test I – Condensate Accumulation**

The total, sensible and latent energies (integration over the entire simulation period) are given in Figure 2-28. It can be observed that the agreement is very good (1.3% for the total cooling energy, 1.5% for the sensible cooling energy and 21.4% for the latent cooling energy).

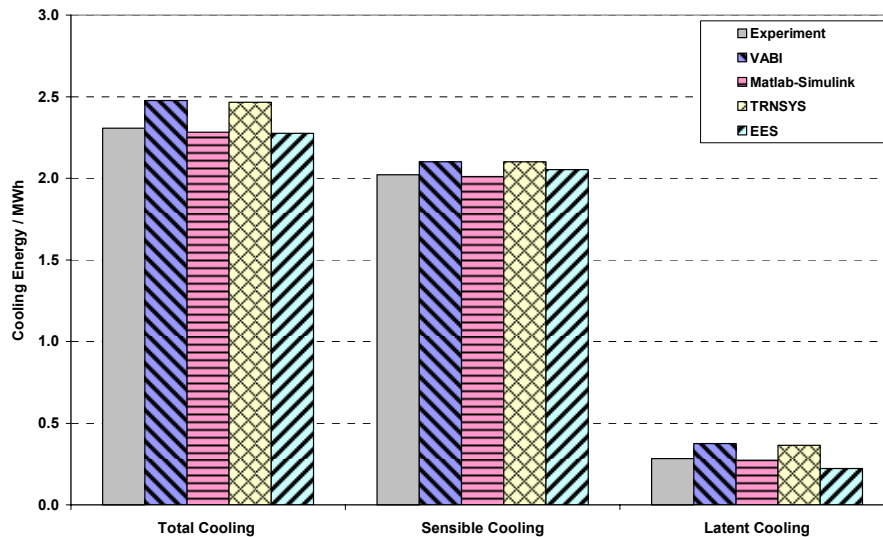


Figure 2-28 Cooling Coil Empirical Test I – Total, Sensible and Latent Energies

### 3 Condensing Boiler

#### 3.1 Description of the model

The condensing boiler model associates a classical boiler model and a cooling coil model, which takes into account the latent heat exchange. This coil works in dry or humid regime depending on the boiler supply (return) water temperature. Figure 3-1 shows a schematic representation of the model.

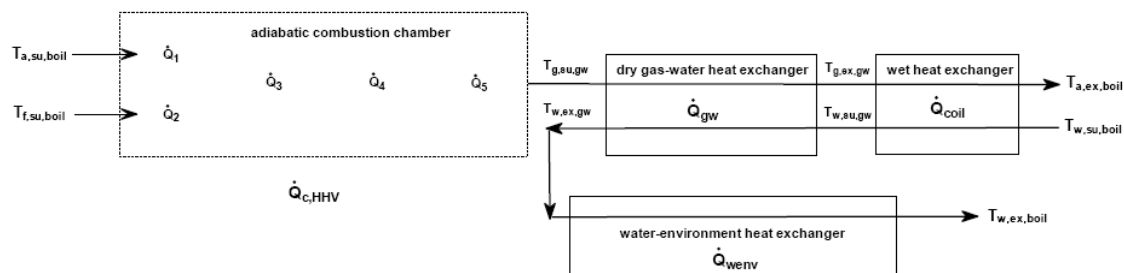


Figure 3-1 : Principle scheme of the condensing boiler modeling

The main components of the model are:

1. The adiabatic combustion chamber
2. The dry gas-water heat exchanger
3. The wet gas-water heat exchanger
4. The water-environment heat exchanger

#### *The Adiabatic Combustion Chamber*

For the purpose of the modeling, the combustion process is decomposed into different heat transfers. First of all, air and fuel are heated up or cooled down to the reference temperature

$T_{ref}$ , at which the low heating value LHV of the fuel is defined:

$$\dot{Q}_1 = \dot{M}_{a,boil} \cdot c_{p,a,boil} \cdot (T_{ref} - T_{a,su,boil}) \quad (3-1)$$

$$\dot{Q}_2 = \dot{M}_{f,boil} \cdot c_{p,f} \cdot (T_{ref} - T_{f,su,boil}) \quad (3-2)$$

The combustion is then assumed to be isothermal and complete:

$$\dot{Q}_3 = - \dot{M}_{f,boil} \cdot \text{LHV} \quad (3-3)$$

A “dissociator” could account for an eventual incomplete combustion:

$$\dot{Q}_4 = \dot{M}_{co} \cdot \text{LHV}_{co} \quad (3-4)$$

The combustion gas is then heated up to the combustion chamber exhaust temperature. The specific heat  $c_{p,g}$  of combustion gas is computed by means of a subroutine on the basis of molar coefficients  $m$  and  $n$  characterizing the combustible  $C_mH_n$  and fuel air ratio  $f$ .

$$\dot{Q}_5 = \dot{M}_{g,boil} \cdot c_{p,g} \cdot (T_{adiab} - T_{ref}) \quad (3-5)$$

Since the combustion chamber is considered as adiabatic, the sum of these terms must be equal to zero. By definition, the exhaust temperature from the combustion chamber is the adiabatic temperature.

$$\dot{Q}_1 + \dot{Q}_2 + \dot{Q}_3 + \dot{Q}_4 + \dot{Q}_5 = 0 \quad (3-6)$$

#### *The dry gas-water heat exchanger*

It is modeled by its heat transfer coefficient  $AU_{gw}$ , which varies with the gas flow rate  $\dot{M}_{g,boil}$ , according to:

$$AU_{gw} = AU_{gw,N} \cdot \left[ \frac{\dot{M}_{g,boil}}{\dot{M}_{g,boil,n}} \right]^{a_{gw}} \quad (3-7)$$

Nominal values  $AU_{gw,n}$  and  $\dot{M}_{g,boil,n}$  of the heat transfer coefficient and of the gas flow rate and a value of the exponent  $a_{gw}$  have to be identified.

#### *The wet heat exchanger*

It is proposed to represent the wet heat exchanger by a cooling coil, working either in dry or wet regime, depending on the boiler supply temperature. In order to use the previously explained model of a cooling coil, an equivalent air is defined as substitute to the gas at the exhaust of the dry gas-water heat exchanger.

The cooling coil air supply temperature is the gas temperature at the exhaust of the gas-water heat exchanger:

$$T_{a,su,coil} = T_{g,ex,gw} \quad (3-8)$$

The equivalent air mass flow rate is defined by expressing the energy conservation:

$$\dot{M}_{a,coil} \cdot c_{p,a,coil} = \dot{M}_{g,boil} \cdot c_{p,g,coil} \quad (3-9)$$

Mean values of air and gas specific heat are calculated between the cooling coil supply and exhaust:

$$c_{p,a,coil} = \mathbf{Cp} ( \text{'AirH2O'} , T = T_{a,coil,m} , P = P_{atm} , W = W_{a,su,coil} ) \quad (3-10)$$

$$c_{p,g,coil} = \mathbf{cpbar} ( m , n , f , T_{a,su,coil} , T_{a,ex,coil} ) \quad (3-11)$$

$$T_{a,coil,m} = \frac{T_{a,su,coil} + T_{a,ex,coil}}{2} \quad (3-12)$$

Equivalent specific air humidity at the cooling coil supply is defined on the basis of water content in gas:

$$\dot{M}_{H_2O,g} = \dot{M}_{a,coil} \cdot W_{a,su,coil} \quad (3-13)$$

Water content in gas at the exhaust of the gas-water heat exchanger is the sum of both water initially present in combustion air and water resulting from the combustion of the fuel:

$$\dot{M}_{H_2O,g} = \dot{M}_{H_2O,comb} + \dot{M}_{H_2O,air} \quad (3-14)$$

$$\dot{M}_{H_2O,air} = W_{a,su,boil} \cdot \dot{M}_{a,boil} \quad (3-15)$$

The modeling of the cooling coil has been presented previously.

#### *Water-environment losses*

This loss is supposed to occur through a semi-isothermal heat exchanger, whose heat transfer coefficient  $AU_{wenv}$  is assumed to be constant:

$$NTU_{wenv} = \frac{AU_{wenv}}{\dot{C}_{w,env}} \quad (3-16)$$

$$\varepsilon_{wenv} = 1 - \exp ( - NTU_{wenv} ) \quad (3-17)$$

$$\dot{Q}_{wenv} = \varepsilon_{wenv} \cdot \dot{C}_{w,env} \cdot ( T_{w,ex,gw} - T_{env} ) \quad (3-18)$$

Water temperature at the condensing boiler exhaust is given by:

$$T_{w,ex,boil} = T_{w,ex,gw} - \frac{\dot{Q}_{w,env}}{\dot{C}_{w,env}} \quad (3-19)$$

### Heating power and efficiency

The total heating power of the boiler is the sum of the heating power exchanged in the gas-water heat exchanger (minus the water-environment losses) and the heating power produced in the wet heat exchanger:

$$\dot{Q}_{u,1,boil} = \dot{M}_{w,boil} \cdot c_w \cdot (T_{w,ex,boil} - T_{w,su,gw}) \quad (3-20)$$

$$\dot{Q}_{u,boil} = \dot{Q}_{u,1,boil} + \dot{Q}_{coil} \quad (3-21)$$

The thermal efficiency of the modeler is the ratio between the heating capacity and the heat input of the boiler:

$$\eta_{HHV} = \frac{\dot{Q}_{u,boil}}{\dot{Q}_{c,HHV}} \quad (3-22)$$

The heat input is here defined on the basis of the high heating value (*HHV*) of the fuel:

$$\dot{Q}_{c,HHV} = \dot{M}_{f,boil} \cdot HHV \quad (3-23)$$

## 3.2 Parameters identification

### 3.2.1 Available information

Some general information about the boiler can be taken from Table 3-1.

**Table 3-1 : Condensing boiler general data**

Manufacturer	Aerco International
Boiler Unit Model	KC-1000-GWB
Boiler Type	Natural Gas Fired Hot Water
Fuel Consumption	28.32 m <sup>3</sup> /h @37.25 MJ/m <sup>3</sup> 1,000 CFH gas @ 1,000 BTU/CF
Maximum Capacity	272,6 kW (930,000 BTU/hr)
Water Volume	87.1 l (23 gallons)
Control Range	10 ... 104°C (50 ... 220°F)
Water Flow Range	1.6 ... 9.5 l/s (25 ... 150 gpm)
ASME Working Pressure	1.04 MPa (150 psig)
Rated AFUE	92% (Efficiency varies with entering water temperature and firing rate)

The *burner* is characterized by the information given at Table 3-2. With a modulation turn down ratio of 14:1 the capacity of the burner at the minimum firing rate is approximately 7% of full capacity.

**Table 3-2 : Burner General Data**

Type	Nozzle Port Injection
Modulation Turn Down Ratio	14:1 Turndown
Capacity at Minimum Firing Rate	7% Capacity

The properties of the *fuel* that was used for calculation are taken from Table 3-3

**Table 3-3 : Properties of natural gas**

Properties [Units/Conditions]	Value
Carbon content [mass %]	73.3
Hydrogen content [mass %]	23.9
Oxygen content [mass %]	0.4
Methane concentration [Volume %]	80 - 99
Ethane concentration [Volume %]	2.7 - 4.6
Nitrogen concentration [Volume %]	0.1 - 15
Carbon dioxide concentration [Volume %]	1 - 5
Sulphur concentration [ppm, mass]	<5
Methane number	69 - 99
Octane number	120 -130
Relative molar mass	17 - 20
Relative density [@15°C / 1 bar]	0.72 - 0.81
Stoichiometric air/fuel ratio [mass]	17.2
Lower heating/calorific value [MJ/kg]	38 - 50
Stoichiometric lower heating value [MJ/kg]	2.75
Flammability limits [lambda]	0.7 - 2.1

The total electricity consumption for the hydraulic boiler includes the combustion air fan (blower) as well as the control panel, air/fuel valve and safety shut off valve. When the boiler is in stand by, the only electrical usage is to power the control panels, lights, relays, etc. The combustion air fan has some variation in power, depending on the modulation of the air/fuel valve. The air/fuel valve acts as a discharge damper on the combustion air fan to reduce the

amount of combustion air flow while also modulating the gas flow to the burner. As the firing rate of the boiler decreases, the volume of combustion air (and fuel) is reduced by the air/fuel valve. Consequently, the electrical power of the combustion air fan decreases. A previous test on the boiler gave the results shown in Table 3-4:

**Table 3-4 : Total electrical consumption for the hydraulic boiler**

Status	Firing Rate	Power
Standby Mode	No call for heat, control panel only	27 W
Minimum Fire	10%	430 W
Mid Range Fire	64%	770 W
Full fire	100%	860 W

In total, 18 performances points are given by the manufacturer presented under the form of a single graph, in which the performance is given as function of water supply temperature and firing rate. The difference between supply and exhaust temperature is been fixed to 11 K. These points are presented in Figure 3-2.

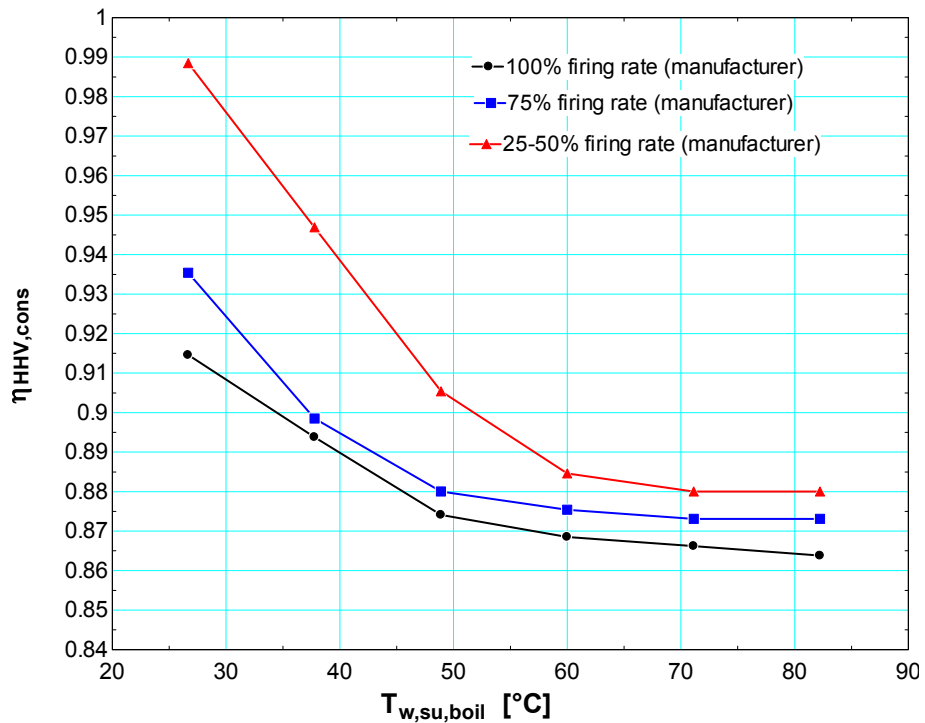


**Figure 3-2 : Evolution of measured (given by the manufacturer) boiler efficiency**

### 3.2.2 Procedure for identifying the parameters

The parameters of the model are tuned in order to bring the values predicted by the model as close as possible to the values announced by the manufacturer. Identified parameters are given in the information diagram shown in Figure 3-3. In practice, the tuned parameters were  $AU_{gw,n}$ ,  $\dot{M}_{g,boil,n}$ ,  $a_{gw}$ ,  $AU_{wenv}$ ,  $R_{a,coil,n}$ ,  $R_{w,coil,n}$ ,  $R_{m,coil,n}$ . The other parameters were information given by the manufacturer for these 18 points. The criterion to minimize the difference between the manufacturer data and the model results was the least squares method. This diagram shows also that for this identification, the water supply temperature, the temperature difference between the supply and the exhaust, the ambient conditions (temperature, atmospheric pressure and humidity ratio), the air supply temperature and the firing rate are inputs of the model. The model calculates the useful power, the efficiencies, the condensate mass flowrate, the gas exhaust temperature and mass flowrate, and the sensible and latent power in the wet heat exchanger.

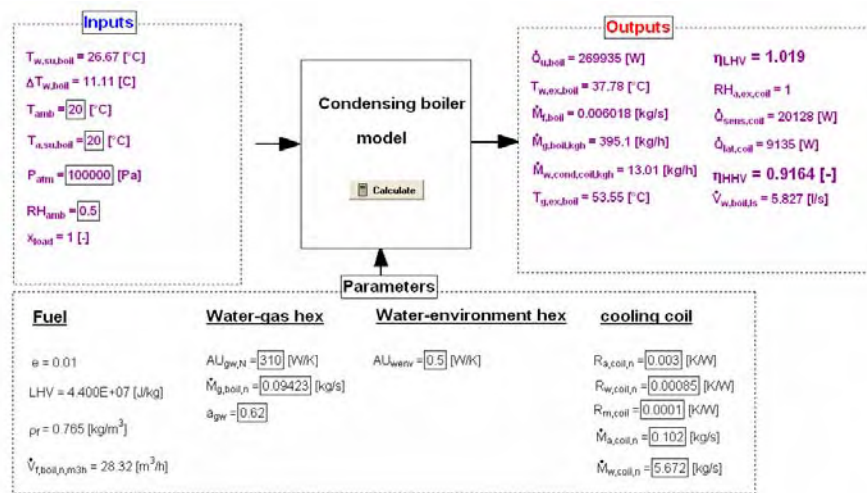


Figure 3-3 : Inputs, outputs and parameters of the condensing boiler model

Figure 3-4 shows the evolution, with the supply water temperature, of both predicted values of the efficiency and values announced by the manufacturer. Even if the model is ‘mechanistic’, some physical phenomenon are probably escaping (quantitatively or qualitatively) from the modelling. For example, the model seems not to describe well the behaviour of the boiler for high return water temperatures and for low return temperatures and low firing rates. For the other points, the agreement between measured and calculated values is pretty good.

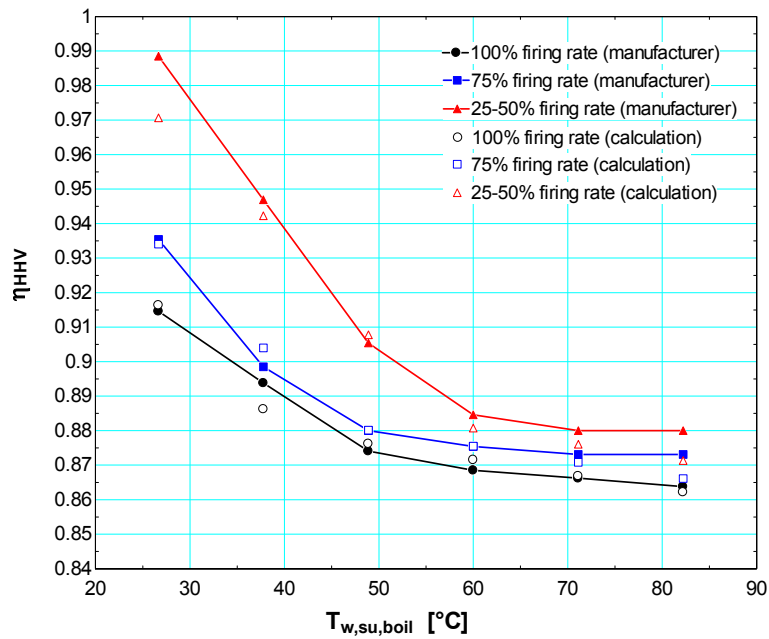


Figure 3-4 : Evolution of the calculated and measured boiler efficiency

### 3.3 Simulation results analysis

#### 3.3.1 Analysis of the comparative tests

This comparative investigation includes 8 different tests, in which basically two different control strategies are considered: one in which the distribution boiler exhaust water temperature set point is constant and independent on outside air temperature, the return temperature entering the boiler is known and function of the outside air temperature as well as the heating water flowrate (cases HWB 100-220). In the other one, the heating water flowrate is a constant and supply water temperature and return temperature depend on the outside air temperature. Table 3-5, Figure 3-5 and Figure 3-6 summarize these tests.

Table 3-5 : Summary of the Boiler comparative test

Test Case	Configuration	Combust. Air	Condensing Boiler
HWB100	SPT=const HWFR=f(OA)	inside	Yes
HWB120			No
HWB200		outside	Yes
HWB220	No		
HWB300	SPT=f(OA) HWFR=const	inside	Yes
HWB320			No

HWB400		outside	Yes
HWB420			No

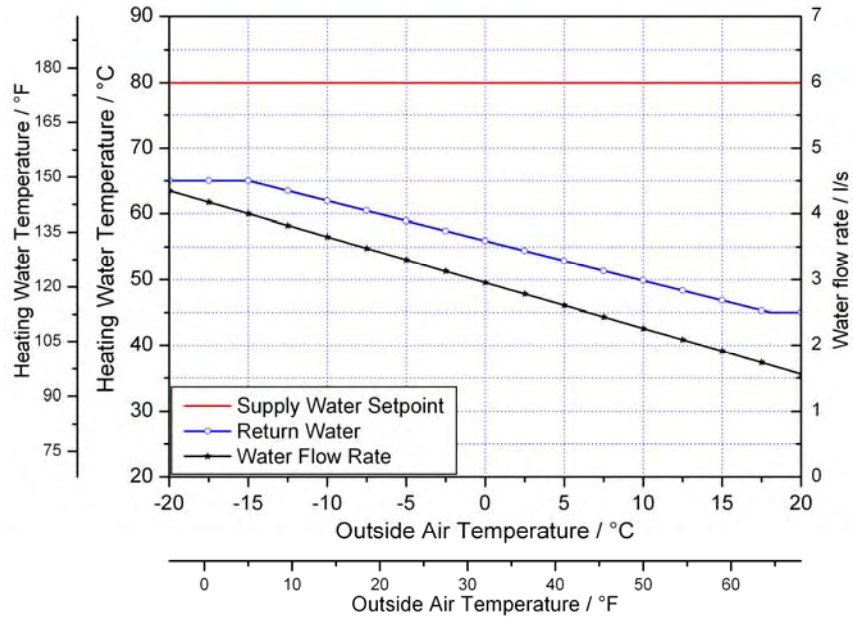


**Figure 3-5 : Distribution water setpoint temperature, return water temperature and water flow rate for cases HWB 100-220**

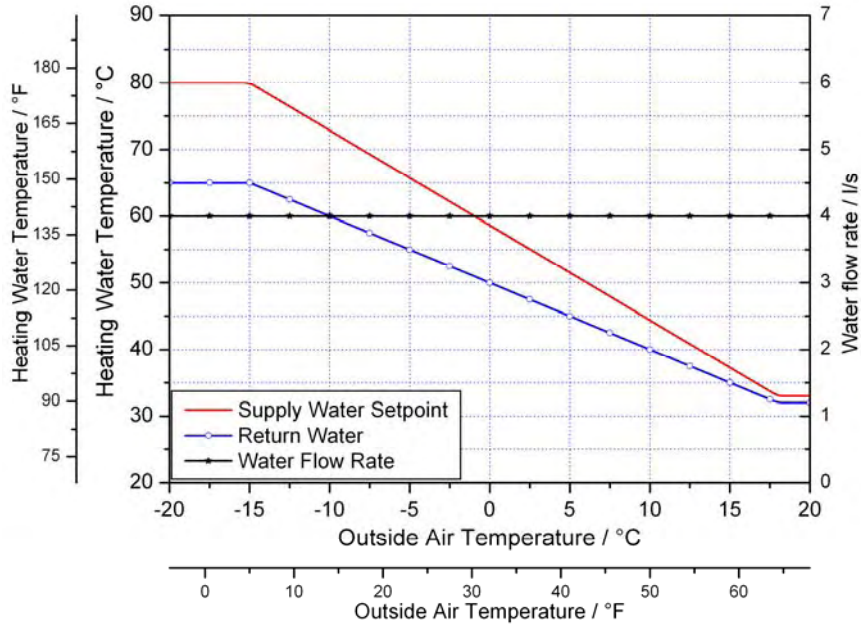


**Figure 3-6 : Distribution water setpoint temperature, return water temperature and water flow rate for cases HWB 300-420**

Main results of this comparative test are shown in Figure 3-7 and Figure 3-8. These figures give the total heating energy (integration of the heating power over the simulation) and the mean leaving water temperature.

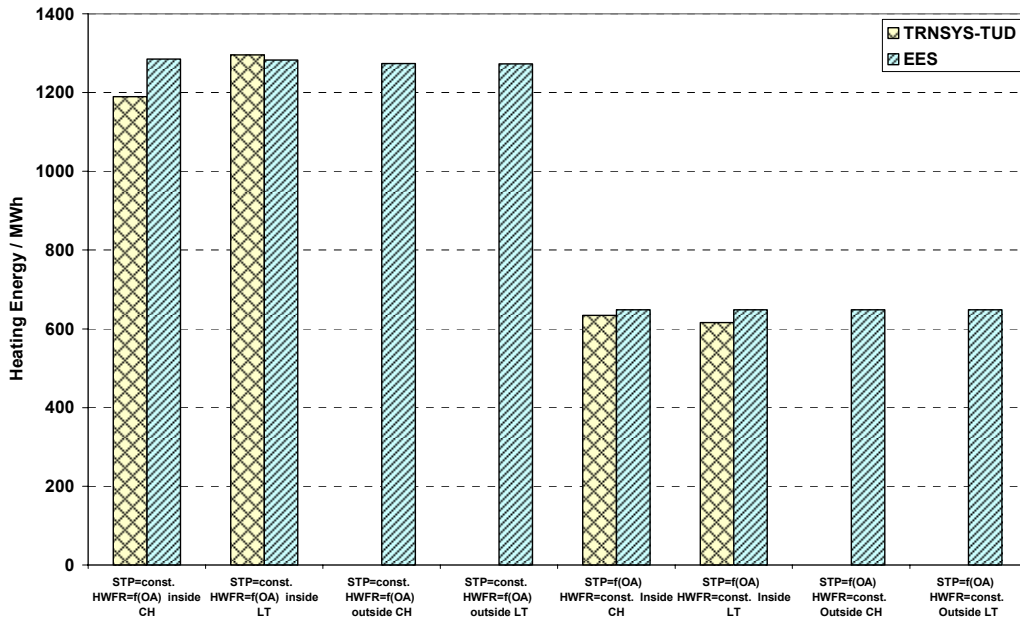


**Figure 3-7 : Heating energy of the boiler for the different test cases**

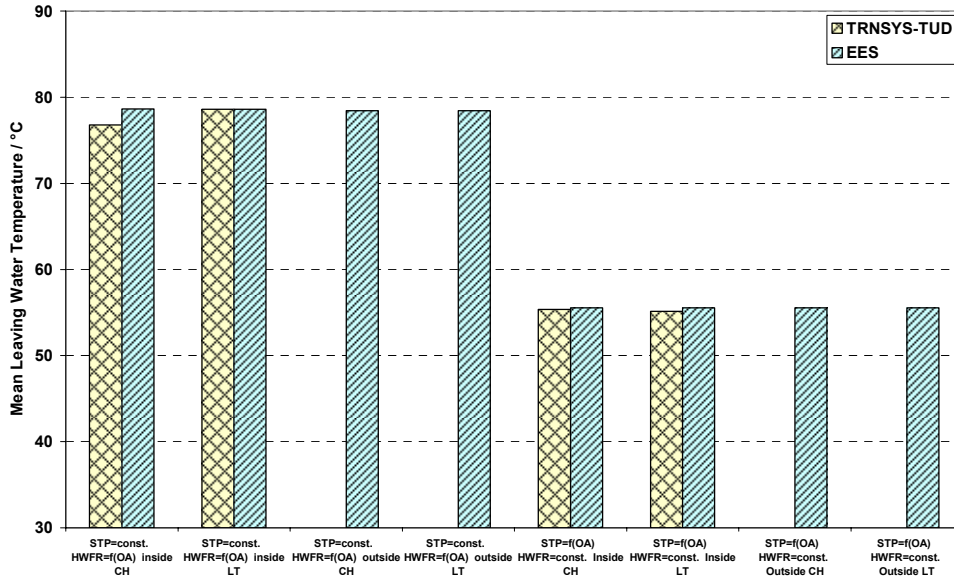


**Figure 3-8 : Mean Leaving Water Temperature for the different test cases.**

From Figure 3-7 and Figure 3-8, it can be seen a very good agreement between TRNSYS and EES simulation. However, these two figures do not represent well the ability of the two models to predict the performances of the boiler. Actually, the entering water temperature,

the heating water flow rate and the leaving water temperature set point are given. In fact, if the control of the boiler is the same, the results of both simulations must be also the same. In the case of EES a perfect control is assumed, i.e., the set point is always achieved if the boiler capacity is big enough. That is the reason because the mean leaving temperature and heating energy of the boiler are always higher, with exception of the heating energy in the test HWB120 (STP=const, HWFR=f(OA), inside LT).

So, a more useful variable of comparison is shown in Figure 3-9 and Figure 3-10: the firing rate. Its mean value over the evaluated period and also the hourly behavior on a 3 day period chosen in a random way for the test HWB-100 are shown respectively.

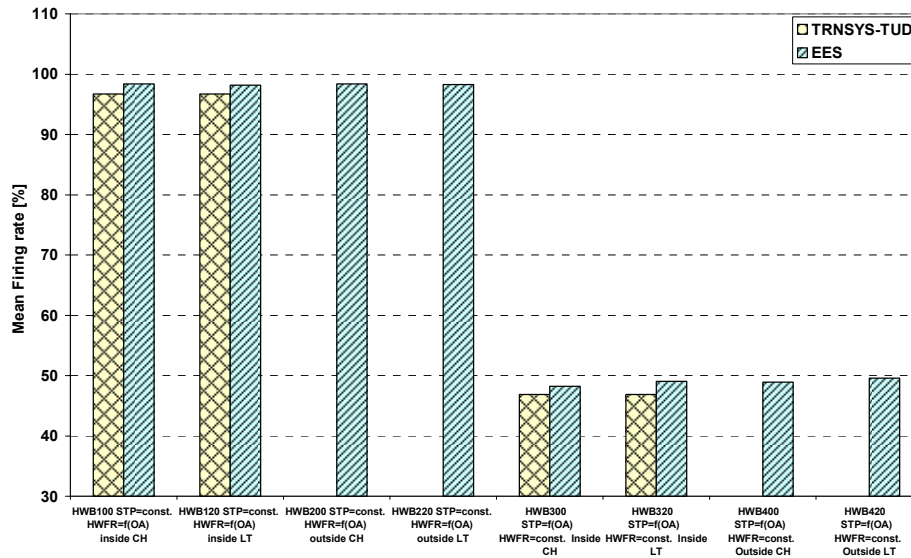


Figure 3-9 : Mean Firing Rate for the different test cases.

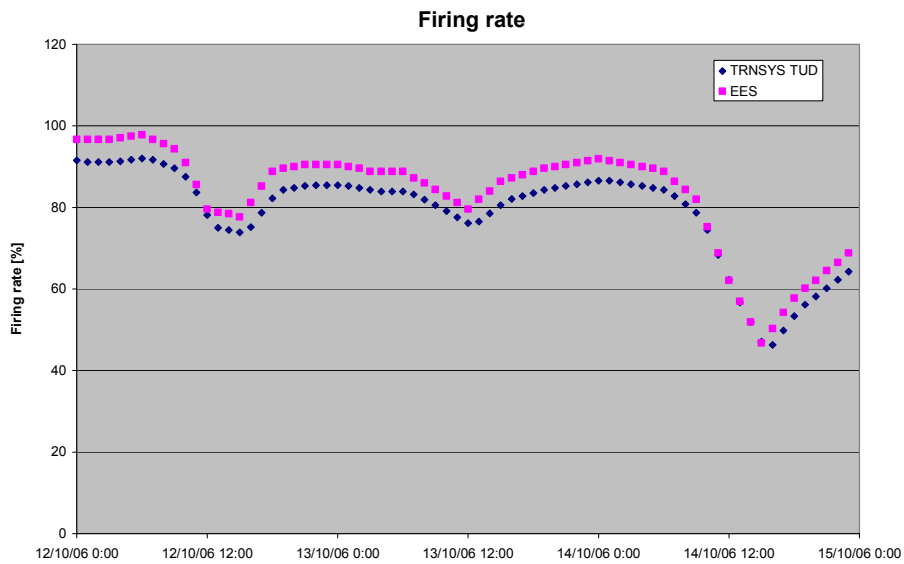


Figure 3-10 : Firing rate between 12/10/2006 and 14/10/2006 for the HWB-100 test

The results show a similar behavior between the two simulations, but EES is always giving a higher firing rate due to the, already explained, control strategy.

### 3.3.2 Analysis of the empirical test

The goal of this empirical test is to predict both heating loads as well as conditions of both air and water leaving the boiler. Input data come from an experiment which was conducted at the ERS during February 21-28, 2006. Due to a system fault that occurred during the experiment data of February 26, are not available for further analysis. Simulation results will be compared to the measurements.

For boiler empirical test, no data compensation was required. Thus, no raw data are provided. At the beginning, the same perfect control as the comparative test was assumed for this case, i.e., the set point temperature was always achieved in case that the boiler was big enough. In this empirical test, a proportional control was included. The gain was tuned in order to get as closer as possible to the experimental results. The following equations summarize this control strategy.

$$G_{\text{boil}} = 0.21 \quad (3-24)$$

$$x_{\text{load,min}} = 0.1 \quad (3-25)$$

$$x_{\text{load,max}} = 1 \quad (3-26)$$

$$X_{\text{boil,control,1}} = G_{\text{boil}} \cdot (T_{\text{w,ex,boil,set}} - T_{\text{w,ex,boil}}) \quad (3-27)$$

$$X_{\text{boil,control,2}} = \mathbf{Min} ( X_{\text{boil,control,1}}, 1 ) \quad (3-28)$$

$$X_{\text{boil,control}} = \mathbf{Max} ( X_{\text{boil,control,2}}, 0 ) \quad (3-29)$$

$$x_{\text{load}} = x_{\text{load,min}} - X_{\text{boil,control}} \cdot ( x_{\text{load,min}} - x_{\text{load,max}} ) \quad (3-30)$$

Results of this empirical test are summarized in the following chapters:

#### 3.3.2.1 *Leaving water temperature*

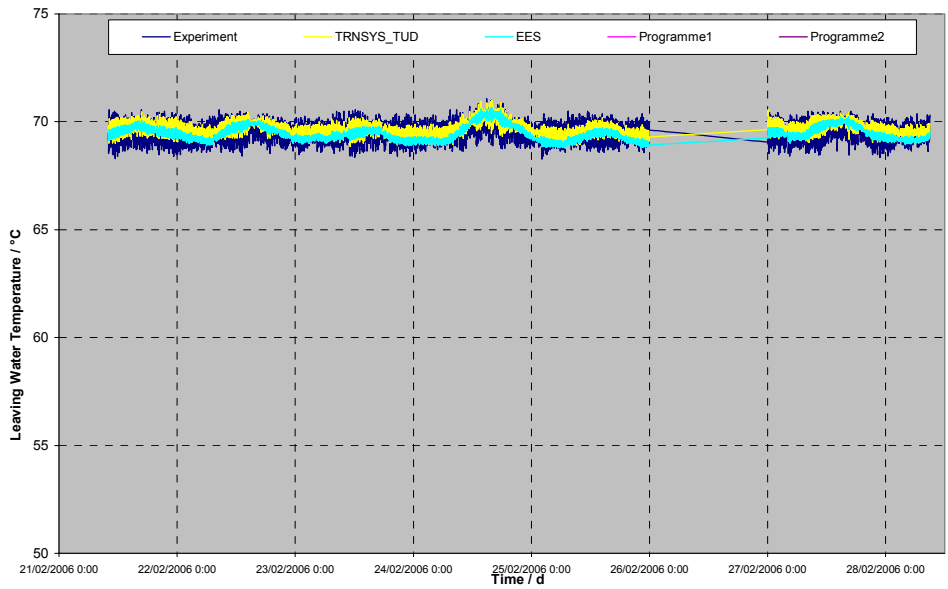


**Figure 3-11 : Leaving water temperature for all the studied period**

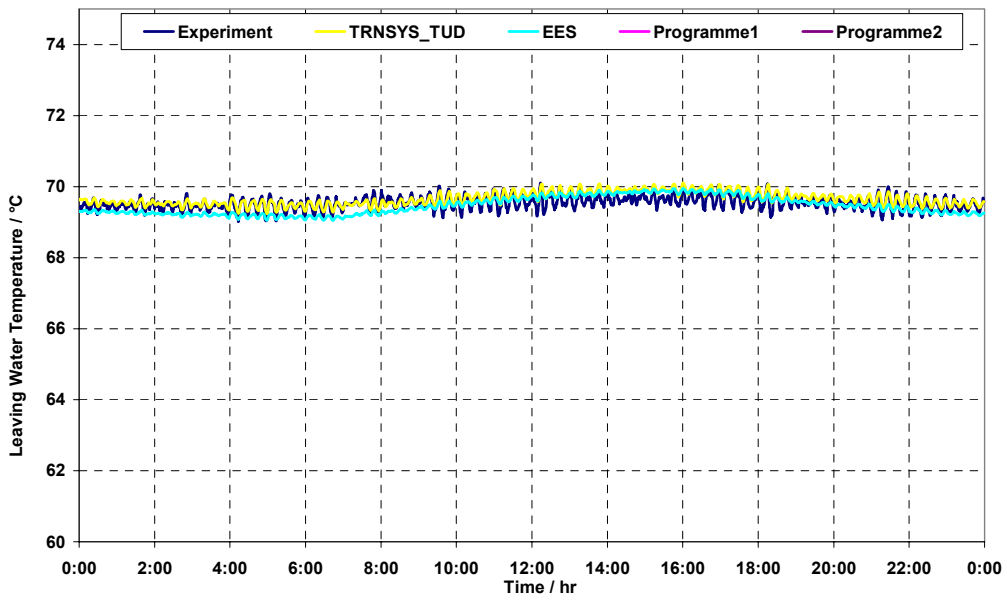


**Figure 3-12 : Averaged daily leaving water temperature**

The results on this variable show a good agreement between both simulations and the experimental results. Nevertheless, this variable does not represent well the ability of the models to predict the boiler performances, since the set point leaving temperature is an input, so the differences are related only to the control hypotheses and not to the accuracy of the models.

The mean leaving water temperature for all the studied period is summarized in Table 3-6 for experimental data and both simulation data.

**Table 3-6 : Mean leaving water temperature in all the studied period**

	Experimental	TRNSYS TUD	EES
Mean Leaving Temperature [°C]	69.54	69.65	69.46

It can be seen from Table 3-6 that the agreement of both simulations and experimental data is good. TRNSYS\_TUD is overpredicting a bit the leaving water temperature, while EES is underpredicting it.

To avoid the influence of the control strategy, the leaving water temperature could be imposed and the control taken out from the simulation for this empirical test.

### 3.3.2.2 Boiler heating power

Figure 3-13 and Figure 3-14 show the variations of the boiler heating power for all the period and in averaged daily values respectively.

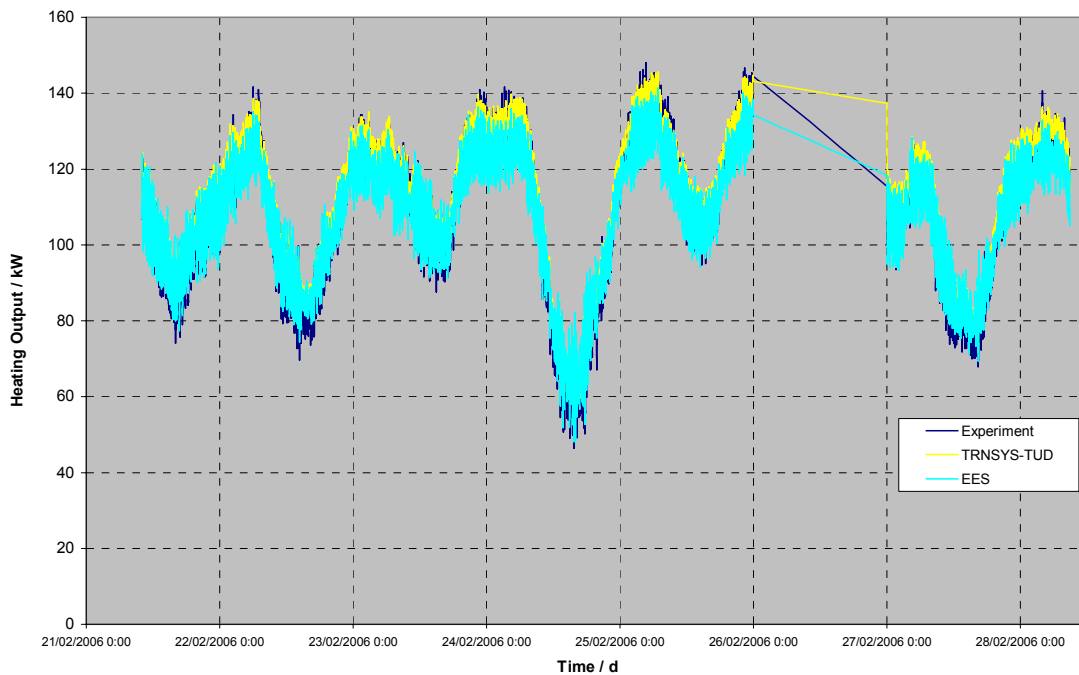


**Figure 3-13 : Boiler heating power for all the studied period**

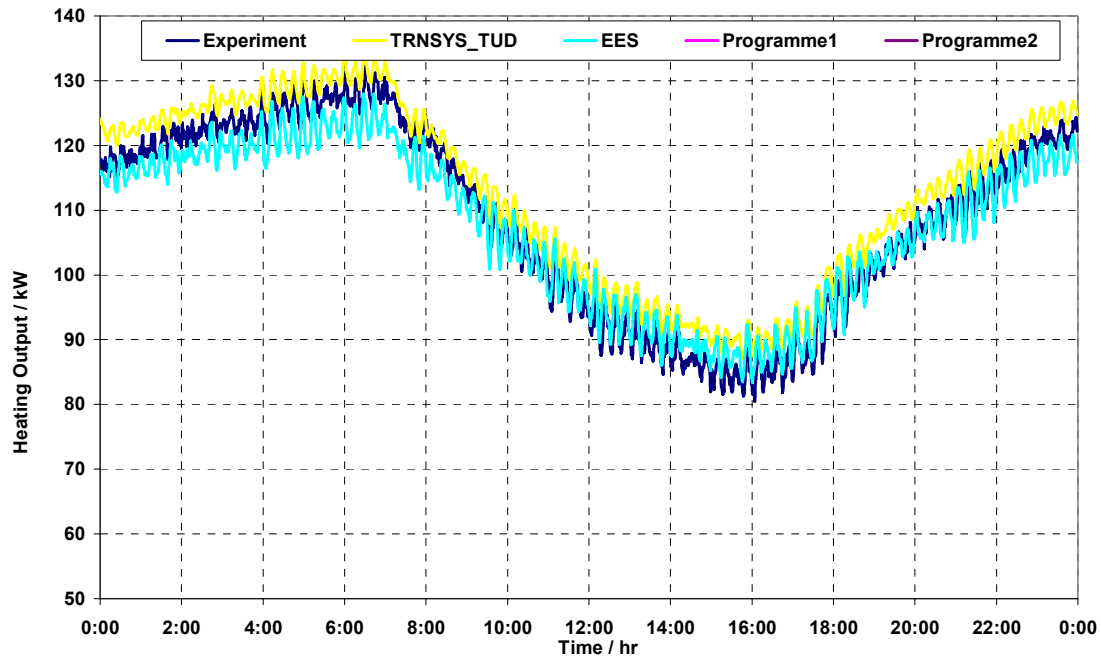


**Figure 3-14 : Averaged daily boiler heating power**

Table 3-7 shows the total heating power of the boiler for the whole period. Obviously, and in agreement with the mean leaving water temperature results, TRNSYS\_TUD overpredicts a bit the boiler heating power, while EES underpredict it.

**Table 3-7 : Total boiler heating power for all the studied period**

	Experimental	TRNSYS TUD	EES
Total boiler heating power [kW]	932.5	966.9	923.5

The same remark as for the leaving water temperature can be made for the boiler heating power, because inputs of the simulation are: the water flowrate, the entering water temperature and the leaving water temperature set point, so the results shown in Figure 3-13 and Figure 3-14 only test the accuracy of the simulated control strategy.

### 3.3.2.3 Natural gas flowrate

As well as for the comparative test, the natural gas flowrate is a good variable in order to test and compare the performance of the models. Figure 3-15 and Figure 3-16 show the behaviour of this variable in the whole period and in averaged daily values respectively. Table 3-8 summarizes the total natural gas consumption of all the period.

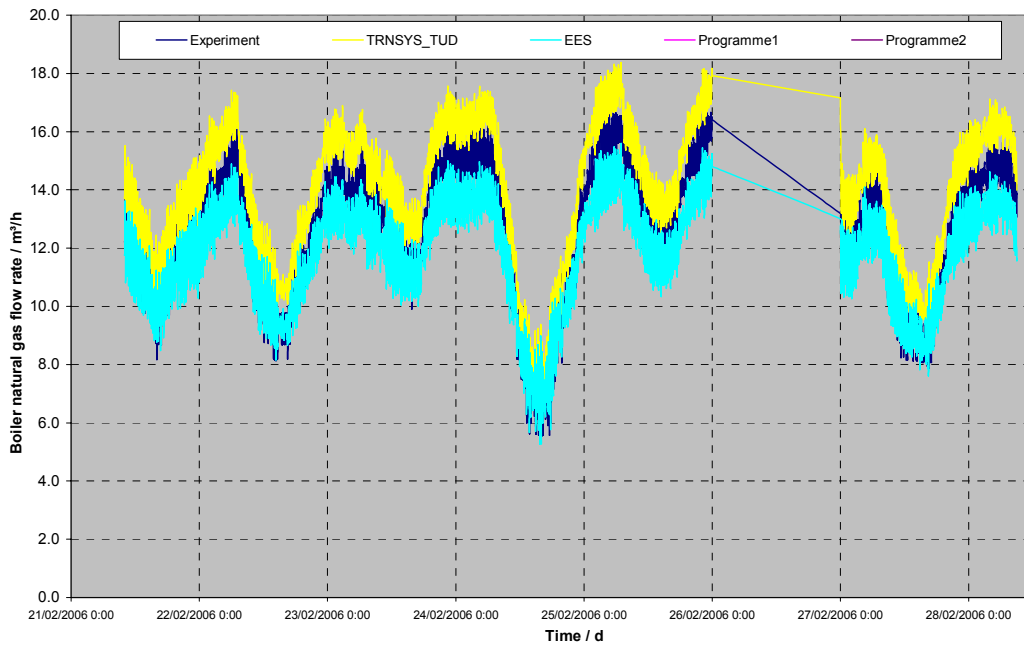


**Figure 3-15 : Natural gas flowrate for all the studied period**

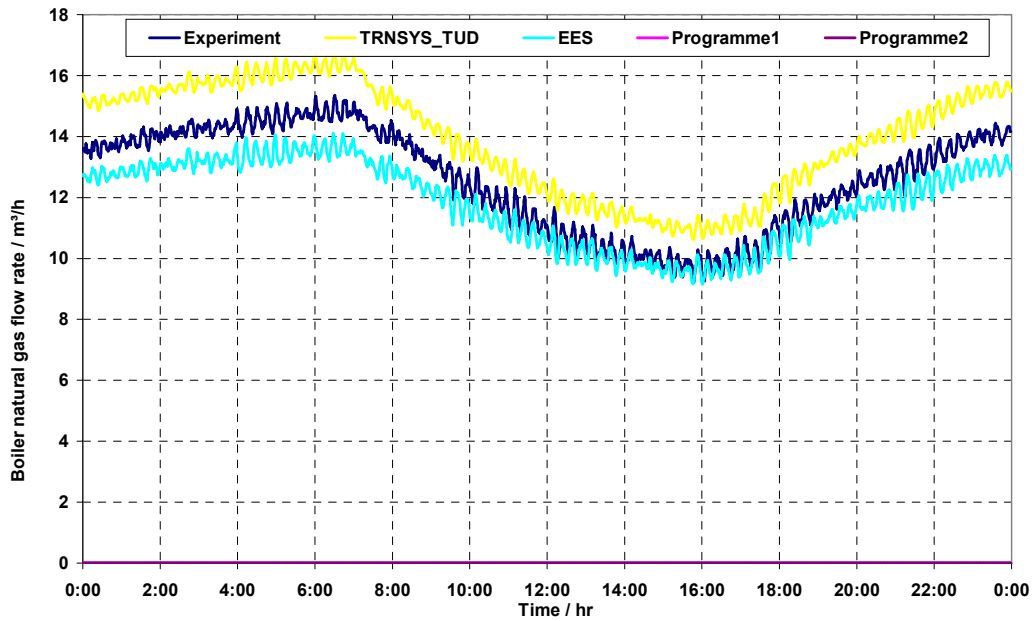


**Figure 3-16 : Averaged daily natural gas flowrate**

**Table 3-8 : Total natural gas flowrate of all the studied period**

	Experimental	TRNSYS TUD	EES
Total natural gas flowrate [m <sup>3</sup> /h]	108037	119498	101531
Deviation [%]	-	10.6	-6.0
Average absolute difference [m <sup>3</sup> /h]	-		0.89
Average relative difference [%]	-		6.90

In general, there is a good agreement between both models and the experimental values. EES is underestimating the total gas flowrate in a 6 %, while TRNSYS\_TUD is overestimating it in a 10.6 %. The average absolute error and average relative error of EES in all the period for this variable is of 0.89 [m<sup>3</sup>/h] and 6.9%. These errors are calculated as follows:

$$ERR [m^3 / h] = \frac{\sum_{i=1}^n |NGFR_{model,i} - NFGR_{meas,i}|}{n} \quad (3-31)$$

$$ERR [%] = \frac{\sum_{i=1}^n \frac{|NGFR_{model,i} - NFGR_{meas,i}|}{NGFR_{meas,i}}}{n} \cdot 100 \quad (3-32)$$

This can be partly explained by the behaviour of the precedent variables. As we already pointed out, a good way to avoid the influence of the control and to evaluate the model, is to include as an input the leaving water temperature. More ahead in the report, these results will be shown.

#### 3.3.2.4 Electrical power

As it was shown in Table 3-4, four points of electrical consumption are available at four different firing rates. Between the minimum, mid range and full firing rate, a lineal interpolation was done in order to have a continuous law that predicts the electrical consumption for all the range of firing rates.

Results are shown in Figure 3-17 and Figure 3-18. Differences between the model and the experiments are summarized in Table 3-9.

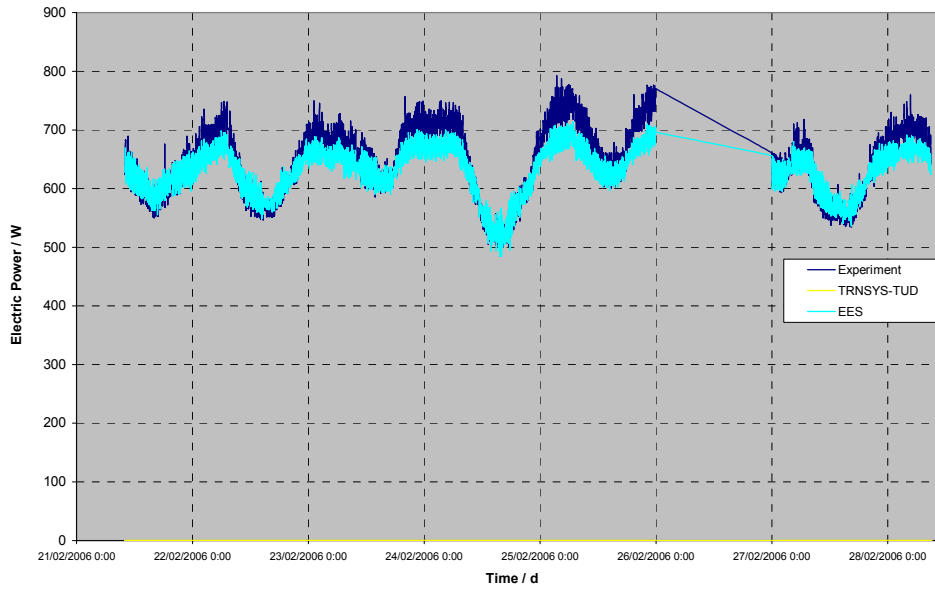


**Figure 3-17 : Electrical power for all the studied period**

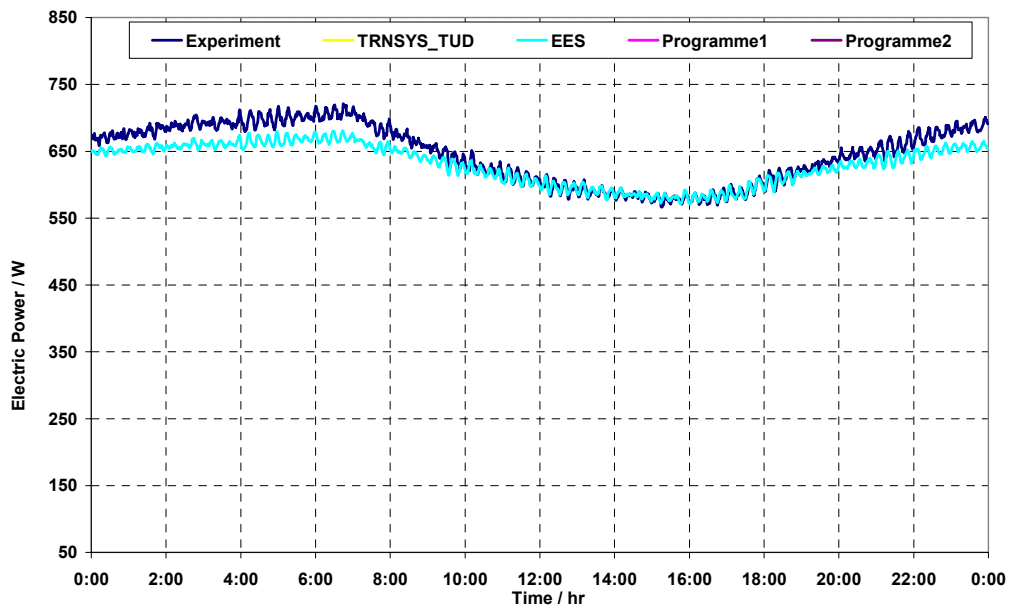


**Figure 3-18 : Averaged daily electric power**

**Table 3-9 : Summary of deviations in the electrical power consumption**

	Experimental	EES
Total electrical power consumption [kW]	5544	5406
Deviation [%]	-	-2.49
Average absolute difference [W]	-	22.69
Average relative difference [%]	-	3.36

The electric power consumption is slightly underpredicted by the model. This is direct consequence of the underprediction of the natural gas flowrate and, therefore, the boiler firing rate.

Maybe, this prediction could be slightly improved if a quadratic was used instead of a linear interpolation. However, this improvement would be very slight as it can be seen in Figure 3-19.

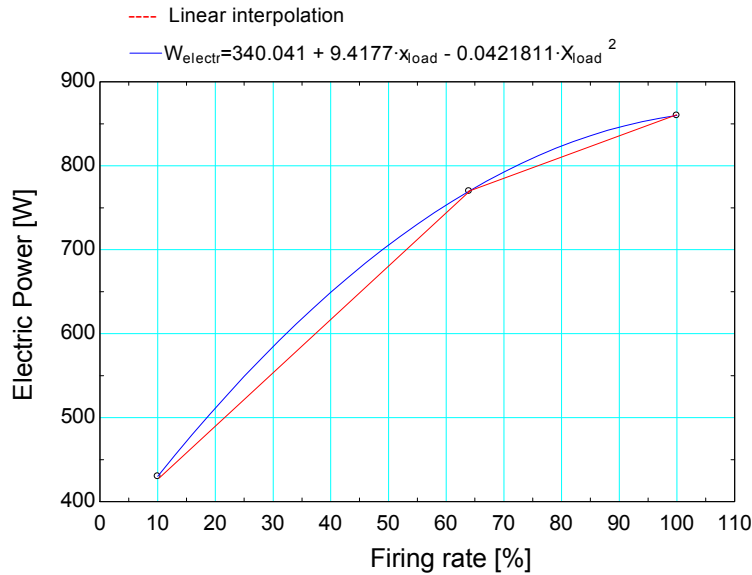


**Figure 3-19 : Electric power consumption vs firing rate in the condensing boiler**

### 3.3.2.5 Flue gas temperature

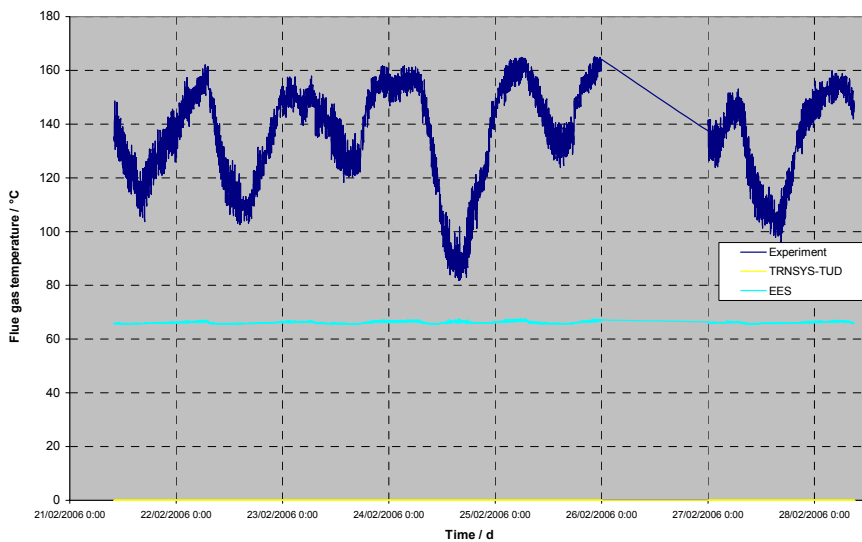


**Figure 3-20 : Flue gas temperature for all the studied period**

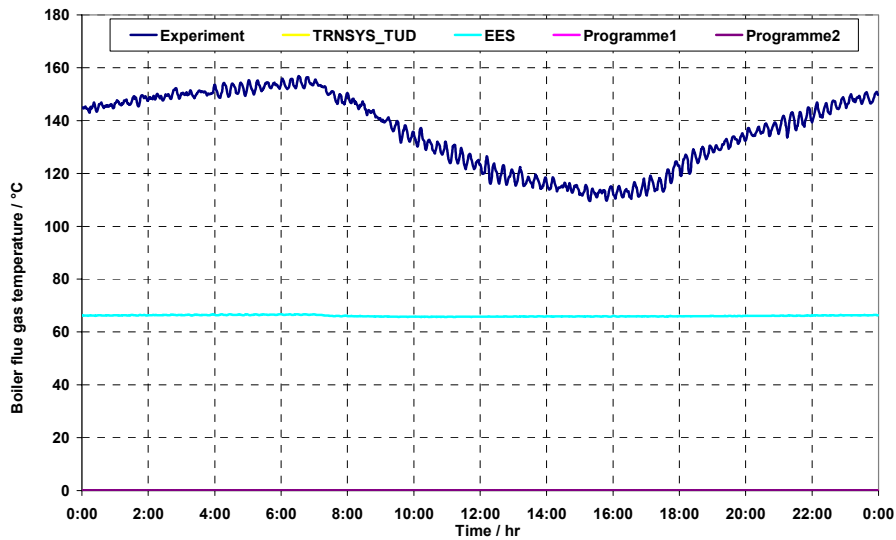


**Figure 3-21 : Averaged daily boiler flue gas temperature**

It can be seen that the flue gas temperature is underpredicted by the model. This can be explained by a bad tuning of it and an overestimation of the AU values of the heat exchangers (especially the wet heat exchanger), what conduce to a very high approximation of the flue gas temperature to the entering water temperature.

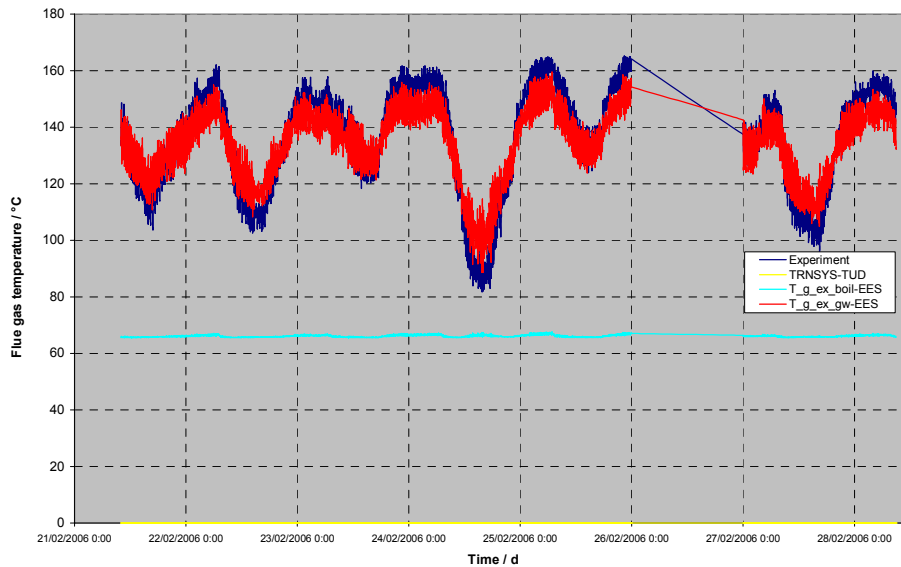


**Figure 3-22 : Flue gas temperature behaviour**

In Figure 3-22, it can be seen that the gas temperature at the exhaust of the dry heat exchanger ( $T_{g\_ex\_gw-EES}$ ) has relatively a good agreement with the experimental flue gas temperature (in magnitude and trend), but at the exhaust of the wet heat exchanger ( $T_{g\_ex\_boil-EES}$ ) is clearly underpredicted. This is the reason for which it was affirmed that the AU of the wet heat exchanger was the one more overpredicted, because is precisely, in this heat exchanger where the flue temperature diminishes to values near the water entering

temperature as it can be seen in Figure 3-23 where the maximum difference between the flue gas temperature and the water supply temperature arise to 5°C. This is also reaffirmed with the effectiveness obtained for the coil which ranges between 92 and 99% in the simulation (clearly overpredicted).

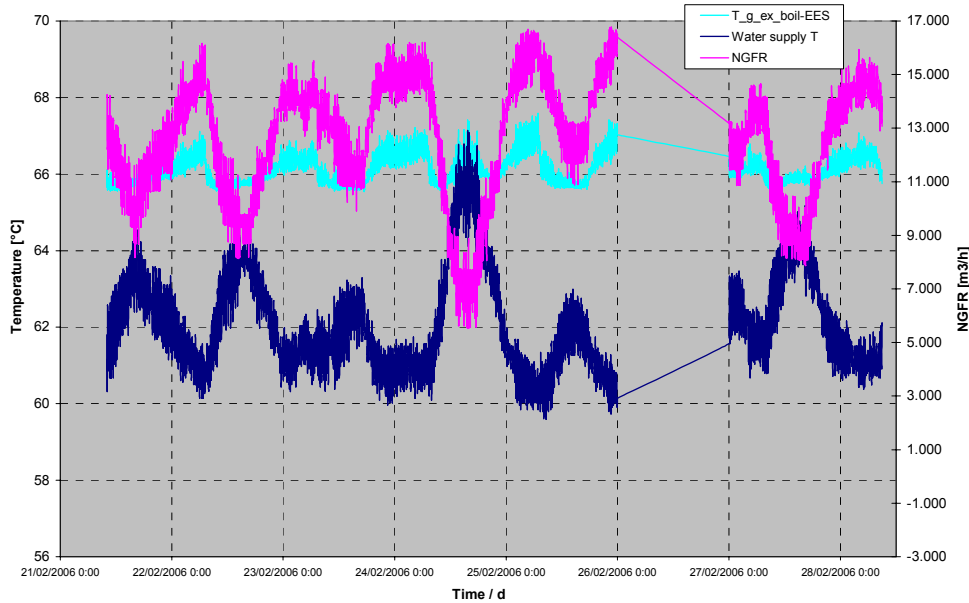


**Figure 3-23 : Superposition of boiler water supply temperature, flue gas temperature and natural gas flowrate**

At this point, someone could ask himself, why the heat balance at the water side (temperatures and flowrates) and the natural gas flowrate have a good agreement with the experiments and the flue gas temperature does not. The answer is that an error of approx.  $\pm 5\%$  in the prediction of the fuel flowrate or firing rate (the average absolute error was of 6.9%), produces an error in the flue gas temperature of more than 150 [K]. Let's see a brief example to illustrate this with typical values of the test:

$$\begin{aligned} Q_{\dot{u}_{\text{boil}}} &= 107274 \text{ [W]} \\ Q_{\dot{c}_{\text{HHV}}} &= 123159 \text{ [W]} \\ Q_{\dot{c}_{\text{LHV}}} &= 110685 \text{ [W]} \end{aligned}$$

An error of  $\pm 5\%$  in the prediction of the fuel flowrate means that  $Q_{\dot{c}_{\text{LHV}}}$  ranges between 105150 [W] and 116219[W]. This means that the loss power  $Q_{\dot{\text{loss}}} = Q_{\dot{c}_{\text{LHV}}} - Q_{\dot{u}_{\text{boil}}}$  ranges between 0 [W] and 8945 [W]. Now, this loss power can be expressed approx. by:

$$Q_{\dot{\text{loss}}} = C_{\dot{g}} \cdot (t_{\text{ex}_g} - t_{\text{su}_g}) \text{ with } t_{\text{su}_g} = 20^\circ\text{C. So, resolving the equation, we have that } t_{\text{ex}_g} \text{ can vary between } 20^\circ\text{C and } 169^\circ\text{C.}$$

Regarding the whole empirical test, it is important to point out that, unfortunately, at no moment, condensation did occur. This makes that no validation of the whole model can be performed with this data. In fact, only a dry heat exchange is always occurring in the boiler, so is the same phenomenon that occurs in a classical boiler.

Moreover, we can demonstrate with Figure 3-24 that with the manufacturer data is impossible to reach a good tuning and information is missing to tune the parameters in a correct way.

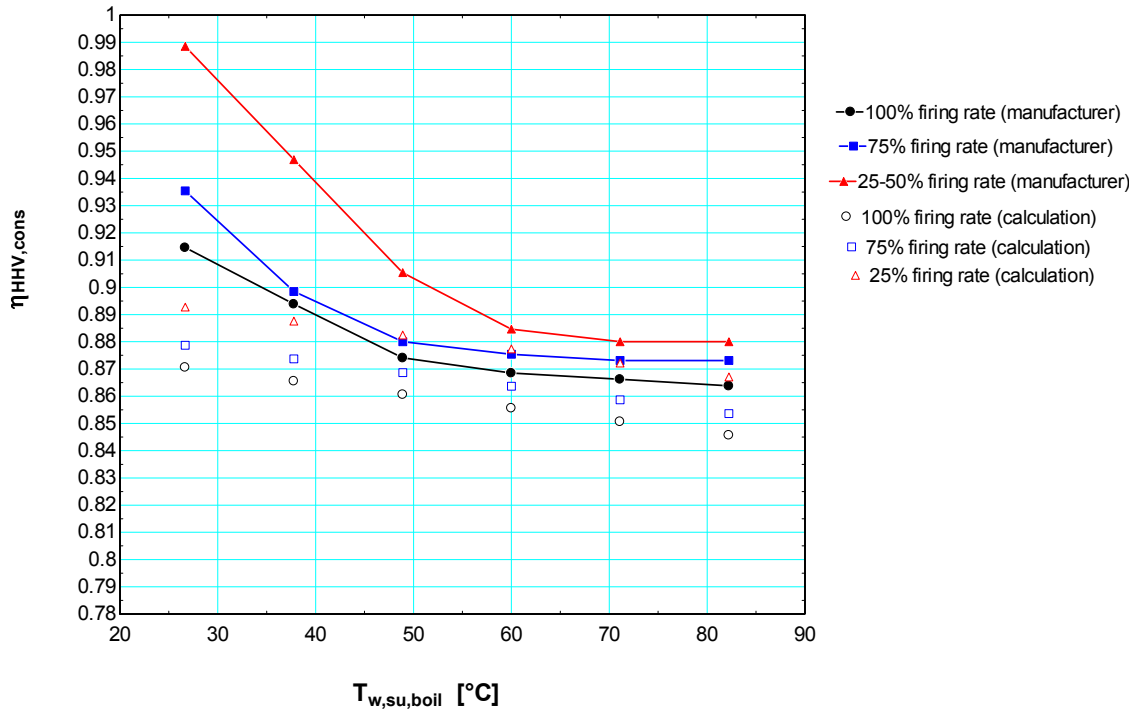


**Figure 3-24 : Evolution of the measured and calculated (with a classical boiler model) boiler efficiency**

This simulation was done with a classical boiler without condensation model (as was the case of the empirical test). In all these points, the effectiveness of the heat exchanger is more than 96%. In fact, for a firing rate of 25-50 % the effectiveness is more than 99% (see Table 3-10) and even in this case, the overall boiler efficiency is not reached. This means that the manufacturer data is not accurate enough or that some information is missing. For example, the catalogue does not specify accurately the fuel used to obtain these results and maybe is different as the one used in the Empirical Test. In other words, we don't have the enough information to tune the model with the manufacturer data. So, we are going to make the parameter identification of the model with the available experimental information.

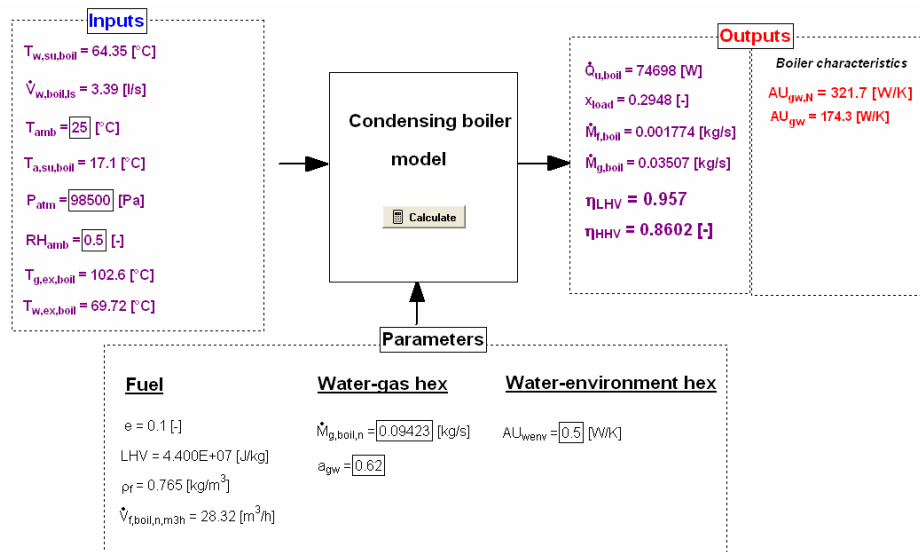
**Table 3-10 : Information of the simulation done with a classical boiler model in order to fit the manufacturer data**

i	x_load [-]	$T_{w,su,boil\_F}$ [°F]	$T_{w,su,boil}$ [°C]	eta_HHV [-]	eta_HHV_manuf [-]	epsilon_gw [-]
1	1	80	26.67	0.8706	0.9146	0.9675
2	1	100	37.78	0.8656	0.8938	0.9673
3	1	120	48.89	0.8606	0.8741	0.9672
4	1	140	60	0.8556	0.8685	0.9671
5	1	160	71.11	0.8507	0.8662	0.967
6	1	180	82.22	0.8457	0.8638	0.9668
7	0.75	80	26.67	0.8787	0.9354	0.9782

8	0.75	100	37.78	0.8737	0.8985	0.9781
9	0.75	120	48.89	0.8687	0.88	0.978
10	0.75	140	60	0.8637	0.8754	0.978
11	0.75	160	71.11	0.8587	0.8731	0.9779
12	0.75	180	82.22	0.8536	0.8731	0.9778
13	0.25	80	26.67	0.8927	0.9885	0.997
14	0.25	100	37.78	0.8876	0.9469	0.997
15	0.25	120	48.89	0.8825	0.9054	0.997
16	0.25	140	60	0.8774	0.8846	0.997
17	0.25	160	71.11	0.8722	0.88	0.997
18	0.25	180	82.22	0.8671	0.88	0.997

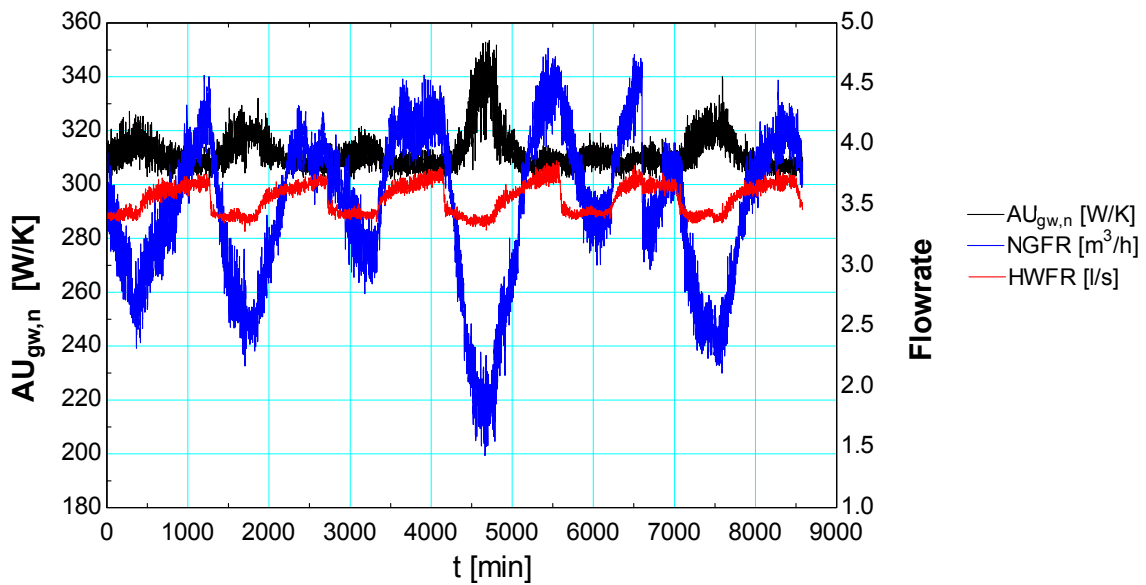
Tuning with experimental data

Due to the fact that no condensation occurs during the experiments, the model was tuned without using the cooling coil model, i.e., it was used a classical boiler model with only the dry heat exchanger. In this tuning, the leaving water temperature was an input in order to avoid the influence of the control strategy. Also, the flue gas temperature was an input in order to identify the overall heat transfer coefficient in nominal conditions  $AU_{gw\_n}$  that is the main parameter of the reference boiler model. A scheme of this parameter identification is shown in Figure 3-25.

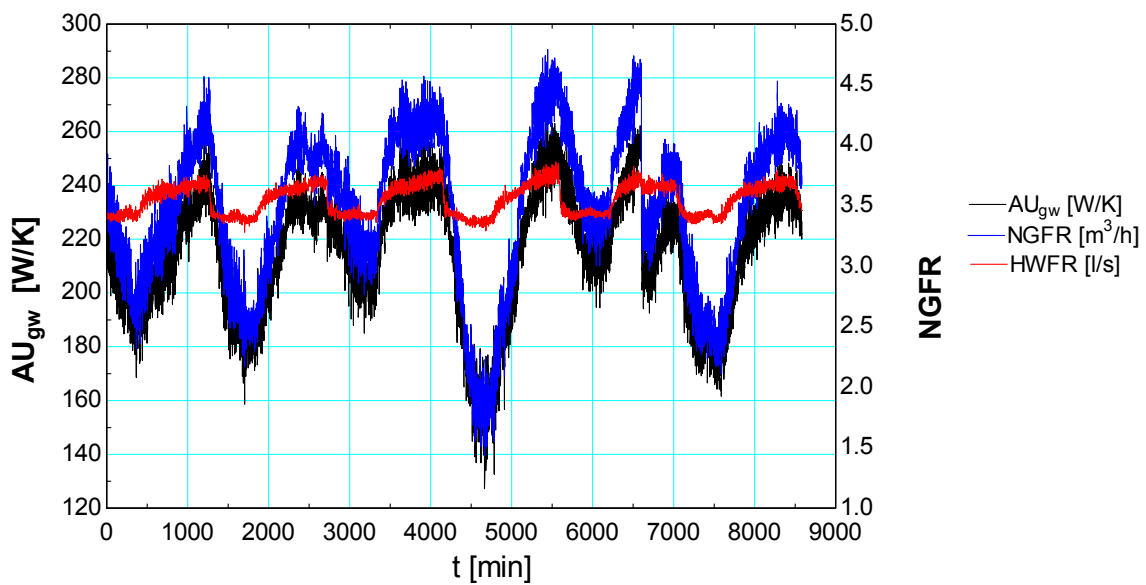


**Figure 3-25 : Scheme of the parametric identification of the boiler with the experimental data**

The results of this identification simulation are shown in Figure 3-26, 3-27 and 3-28

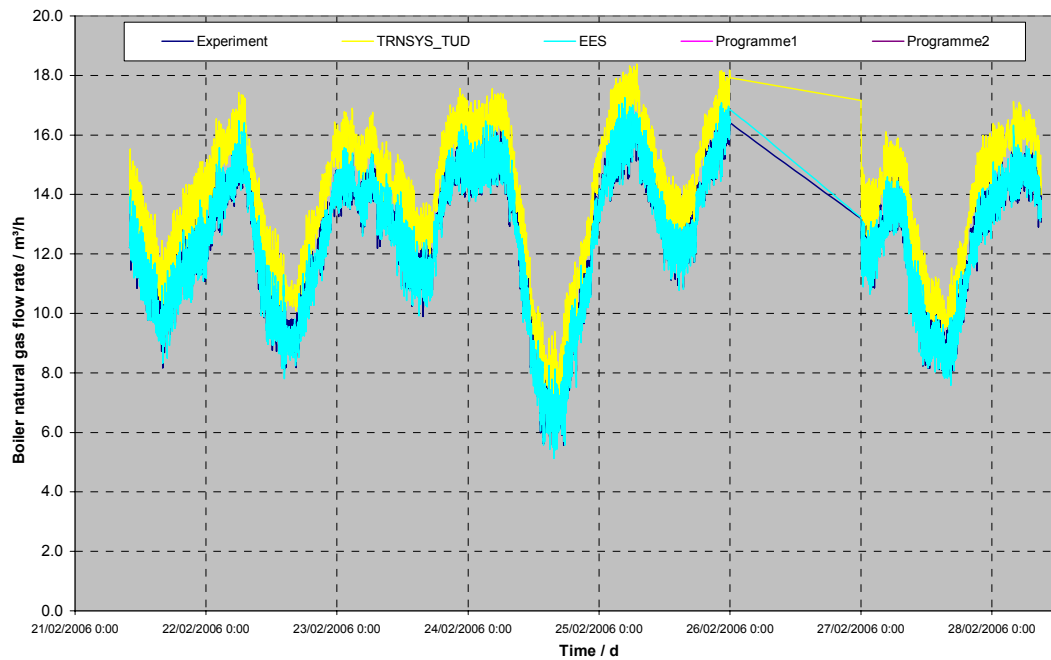


**Figure 3-26 : Evolution of the  $AU_{gw,n}$ , Natural gas Flowrate and Heating Water Flowrate during the whole period**



**Figure 3-27 : Evolution of the  $AU_{gw}$ , Natural gas Flowrate and Heating Water Flowrate during the whole period**

In Figure 3-26, it can be seen that the identified overall heat transfer coefficient in nominal conditions is relatively constant during the period and ranges between 310 and 320 [W/K] with the exception of the period between  $t = 4500$  and  $4900$  [min] (12:00 and 20:00 of 24/02/2007), period in which the outside air temperature arises over  $16^{\circ}\text{C}$  and also the entering water temperature over  $67^{\circ}\text{C}$ . This period is also the one in which the NGFR and HWFR are the lowest.



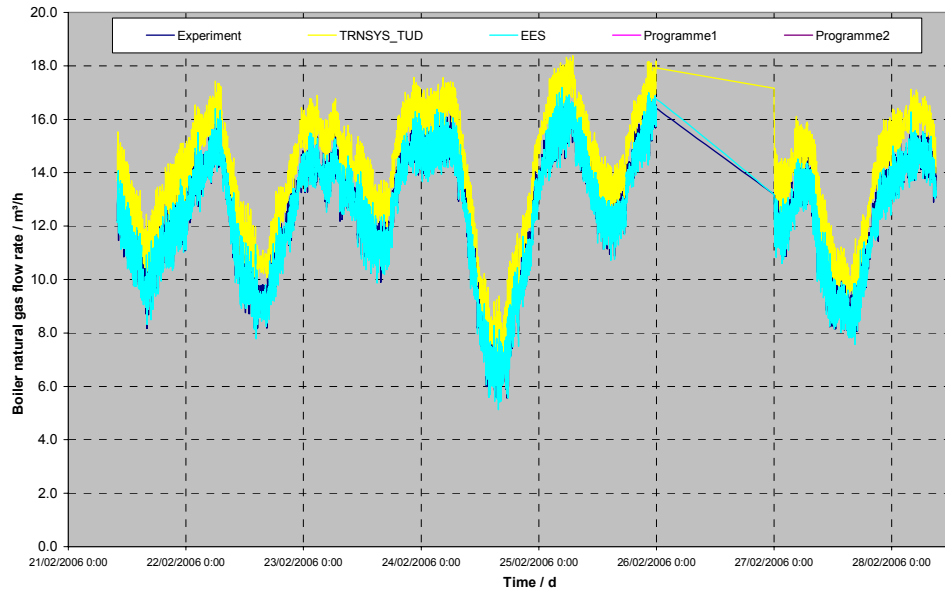
**Figure 3-28 : Natural gas flowrate for all the studied period with the parameter identification model**

Figure 3-28 shows that with the flue gas temperature as input and therefore using the identified (and relatively constant)  $AU_{gw,n}$  the model predicts in a good way the firing rate or natural gas flowrate. The average absolute error is of 2,2 %.

So, now that the parameter identification has been done with the experimental results, another simulation was done taking the average  $AU_{gw,n}$  of 320 [W/K] obtained in the latter parameter identification. The results are shown below.

### Natural gas flowrate

Figure 3-29 and Figure 3-30 show the evolution of the natural gas flowrate and Table 3-11 summarizes the deviations between the model and the experiments



**Figure 3-29 : Evolution of the natural gas flowrate**

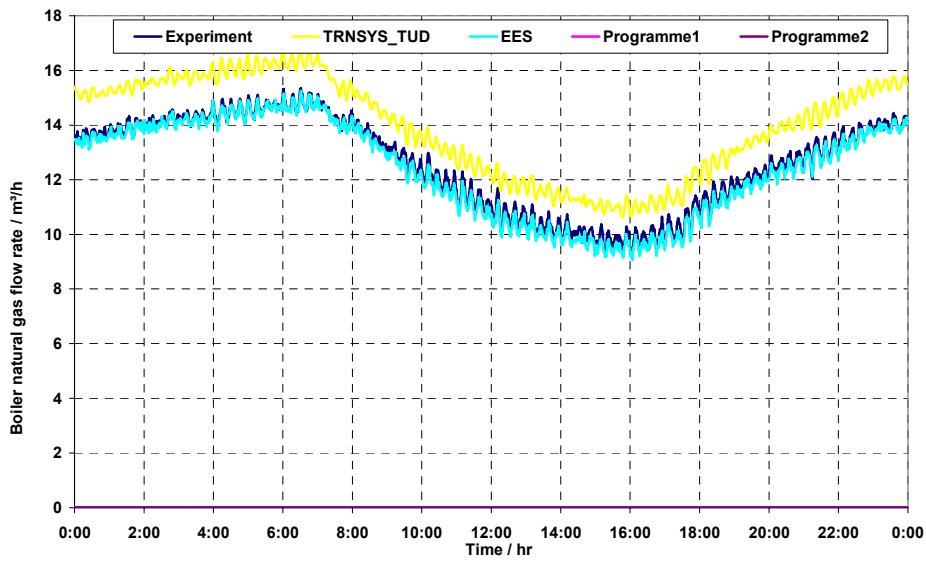


**Figure 3-30 : Averaged daily natural gas flowrate**

**Table 3-11 : Summary of deviations between the simulation and experimental data**

	Experimental	EES
Total natural gas flowrate [m <sup>3</sup> /h]	108037	106409
Deviation [%]	-	-1.5
Average absolute difference [m <sup>3</sup> /h]	-	0.29
Average relative difference [%]	-	2.41

It can be seen that with the new identified parameters, the results on the natural gas flowrate have improved. The deviation on the total consumption over the period predicted by the model diminished from -6% to -1.5%. Also, the average absolute and relative errors diminish from 0.89 [m<sup>3</sup>/h] to 0.29 [m<sup>3</sup>/h] and from 6.90 [%] to 2.41 [%] respectively.

Electrical power

Figure 3-31 and Figure 3-32 show the evolution of the electrical power and Table 3-12 summarizes the deviations between the model and the experiments

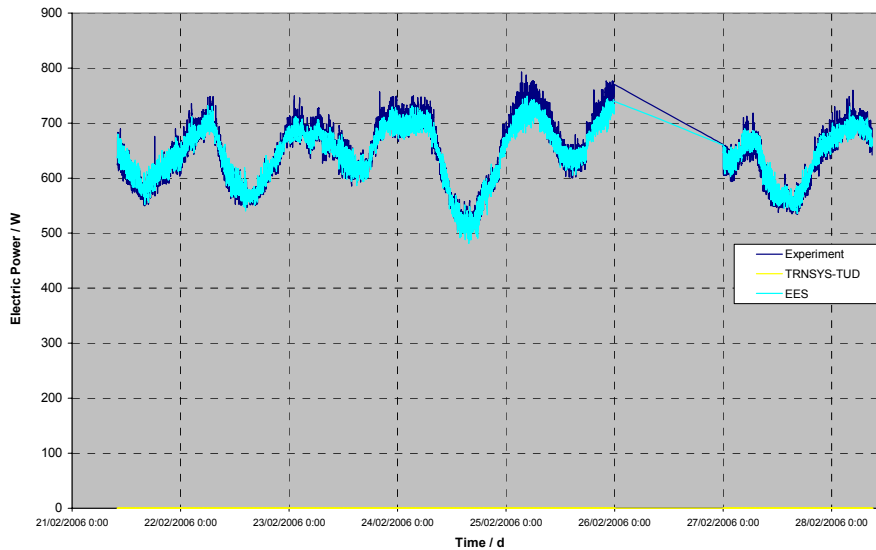


**Figure 3-31 : Electrical power for all the studied period**

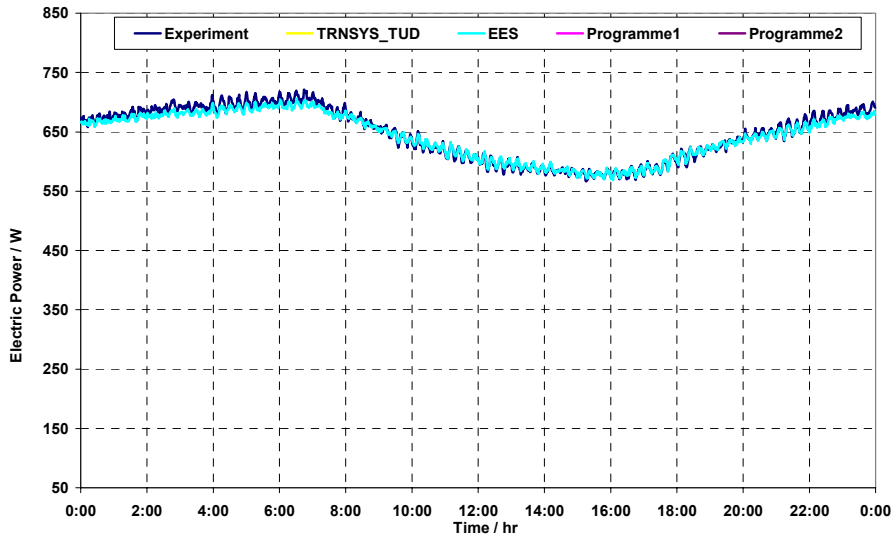


**Figure 3-32 : Averaged daily electric power**

**Table 3-12 : Summary of deviations in the electrical power prediction**

	Experimental	EES
Total electrical power consumption [kW]	5544	5515
Deviation [%]	-	-0.52
Average absolute difference [kW]	-	11.10
Average relative difference [%]	-	1.68

The results on the electrical power have improved. The deviation on the total electrical consumption in the period predicted by the model diminishes from -2.49 % to -0.52 %. Also, the average absolute and relative errors diminish from 22.69 [W] to 11.10 [W] and from 3.36 [%] to 1.68 [%] respectively. This is a direct consequence of the better prediction of the natural gas flowrate and therefore the firing rate.

Flue gas temperature

Figure 3-33 and Figure 3-34 show the evolution of the flue gas temperature over the whole period with the new identified parameters.

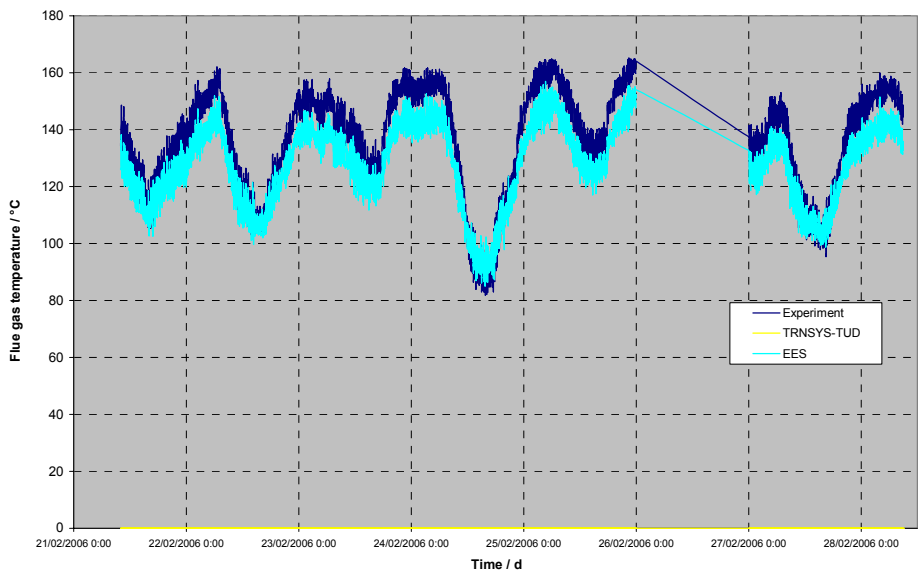


**Figure 3-33 : Evolution of the flue gas temperature for all the period**

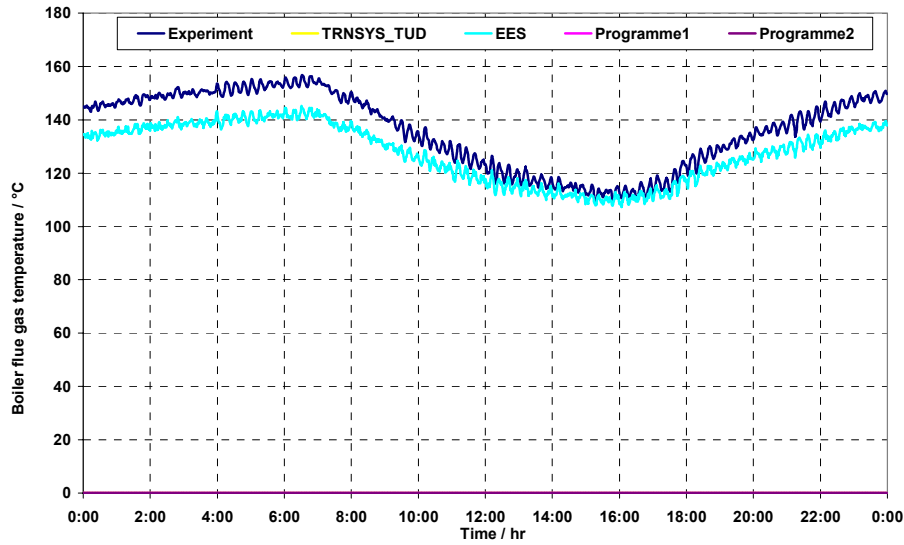


**Figure 3-34 : Averaged daily flue gas temperature**

The average absolute difference in the prediction of this variable is of 8.64 [K] calculated as follows:

$$ERR [K] = \frac{\sum_{i=1}^n |FGT_{model,i} - FGT_{meas,i}|}{n} \quad (3-33)$$

It can be seen that the flue gas temperature predicted by the model has now a good agreement with the experimental one, not only in trend but also in order of magnitude. However, it is slightly underpredicted by the model. This is due to the slight underprediction of the gas flowrate. We have already pointed out that a small deviation in the firing rate or gas flowrate has a big impact in the flue gas temperature.

In order to improve the model, it must be taken into account the variation of the heat transfer coefficient with the variation of the water flowrate. So, instead of an overall heat transfer coefficient varying with the gas mass flowrate, it should be modeled with the typical 3 resistances in series, as it was explained in Chapter 2. In this case, the resistances are: the convective resistance on the gas side, the conduction resistance of the metal and the convective resistance on the water side. This gives:

$$\frac{1}{AU_{boiler}} = R_{g,boiler} + R_{m,boiler} + R_{w,boiler}$$

With:

$$R_{g,boiler} = R_{g,boiler,n} \cdot \left[ \frac{\dot{M}_{g,boiler,n}}{\dot{M}_{g,boiler}} \right]^{0.62}$$

$$R_{w,boiler} = R_{w,boiler,n} \cdot \left[ \frac{\dot{M}_{w,boiler,n}}{\dot{M}_{w,boiler}} \right]^{0.8}$$

The Wilson-plot method (Wilson, 1915) may be used here to calculate the heat transfer resistance on the water-side. This method consists in plotting the overall heat transfer resistance as a function of  $\dot{M}_1^{-n}$  for a constant mass flow rate of the other fluid  $\dot{M}_2$ . Provided the exponent  $n$  is chosen correctly, the points should fall on a straight line. All the experimental points are obtained with water flow rates very close to each other and by gas flow rates between 0.021 and 0.072 [kg/s]. The evolution of the overall heat transfer resistance with  $K_w$  (defined as the gas mass flow rate exponent (-0.62)) for these points is given in Figure 3-35. Two sources of information can be drawn from the Wilson-plot method:

1. If the line is extrapolated to  $K_w = 0$  ( $\dot{M}_g \rightarrow \infty, R_g \rightarrow 0$ ), the intersection with the R-axis gives the value of the metal plus water-side resistance ( $R_w + R_m$ ). Making a linear curve fit, the metal plus water-side resistance appears to be close to 0.0006838 K/W. The range of water mass flow rates is not wide enough to identify clearly any dependency between this total resistance and the water mass flow rate. Consequently, it is not possible to distinguish between the water-side and metal resistance.
2. The nominal gas-side resistance can be identified from the slope of the linear regression. The slope associated to the linear fit is 0.000633338. Hence, the nominal water-side resistance can be computed by:

$$R_{g,n} = \frac{0.000633338}{\dot{M}_{g,boiler,n}^{0.62}}$$

The identified nominal gas-side resistance  $R_{g,n}$  is **0.002744 K/W**.

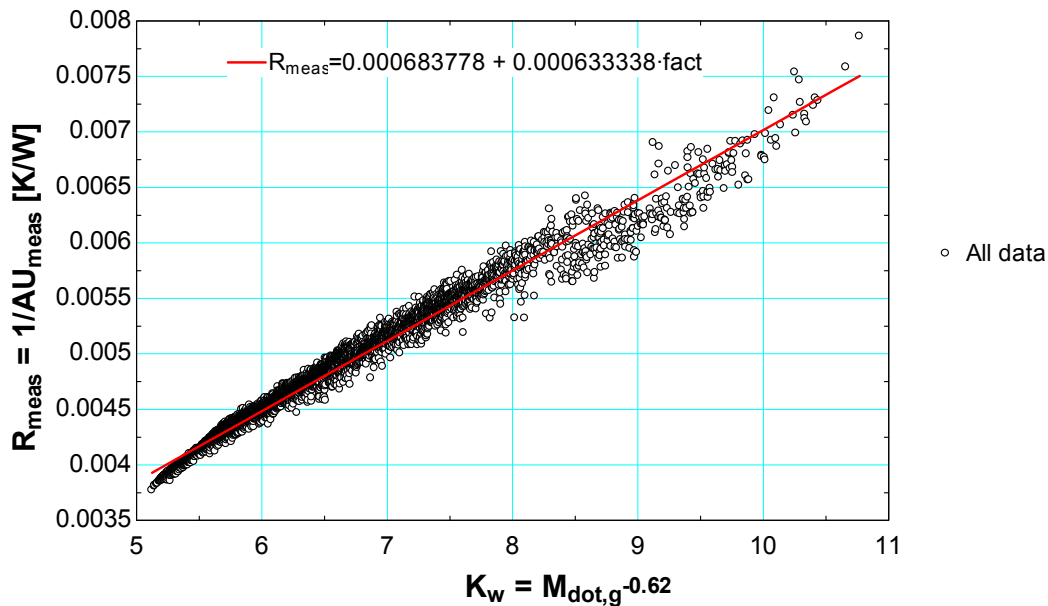


**Figure 3-35 : Evolution of the overall heat transfer resistance with the gas flow rate exponent -0.62 (all the data plotted)**

## 4 Heating coil

### 4.1 Description of the model

The modeling of the heating coil is similar to the one of the cooling coil. Here also, the model treats the coil as a one-zone counter-flow heat exchanger. All the equations are exactly the same as for the cooling coil in dry regime.

### 4.2 Parameters identification

#### 4.2.1 “Nominal” point given by the manufacturer (comparative test)

##### 4.2.1.1 Consistency of the point

For the comparative tests, the only information which can be used to identify the parameters of the model is the nominal performance point given by the manufacturer. This point is detailed in Table 4-1.

**Table 4-1 Cooling coil performance data (Data marked with \* were calculated and are not part of the equipment submittal)**

Heating Coil Performance		
Barometric pressure *	kPa	101.3
Supply Air Temperature	°C Dry bulb	4.44
Supply Air Relative Humidity *	%	50
Supply Air Moisture *	kg/kg	0.00259
Supply Air Density *	kg/m <sup>3</sup>	1.27
Exhaust Air Temperature	°C Dry bulb	37.78
Exhaust Air Moisture *	kg/kg	0.0026
Exhaust Air Density *	kg/m <sup>3</sup>	1.13
Air Flow Rate at coil leaving air conditions *	m <sup>3</sup> /h	5780
Air Pressure Drop	kPa	0.0498
Entering Liquid Temp.	°C	82.28
Leaving Liquid Temp.	°C	71.06
Liquid Flow (pure water)	l/s	1.33
Liquid Pressure Drop	kPa	3.67
Total Cooling Capacity	kW	61

The *heating capacity* is calculated on the water side by (the subscript *r* denotes here *water*):

$$\dot{Q}_{\text{coil}} = \dot{C}_{r,\text{coil}} \cdot (T_{r,\text{su,coil}} - T_{r,\text{ex,coil}}) \quad (4-10)$$

With the water capacity flow rate defined as:

$$\dot{C}_{r,\text{coil}} = \dot{M}_{r,\text{coil}} \cdot c_{p,r,\text{coil}} \quad (4-11)$$

The water mass flow rate is expressed as a function of the water volume flow rate and the water density:

$$\dot{M}_{r,\text{coil}} = \dot{V}_{r,\text{coil}} \cdot \rho_{r,\text{coil}} \quad (4-12)$$

A total capacity of 60801 W is calculated, which corresponds to the value given in Table 4-1. Values of the main variables involved in this calculation are listed in Table 4-2.

**Table 4-2 Values of the variables involved in the total cooling capacity calculation**

---

$C_{\text{dot}_r_{\text{coil}}}$	=5429 [J/m <sup>3</sup> -K]
$c_{p_r_{\text{coil}}}$	=4191 [J/kg-K]
$M_{\text{dot}_r_{\text{coil}}}$	=1.295 [kg/m <sup>3</sup> ]
$Q_{\text{dot}_{\text{coil}}}$	=60801 [W]
$\rho_{r_{\text{coil}}}$	=973.8 [kg/m <sup>3</sup> ]
$T_{r_{\text{ex}_{\text{coil}}}}$	=71.1 [C]
$T_{r_{\text{su}_{\text{coil}}}}$	=82.3 [C]
$V_{\text{dot}_r_{\text{coil}}}$	=0.00133 [m <sup>3</sup> /s]

---

The *air mass flow rate* is not given by the manufacturer, but is calculated from the energy balance on the air-side:

$$\dot{Q}_{\text{coil}} = \dot{M}_{a,\text{coil}} \cdot (h_{a,\text{ex,coil}} - h_{a,\text{su,coil}}) \quad (4-13)$$

The inlet and outlet air specific enthalpies are calculated for humid air, with the pressure, and the dry- and wet-bulb temperatures:

$$h_{a,\text{su,coil}} = h ('AirH2O', T_{a,\text{su,coil}}, P = P_{\text{atm}}, R = RH_{\text{su,coil}}) \quad (4-14)$$

$$h_{a,\text{ex,coil}} = h ('AirH2O', T_{a,\text{ex,coil}}, P = P_{\text{atm}}, R = RH_{\text{ex,coil}}) \quad (4-15)$$

The air mass flow rate is converted into volume flow rate (expressed conventionally at outlet coil conditions) by:

$$\dot{M}_{a,\text{coil}} = \dot{V}_{a,\text{coil}} \cdot \rho_{a,\text{ex,coil,meas}} \quad (4-16)$$

$$\dot{V}_{a,coil,m3h} = \dot{V}_{a,coil} \cdot 3600 \quad (4-17)$$

The calculated air volume flow rate (5748 m<sup>3</sup>/h) only slightly differs from the value given in Table 2-1 (difference of 0.55%).

**Table 4-3 Values of the variables involved in the air flow rate calculation**

---

$h_{a\_ex\_coil}$	=44581 [J/kg]
$h_{a\_su\_coil}$	=10900 [J/kg]
$\dot{M}_{a\_coil}$	=1.805
$RH_{ex\_coil}$	=0.06414
$RH_{su\_coil}$	=0.5
$t_{a\_ex\_coil}$	=37.7 [C]
$t_{a\_su\_coil}$	=4.4 [C]
$v_{a\_ex\_coil}$	=0.8844 [m <sup>3</sup> /kg]
$v_{a\_su\_coil}$	=0.7897 [m <sup>3</sup> /kg]

---

#### 4.2.1.2 Procedure for identifying the parameters

Since only one performance point is available, the parameters of the model are identified by imposing both the ratio between the air- and water-side resistances and the ratio between the metal and the air-side resistances. As for the cooling coil, these two ratios are chosen according to good practice rules:

- The air-side resistance is supposed to be 10% higher than the water-side resistance. Actually, following a simple design rule, the resistances on both sides should be equal. The air-side resistance is usually reduced by using fins, so that it is closer to the water-side resistance.
- The metal resistance is fixed at 5% of the air-side resistance. Actually, the metal resistance is usually small. However, nominal performances of the coil sometimes account for some fouling in the water piping. This fouling fictitiously results in a higher metal resistance.

Results obtained by imposing these two resistances ratios are shown in Figure 4-1. The heating capacity is implicitly imposed since the water flow rate as well as inlet and outlet temperatures are inputs. The model calculates the outlet air temperature.

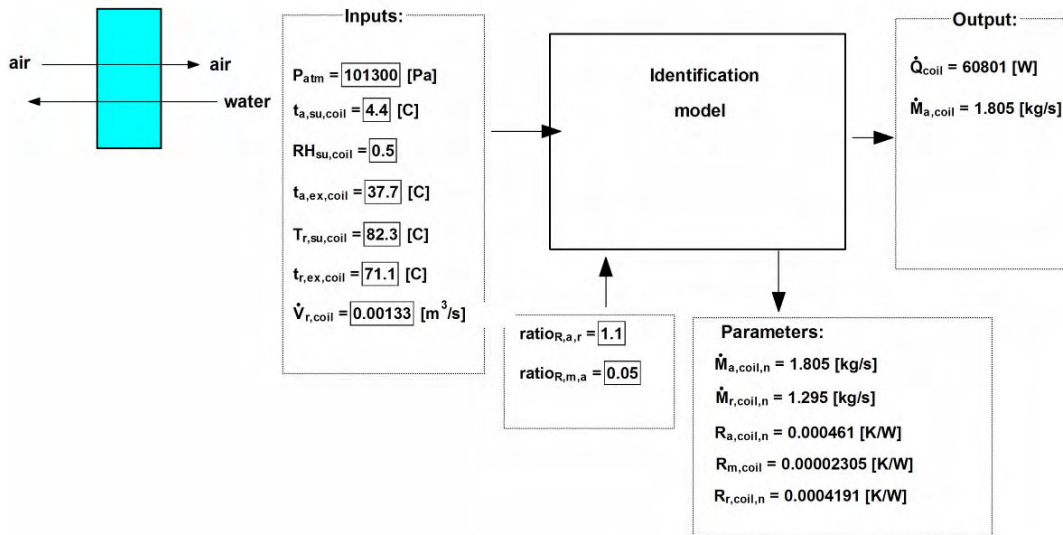


**Figure 4-1 Identification of the parameters of the model on the basis of the nominal point (parameters used for the comparative tests)**

#### 4.2.2 Quasi steady-state points extracted from experimental data (empirical tests)

In addition to the nominal performance point given by the manufacturer, two quasi-steady state points have been extracted from the experimental data and can be used to calibrate the heating coil model. These two points are given in Table 4-4.

**Table 4-4 Quasi-steady state points based on experimental data for the empirical test (Data marked with \*) have been calculated and are not part of the recorded experimental data)**

Heating Coil Performance		#1	#2
Barometric pressure*)	kPa	99.0	97.7
Entering Air Temp.	°C	0.1	16.2
Leaving Air Temp.	°C	25.1	23.0
Leaving Air Moisture	kg/kg	0.00187	0.00389
Leaving Air Density*)	kg/m <sup>3</sup>	1.16	1.15
Air Flow Rate at coil leaving air conditions*)	m <sup>3</sup> /h	5470	5460
Entering Liquid Temp.	°C	69.3	69.9
Leaving Liquid Temp.	°C	50.9	37.4
Mixing Liquid Temp.	°C	62.2	67.9

Liquid Flow*)	l/s	0.59	0.09
Total Heating Capacity*)	kW	44.1	12.2

#### 4.2.2.1 Consistency of the points

Before attempting to use the points given in Table 4-4 for identifying the parameters of the heating coil model, their consistency is checked. This is done by comparing the heating capacities measured on both sides. As shown in Figure 4-2, the agreement is very good.

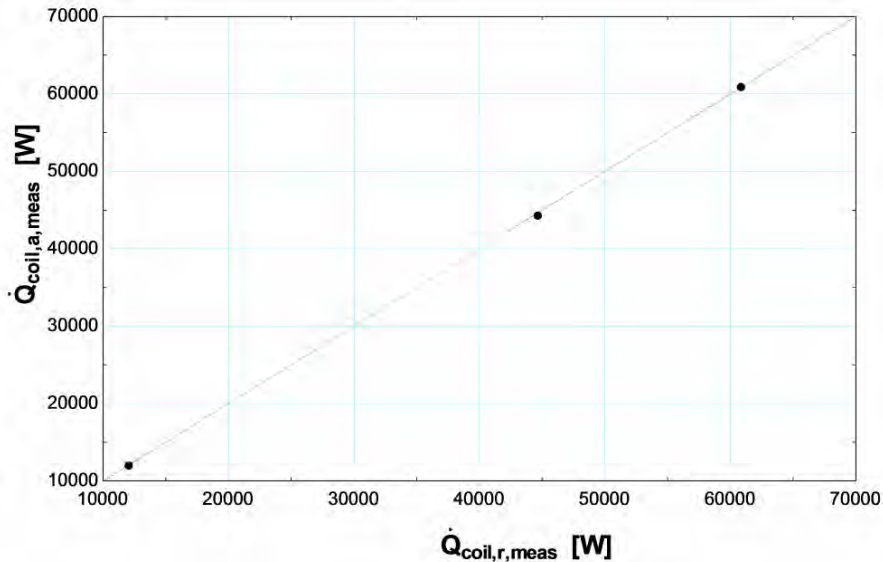


**Figure 4-2 Comparison between the heating capacities calculated on the air-side (y-axis) and on the water side (x-axis)**

#### 4.2.2.2 Identified parameters

First of all, the heating capacity predicted by the model, with the parameters identified on the basis of the nominal point is compared to the measured heating capacity. As shown in Figure 4-3 (square points), the model under-predicts the heating capacity for the two new points.

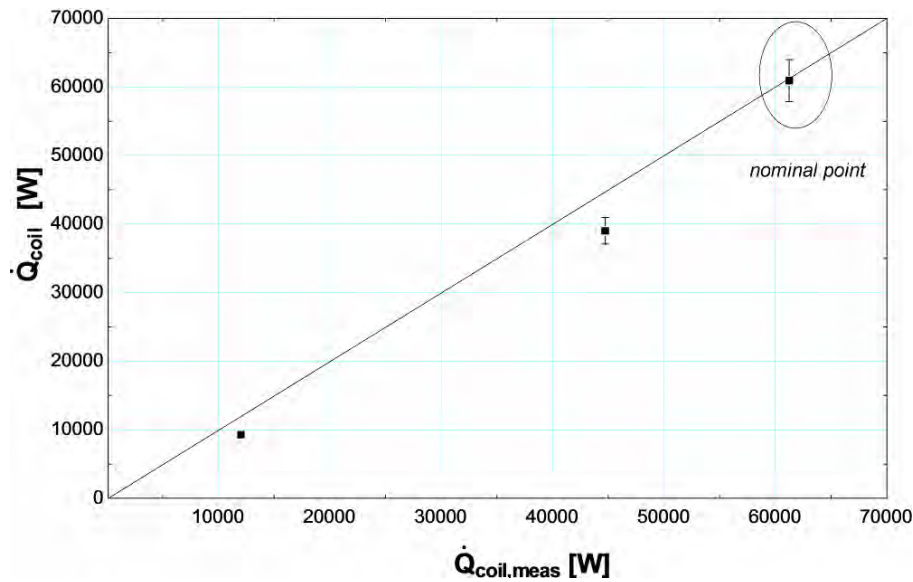


Figure 4-3 Prediction by the model of the heating coil capacity

The two new points differ from the nominal point only by the water flow rate (the air flow rate is close to the nominal one). One explanation would be that water-side resistance should have been smaller in proportions to the other resistances. Actually, the metal resistance may have been underestimated and the water- and air-side resistances overestimated. This assumption tends to be confirmed by previous work carried out on (cooling) and heating in the frame of the ECBCS Annex 10 (Holmes, 1988). The authors showed the importance of the metal resistance in proportion to the two other resistances.

The Wilson-plot method (Wilson, 1915) may be used here to calculate the heat transfer resistance on the water-side. This method consists in drawing the total heat transfer resistance as a function of  $\dot{M}_1^{-n}$  for a constant mass flow rate of the other fluid  $\dot{M}_2$ . Provided the exponent  $n$  is chosen correctly, the points should fall on a straight line. The three performance points given in Table 4-1 and Table 4-4 are characterized by air flow rates very close to each other and by water flow rates ranging from 0.09 to 1.33 l/s. The evolution of the overall heat transfer resistance with  $K_w$  (defined as the water mass flow rate exponent (-0.8)) for these three points is given in Figure 4-4. Two sources of information can be drawn from the Wilson-plot method:

3. If the line is extrapolated to  $K_w = 0$  ( $\dot{M}_w \rightarrow \infty, R_w \rightarrow 0$ ), the intersection with the R-axis gives the value of the metal plus air-side resistance ( $R_a + R_m$ ). Taking an average value from the four curve fits, the metal plus air-side resistance appears to be close to 0.0006297 K/W. The range of air mass flow rates is not wide enough to identify clearly any dependency between this total resistance and the air mass flow rate. Consequently, it is not possible to distinguish between the air-side and metal resistance.
4. The nominal water-side resistance can be identified from the slope of the linear regression. The mean slope associated to the four evolutions is 0.000302264. Hence, the nominal water-side resistance can be computed by:

$$R_{r,coil,n,bis} = \frac{0.000302264}{\dot{M}_{r,coil,n}^{0.8}}$$

The identified nominal water-side resistance  $R_{w,n}$  is **0.0002458 K/W**.

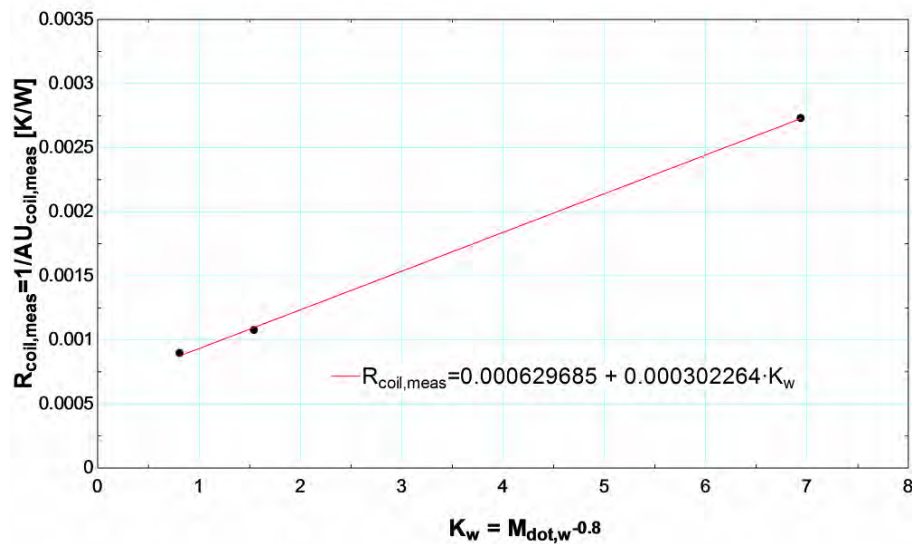


**Figure 4-4 Evolution of the overall heat transfer resistance with the water flow rate exponent - 0.8 (Three points used to calibrate the model for the empirical test)**

Figure 4-5 shows the comparison between the heating capacity calculated by the model and the measured heating capacity (on the air side) for a nominal water resistance of 0.0002458 K/W and an air-side and a metal resistances of 0.0006297/2 K/W. The latter two resistances have been assumed equal since there is not enough information (such as different air flow rates) to distinguish between both of them. The agreement between the prediction by the model and the measurement is very good.

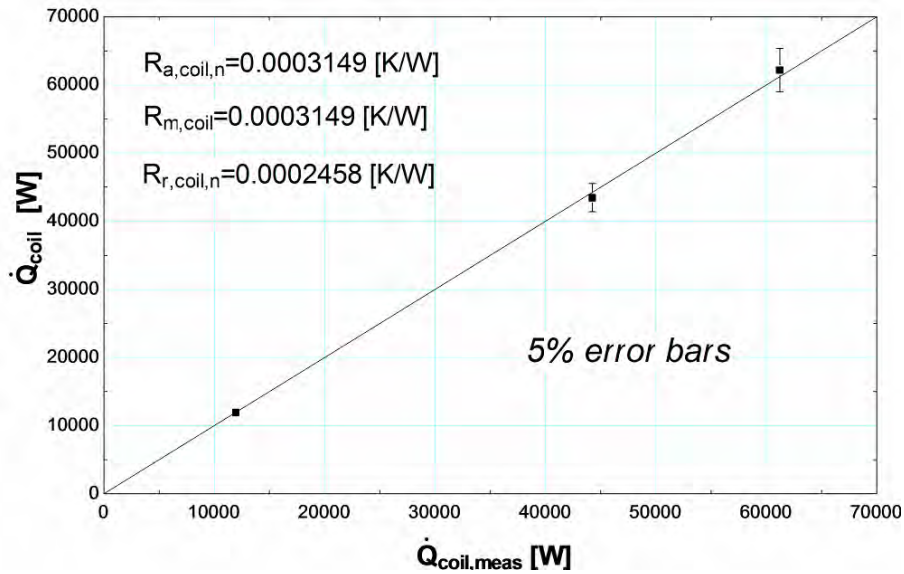


Figure 4-5 Prediction by the model of the heating coil capacity

### 4.3 Simulation results analysis

#### 4.3.1 Analysis of the comparative tests

The comparative test matrix is recalled in Table 4-5. A more detailed description of the tests is given in the main report. The following variables are imposed: the supply air temperature, the exhaust air set point (“DCA-ST”) and the air mass flow rate (Constant Air Volume or Variable Air Volume). The models are compared at almost equal heating loads (the set point may not be achieved). The simulation code must compute the water flow rate (for the four first tests) and the supply water temperature (for the last four tests). Differences between the results generated by the different models only result from differences in the way they evaluate the global heat transfer coefficient  $AU$ .

Table 4-5 Heating coil comparative test case matrix

Test Case	Config	Air Flow	DCA-ST
HX100	$m_{var}$	CAV	13
HX120			18
HX200		VAV	13
HX220			18
HX300	$T_{var}$	CAV	13
HX320			18
HX400		VAV	13
HX420			18

The total heating water volume passing the coil is given in Figure 4-6. For the four last tests, the models compute the same water volume, since the coil is controlled with a varying water temperature at constant water flow rate. For the four first tests, the total volume computed by EES is slightly larger than those computed by the three other simulation codes. This is explained by a lower overall heat transfer coefficient  $AU$ , what is confirmed by Figure 4-7.

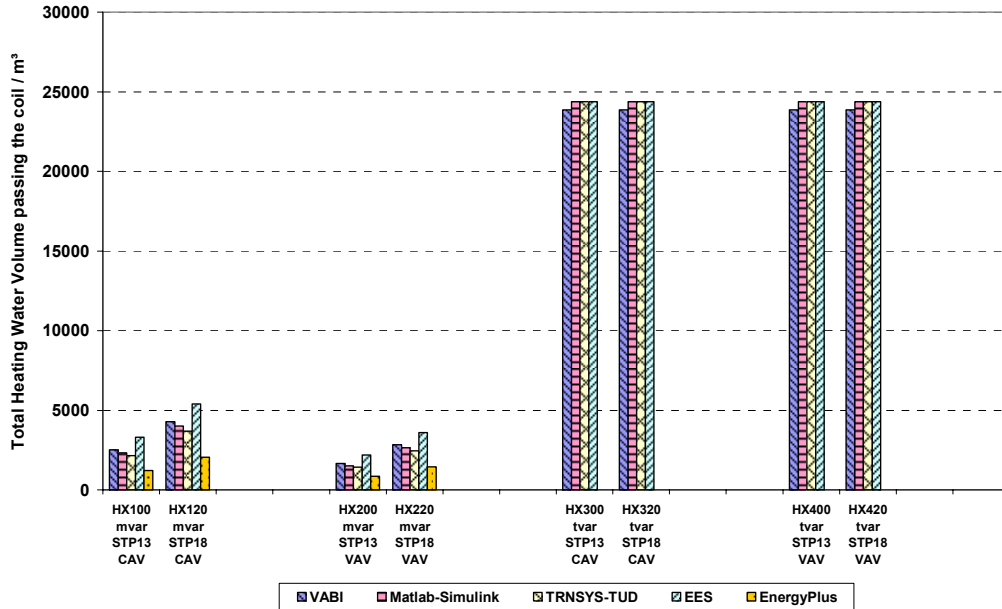
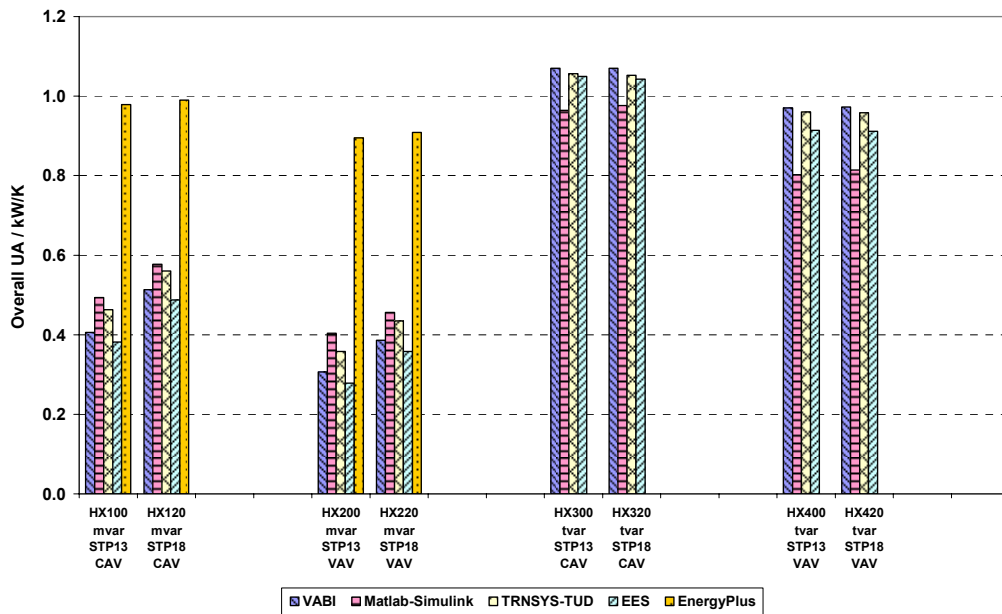


Figure 4-6 Total heating water volume passing the coil

Figure 4-7 actually gives the mean overall heat transfer coefficient  $AU$  for each test. The heat transfer coefficient is averaged over the hours when the heating coil is working ( $T_{a,su,coil} < T_{a,ex,coil,set}$ ).



**Figure 4-7 Mean overall heat transfer coefficient AU**

Figure 4-8 shows the mean leaving water temperature. Here also, this temperature is averaged over the hours where the coil is working. For the first four tests, the mean leaving water computed by EES is larger than those computed by the other simulation codes. This is due to the larger computed water flow rate (remembering that the simulation codes are compared at almost equal heating capacity). For the last four tests, EES predicts a leaving water temperature close the one predicted by TRNSYS-TUD and VABI. Since the heating capacity and the water flow rate are imposed, it means that the computed entering water temperatures, and thus the computed overall heat transfer coefficients, are close.

Comparing results for varying water flow rate (HX100, HX120, HX200 and HX220) and constant water flow rate (HX300, HX320, HX400 and HX420) make appear that the EES model may not describe correctly the dependency of the overall heat transfer coefficient  $AU$  with the water flow rate. The weight given to the water-side resistance may be too large, what is confirmed by the analysis carried out previously in §4.3.1.

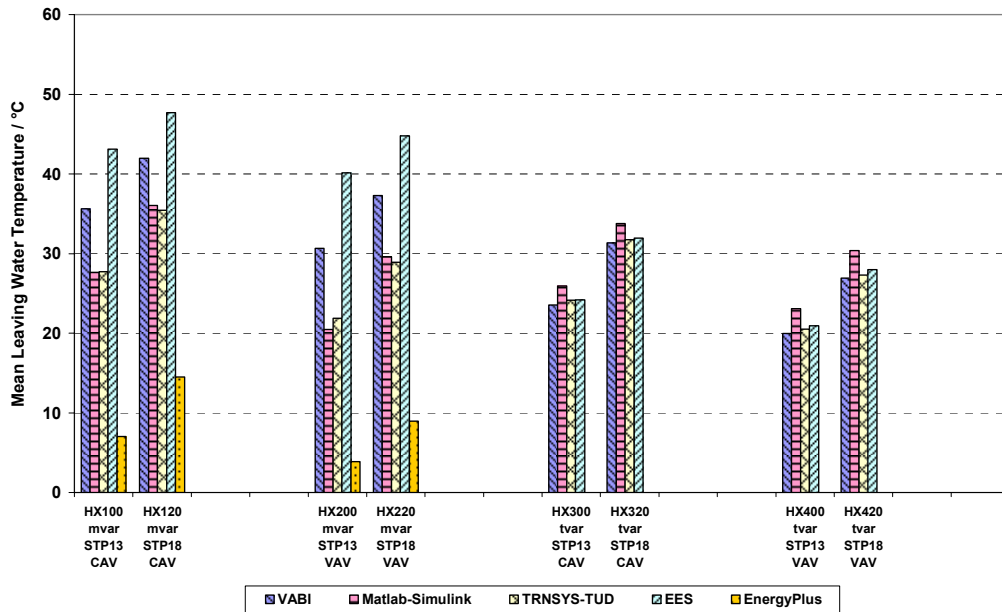


Figure 4-8 Mean leaving water temperature

#### 4.3.2 Analysis of the empirical test

##### 4.3.2.1 Resistances identified on 3 points

This paragraph shows the main results of the simulation carried out with the heating coil model whose parameters have been identified on the basis of the three points given in Table 4-1 and Table 4-4. Identification of these parameters has been presented in §4.2.2.2. The information diagram related to this empirical test is given in Figure 4-9.

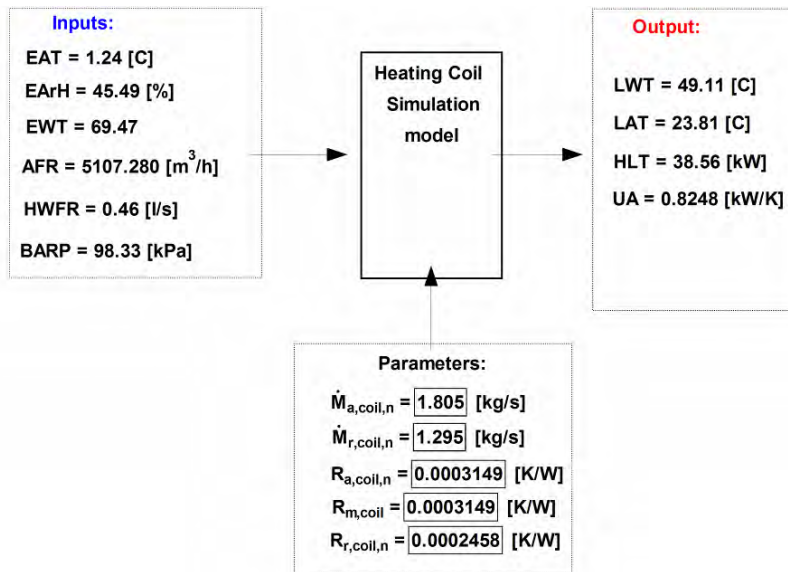


Figure 4-9 Information diagram related to the heating coil empirical test (parameters have been identified on the three performance points presented in §4.2)

The time evolution of the averaged overall heat transfer coefficient predicted by the model is compared to the measured one in Figure 4-10. The EES model slightly under-predicts this heat transfer coefficient.

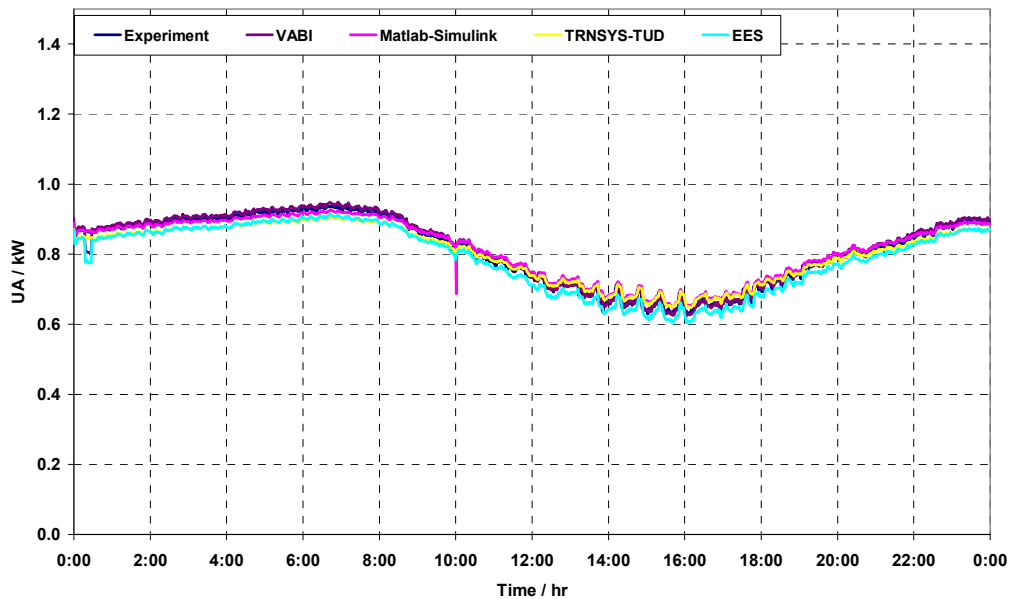
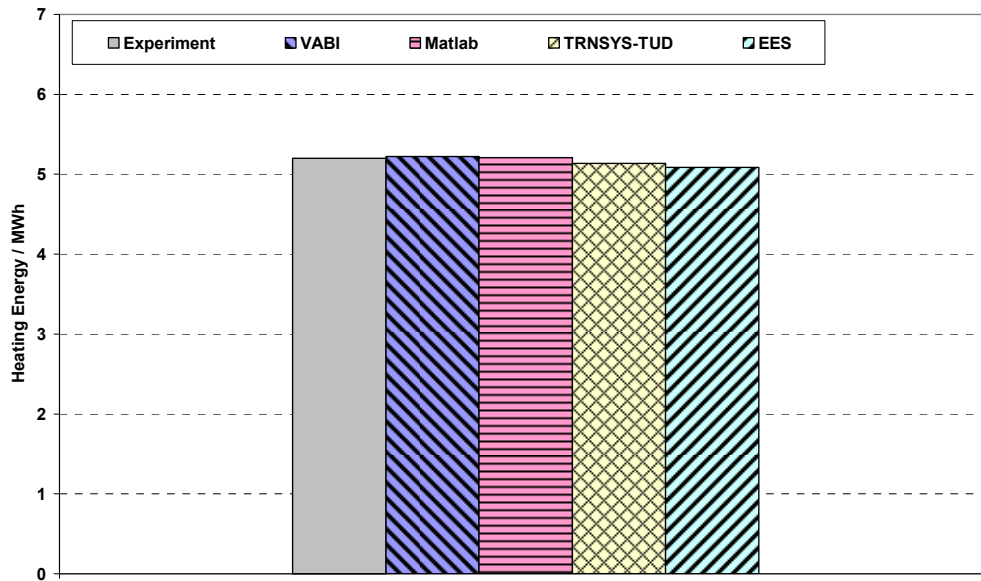


Figure 4-10 Time evolution of the averaged overall heat transfer coefficient  $AU_{coil}$

The underestimation of the overall heat transfer coefficient yields the underestimation of the total heating energy (integration over the 8581 minutes of the simulation), what is shown in Figure 4-11. However, the difference between the prediction by the model (5.09 MWh) and the measurement (5.20 MWh) is only 2.1%.



**Figure 4-11 Total heating energy**

*4.3.2.2 Refinement of the resistances based on more experimental points*

The parameters of the models are refined by applying the Wilson plot method to four series of measurements points extracted from the empirical test and characterized by four different (but quite close) air mass flow rates. Figure 4-12 shows the evolution of the total heat transfer resistance with the water mass flow rate exponent (-0.8). Here also, each of the four evolutions is fairly linear. Curve fits related to the four different air flow rates are given on the same figure. Coefficients of the curve fitting equations are pretty close from each other. The mean offset of the four curve fits is 0.00062 and the mean slope is 0.000296. These values are very close to those given in Figure 4-4. From the value of the slope, a nominal water-side resistance of 0.0002458 K/W is identified.

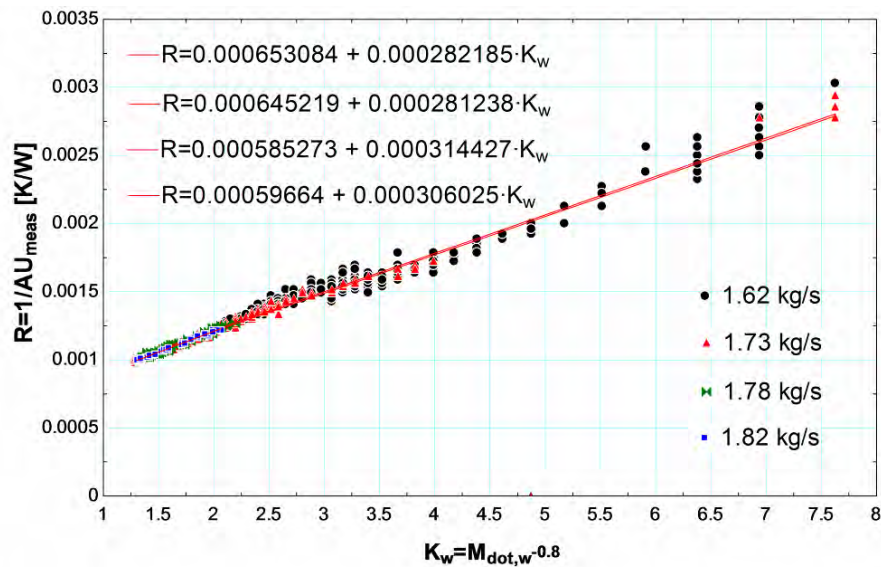


Figure 4-12 Evolution of the overall heat transfer resistance with the water flow rate exponent - 0.8 (measurements related to the empirical test)

The empirical test is run again with the refined resistances: a nominal water-side resistance of 0.0002458 K/W, an air-side resistance of 0.00062/2 K/W and a metal resistance of 0.00062 K/W. Here also, the two latter resistances have been assumed equal; since there is not enough information to distinguish between the air-side and the metal resistances (the experimental air flow rate range is too small).

The information diagram related to the heating coil empirical test with the refined parameters is given in Figure 4-13.

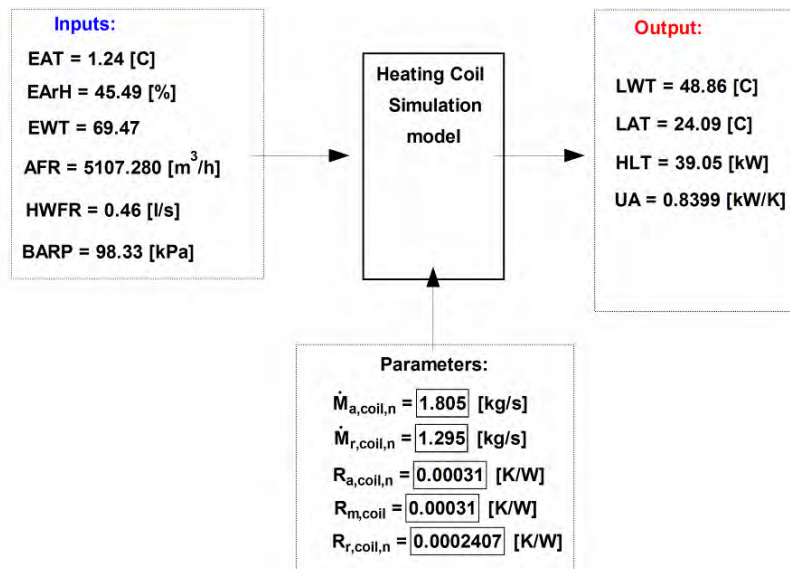


Figure 4-13 Information diagram related to the heating coil empirical test (parameters have been refined based on more experimental points)

The time evolution of the overall heat transfer coefficient  $AU_{coil}$  and the total heating energy are respectively given in Figure 4-14 and Figure 4-15. By refining the values of the heat transfer resistances in the modeling, the agreement between the prediction by the model and the measurements has been improved.

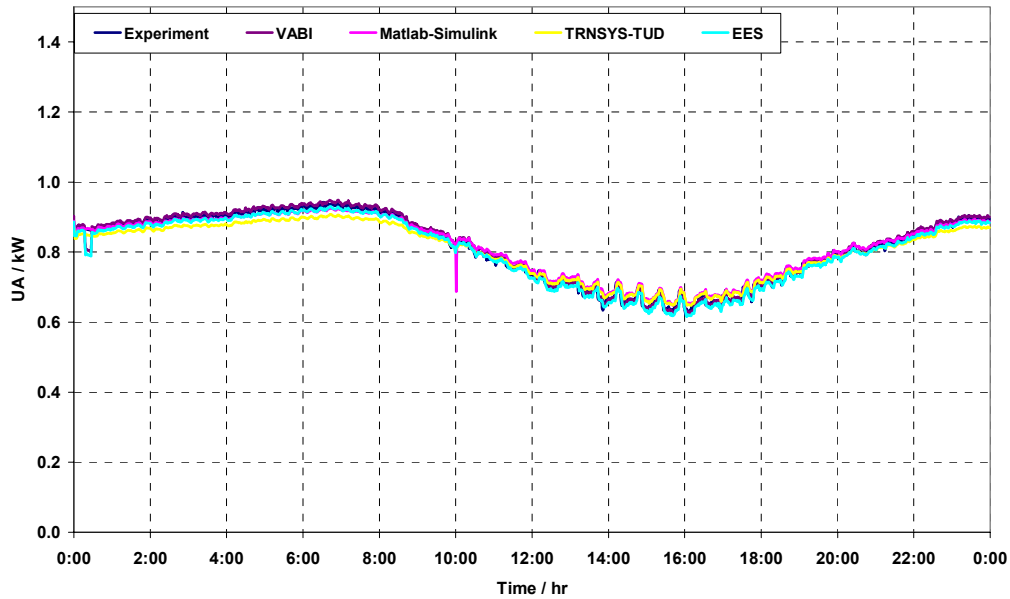


Figure 4-14 Time evolution of the averaged overall heat transfer coefficient  $AU_{coil}$

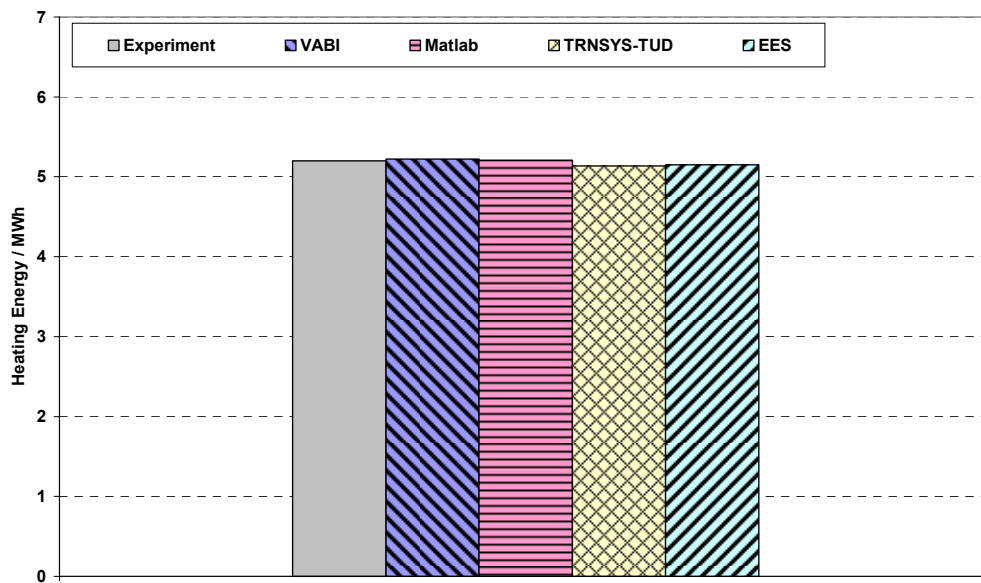


Figure 4-15 Total heating energy

## 5 Conclusions

### 5.1 Chiller

The chiller model parameters identification process, based on *manufacturer catalog data*, revealed that the parameters can easily be identified in two steps: first, the compressor model parameters are identified using compressor performance; then, the heat exchangers model parameters are identified on the basis of chiller performance.

Available information appeared to be too limited for identifying the parameters of the fan control model.

*Analysis of the empirical tests* results made appear that the condensers fan control had to be described in the model, in order to represent the air flow rate decrease when entering air temperature decreases.

*Analysis of all available measurements* (such as evaporating and condensing pressures) allowed evaluating the capability of the compressor model to predict its electrical consumption. This was done by dissociating the compressor model from the heat exchangers models (by imposing both evaporating and condensing pressures). It was observed that the compressor electrical consumption was predicted within 5%. The parameters of the compressor model were those identified based on catalog data and didn't need to be refined.

The analysis of the measurements also revealed that the proposed fan control model is realistic.

The identification of the evaporator and condenser models should be improved. This could be achieved by identifying better quasi steady state periods in the measurement data.

### 5.2 Cooling coil

It appears that the nominal point given by the manufacturer doesn't constitute enough information for identifying the parameters of the model.

The parameters of the model have been retuned using 14 additional quasi-steady state points extracted from experimental data. In order to have a good agreement between the measurements and the predictions by the model, an additional resistance has been added to the metal resistance to account for fouling of the refrigerant pipes.

Results from the empirical tests reveal that the model, with its parameters identified on the basis of the 14 quasi-steady state points, is able to predict both the total and the sensible cooling powers.

### 5.3 Condensing boiler

The available manufacturer data does not constitute enough information in order to identify the parameters of the model. In fact, some important information as the fuel data is missing. It has been demonstrated that even with excessively high heat exchanger efficiencies, the overall boiler efficiency given by the manufacturer is not reached under the conditions of the

empirical test. Therefore, another parameter identification using the available experimental data from the empirical test was done.

With these new identified parameters, the results are pretty good in all the evaluated variables. Unfortunately, the problem of these experimental data is that, at no moment, condensation did occur. This makes that no parameter identification and validation of the whole model can be performed with this data. In fact, only a dry heat exchange is always occurring in the boiler, so is the same phenomenon that occurs in a classical boiler.

#### 5.4 Heating coil

The initial identification of the parameters based only on the manufacturer point seemed to overestimate the water-side convective resistance. The metal resistance was probably underestimated.

This assumption was partially verified with the identification of the parameters based on three performance points (the nominal manufacturer performance points and two quasi-steady state points extracted from experimental data). These three points allowed the identification of the water-side resistance and the combined metal and air-side resistance. However, since the three points are characterized by air mass flow rates close to each other, the identification of the air-side resistance was not possible.

Empirical simulation shows that the model is able to correctly predict the heating capacity, the overall heat transfer coefficient.

#### 5.5 Summary of the models parameters

The parameters of the models of the different components are given their respective information diagrams.

- For the *compressor*, see Figure 1-4
- For the *chiller*, see Figure 1-11 for pure water and Figure 1-16 for glycol water
- For the *cooling coil*, see Figure 2-4
- For the *condensing boiler*, see Figure 3-3
- For the *heating coil*, see Figure 4-13

#### List of references

- ASHRAE. 2000. *2000 ASHRAE handbook—HVAC Systems and Equipment*, Chapter 21. Atlanta: American Society of Heating, Refrigerating and Air-Conditioning Engineers, Inc.
- Braun, J.E., S.A. Klein, and J. Mitchell. 1989. Effectiveness Models for Cooling Towers and Cooling Coils. *ASHRAE Transaction* 95(2):164-173.
- Felsmann, C. 2008. Mechanical Equipment & Control Strategies for a Chilled water and a Hot water system, *A report for the International Energy Agency's SHC Task34/ECBCS Annex 43 Subtask D*.

- Holmes M. J. 1988. ECBCS Annex 10 Report, System Simulation, Heating and Cooling Coils.
- Incropera F. P., D. P. DeWitt, Fundamentals of Heat and Mass Transfer, John Wiley & Sons, 2002.
- Jin, H., and J. Spitler. 2002. Parameters Estimation Based Model of Water-to-Water Heat Pumps with Scroll Compressors and Water/Glycol Solutions, *Proceedings of the Sixth International Conference on System Simulation in Buildings*.
- Lebrun, J., X. Ding, J.-P. Eppe, and M. Wasacz. 1990. Cooling Coil Models to be used in Transient and/or Wet Regimes. Theoretical Analysis and Experimental Validation. *Proceedings of SSB 1990. Liège:405-441*.
- Lemort, V., C. Cuevas, J. Lebrun, and I.V. Teodorese. 2008. Development of Simple Cooling Coil Models for Simulation of HVAC Systems. *ASHRAE Transaction* 114(1).
- Nieter, J. 1988. Dynamic of scroll suction process, Purdue International Compressor Engineering Conference.
- Wilson, E.E. 1915. A Basis for Rational Design of Heat Transfer Apparatus, *ASME Transactions*, Vol. 37, pp. 47-70
- Winandy E., C. Saavedra, and J. Lebrun. 2002. Experimental analysis and simplified modelling of a hermetic scroll refrigeration compressor, *Applied Thermal Engineering* 22: 107-120.